Volume 26, Number 1, 2026 ISSN 1562-8353

NONLINEAR DYNAMICS AND SYSTEMS THEORY
An International Journal of Research and Surveys

Volume 26 Number 1 2026

CONTENTS

NONLINEAR DYNAMICS & SYSTEMS THEORY
Volume 26, No. 1, 2026

Nonlinear Dynamics and Systems Theory

An International Journal of Research and Surveys

EDITOR-IN-CHIEF A.A. MARTYNYUK
S.P. Timoshenko Institute of Mechanics
National Academy of Sciences of Ukraine, Kiev, Ukraine

MANAGING EDITOR I.P. STAVROULAKIS
Department of Mathematics, University of Ioannina, Greece

REGIONAL EDITORS

S.G. GEORGIEV, Paris, France
A. OKNIŃSKI, Kielce, Poland
Europe

M. BOHNER, Rolla, USA
HAO WANG, Edmonton, Canada
North USA and Canada

C. CRUZ-HERNANDEZ, Ensenada, Mexico
Central and South America

M. ALQURAN, Irbid, Jordan
Jordan and Middle East

T. HERLAMBANG, Surabaya, Indonesia
Indonesia and New Zealand

© 2026, InforMath Publishing Group ISSN 1562-8353 Printed in Ukraine
To receive contents and abstracts by e-mail, visit our Website at: **http://www.e-ndst.kiev.ua**

InforMath Publishing Group
http://www.e-ndst.kiev.ua

Nonlinear Dynamics and Systems Theory

An International Journal of Research and Surveys

EDITOR-IN-CHIEF A.A. MARTYNYUK
The S.P. Timoshenko Institute of Mechanics, National Academy of Sciences of Ukraine,
Nesterov Str. 3, 03057, Kyiv-57, UKRAINE / e-mail: journalndst@gmail.com

MANAGING EDITOR I.P. STAVROULAKIS
Department of Mathematics, University of Ioannina
451 10 Ioannina, HELLAS (GREECE) / e-mail: ipstav@cc.uoi.gr

ADVISORY EDITOR A.G. MAZKO,
Institute of Mathematics of NAS of Ukraine, Kiev (Ukraine)
e-mail: mazkoag@gmail.com

REGIONAL EDITORS
S.G. GEORGIEV, France, e-mail: svetlingeorgiev1@gmail.com
A. OKNINSKI, Poland, e-mail: fizao@tu.kielce.pl
M. BOHNER, USA, e-mail: bohner@mst.edu
HAO WANG, Edmonton, Canada, e-mail: hao8@ualberta.ca
C. CRUZ-HERNANDEZ, Mexico, e-mail: ccruz@cicese.mx
M. ALQURAN, Jordan, e-mail: marwan04@just.edu.jo
T. HERLAMBANG, Indonesia, e-mail: teguh@unusa.ac.id

EDITORIAL BOARD

Adzkiya, D. (Indonesia)
Artstein, Z. (Israel)
Awrejcewicz, J. (Poland)
Chen Ye-Hwa (USA)
De Angelis, M. (Italy)
Denton, Z. (USA)
Djemai, M. (France)
Dshalalow, J. H. (USA)
Faria, T. (Portugal)
Gajic, Z. (USA)
Georgiou, G. (Cyprus)
Honglei Xu (Australia)
Jafari, H. (South African Republic)
Kloeden, P. (Germany)
Kokologiannaki, C. (Greece)
Kryzhevich, S. (Poland)
Limarchenko, O.S. (Ukraine)
Lopez Gutierrez, R.M. (Mexico)
Lozi, R. (France)
Mesquita, J.G. (Brazil)
Peterson, A. (USA)
Radziszewski, B. (Poland)
Rasmussen, M. (United Kingdom)
Shi Yan (Japan)
Sivasundaram, S. (USA)
Staicu, V. (Portugal)
Vatsala, A. (USA)

ADVISORY COMPUTER SCIENCE EDITORS
A.N. CHERNIENKO and A.S. KHOROSHUN, Kiev, Ukraine

ADVISORY LINGUISTIC EDITOR
S.N. RASSHYVALOVA, Kiev, Ukraine

© 2026, InforMath Publishing Group, ISSN 1562-8353 print, ISSN 1813-7385 online, Printed in Ukraine
No part of this Journal may be reproduced or transmitted in any form or by any means without permission from InforMath Publishing Group.

INSTRUCTIONS FOR CONTRIBUTORS

(1) General. Nonlinear Dynamics and Systems Theory (ND&ST) is an international journal devoted to publishing peer-refereed, high quality, original papers, brief notes and review articles focusing on nonlinear dynamics and systems theory and their practical applications in engineering, physical and life sciences. Submission of a manuscript is a representation that the submission has been approved by all of the authors and by the institution where the work was carried out. It also represents that the manuscript has not been previously published, has not been copyrighted, is not being submitted for publication elsewhere, and that the authors have agreed that the copyright in the article shall be assigned exclusively to InforMath Publishing Group by signing a transfer of copyright form. Before submission, the authors should visit the website:

http://www.e-ndst.kiev.ua

for information on the preparation of accepted manuscripts. Please download the archive Sample_NDST.zip containing example of article file (you can edit only the file Samplefilename.tex).

(2) Manuscript and Correspondence. Manuscripts should be in English and must meet common standards of usage and grammar. To submit a paper, send by e-mail a file in PDF format directly to

Professor A.A. Martynyuk, Institute of Mechanics,
Nesterov str.3, 03057, Kiev-57, Ukraine
e-mail: journalndst@gmail.com

or to one of the Regional Editors or to a member of the Editorial Board. Final version of the manuscript must typeset using LaTex program which is prepared in accordance with the style file of the Journal. Manuscript texts should contain the title of the article, name(s) of the author(s) and complete affiliations. Each article requires an abstract not exceeding 150 words. Formulas and citations should not be included in the abstract. AMS subject classifications and key words must be included in all accepted papers. Each article requires a running head (abbreviated form of the title) of no more than 30 characters. The sizes for regular papers, survey articles, brief notes, letters to editors and book reviews are: (i) 10-14 pages for regular papers, (ii) up to 24 pages for survey articles, and (iii) 2-3 pages for brief notes, letters to the editor and book reviews.

(3) Tables, Graphs and Illustrations. Each figure must be of a quality suitable for direct reproduction and must include a caption. Drawings should include all relevant details and should be drawn professionally in black ink on plain white drawing paper. In addition to a hard copy of the artwork, it is necessary to attach the electronic file of the artwork (preferably in PCX format).

(4) References. Each entry must be cited in the text by author(s) and number or by number alone. All references should be listed in their alphabetic order. Use please the following style:

Journal: [1] H. Poincare, Title of the article. *Title of the Journal* **volume** (issue) (year) pages. [Language]

Book: [2] A.M. Lyapunov, *Title of the Book.* Name of the Publishers, Town, year.

Proceeding: [3] R. Bellman, Title of the article. In: *Title of the Book.* (Eds.). Name of the Publishers, Town, year, pages. [Language]

(5) Proofs and Sample Copy. Proofs sent to authors should be returned to the Editorial Office with corrections within three days after receipt. The corresponding author will receive a sample copy of the issue of the Journal for which his/her paper is published.

(6) Editorial Policy. Every submission will undergo a stringent peer review process. An editor will be assigned to handle the review process of the paper. He/she will secure at least two reviewers' reports. The decision on acceptance, rejection or acceptance subject to revision will be made based on these reviewers' reports and the editor's own reading of the paper.

NONLINEAR DYNAMICS AND SYSTEMS THEORY
An International Journal of Research and Surveys
Published by InforMath Publishing Group since 2001

Volume 26 Number 1 2026

CONTENTS

Founded by A.A. Martynyuk in 2001.
Registered in Ukraine Number: KB No 5267 / 04.07.2001.

NONLINEAR DYNAMICS AND SYSTEMS THEORY

An International Journal of Research and Surveys

Impact Factor from SCOPUS for 2024: SJR – 0.262, SNIP – 1.098 and CiteScore – 1.5

Nonlinear Dynamics and Systems Theory (ISSN 1562–8353 (Print), ISSN 1813–7385 (Online)) is an international journal published under the auspices of the S.P. Timoshenko Institute of Mechanics of National Academy of Sciences of Ukraine and Curtin University of Technology (Perth, Australia). It aims to publish high quality original scientific papers and surveys in areas of nonlinear dynamics and systems theory and their real world applications.

AIMS AND SCOPE

Nonlinear Dynamics and Systems Theory is a multidisciplinary journal. It publishes papers focusing on proofs of important theorems as well as papers presenting new ideas and new theory, conjectures, numerical algorithms and physical experiments in areas related to nonlinear dynamics and systems theory. Papers that deal with theoretical aspects of nonlinear dynamics and/or systems theory should contain significant mathematical results with an indication of their possible applications. Papers that emphasize applications should contain new mathematical models of real world phenomena and/or description of engineering problems. They should include rigorous analysis of data used and results obtained. Papers that integrate and interrelate ideas and methods of nonlinear dynamics and systems theory will be particularly welcomed. This journal and the individual contributions published therein are protected under the copyright by International InforMath Publishing Group.

PUBLICATION AND SUBSCRIPTION INFORMATION

Nonlinear Dynamics and Systems Theory will have 6 issues in 2026, printed in hard copy (ISSN 1562–8353) and available online (ISSN 1813–7385), by InforMath Publishing Group, Nesterov str., 3, Institute of Mechanics, Kiev, MSP 680, Ukraine, 03057. Subscription prices are available upon request from the Publisher, EBSCO Information Services (`mailto:journals@ebsco.com`), or website of the Journal: `http://e-ndst.kiev.ua`. Subscriptions are accepted on a calendar year basis. Issues are sent by airmail to all countries of the world. Claims for missing issues should be made within six months of the date of dispatch.

ABSTRACTING AND INDEXING SERVICES

Papers published in this journal are indexed or abstracted in: Mathematical Reviews / MathSciNet, Zentralblatt MATH / Mathematics Abstracts, PASCAL database (INIST–CNRS) and SCOPUS.

Nonlinear Dynamics and Systems Theory, **26** (1) (2026) 1–13

Train Departure Scheduling Using Kleene Star and Petri Net Queue Model (Cicalengka–Padalarang)

E. Carnia *, M. Faldiyan, A. A. Permatasari, A. K. Supriatna and M. D. Johansyah

Department of Mathematics, Faculty of Mathematics and Natural Sciences, Universitas Padjadjaran, Sumedang 45363, Indonesia

Received: June 9, 2025; Revised: January 31, 2026

Abstract: The train is one of the public transport used by people to move between regions. PT Kereta Api Indonesia (PT KAI) is an Indonesian State-Owned Enterprise (BUMN) that provides rail transportation services. One of the railway lines belonging to KAI is a line which connects the towns of a province and is called the local railway. An example of a local train in the town is the one which connects Padalarang and Cicalengka subdistricts with the Bandung Raya Ekonomi Railway. The use of this local train is of high enough interest in the community because the price of train tickets is relatively cheap and it is relatively easy for the public to purchase train tickets. Train tickets can be purchased via the KAI Access application online or directly at the counter available at the local station. The entrance to the station is also very practical for the public in general, but because there are two methods of buying train tickets, it sometimes results in many queues in the ticket scanning process. In this paper, we discussed the ticket flow model for entering the Padalarang station in order to avoid any queue during the process of scanning the ticket. In addition, this paper discussed the effective time of train departure so that the time used for train operation is the optimal time. The method applied in this research is a Petri net for station entry flow modeling and the Kleene star algorithm for the effectiveness of train scheduling. The results of this study are useful for reducing queuing time before train departure and for effective train operating time. This research can be a reference for other researchers to develop a Petri net model and a reference for the government to optimize train departure time.

Keywords: *Petri net; queuing system; train; Kleene star algorithm; mathematical model.*

Mathematics Subject Classification (2020): 70K20, 93C85, 93C65, 90B35, 15A80, 68M20.

* Corresponding author: mailto:ema.carnia@unpad.ac.id

© 2026 InforMath Publishing Group/1562-8353 (print)/1813-7385 (online)/http://e-ndst.kiev.ua

1 Introduction

Carl Adam Petri introduced Petri nets in 1962 as a graphical modeling tool similar to flowcharts, capable of representing activities occurring simultaneously [1]. Petri nets employ modeling techniques and network analysis both qualitatively and quantitatively [2], and can be used to model algorithms for specific processes such as rail transportation from the station entry to boarding and traveling to the destination. They are powerful tools for modeling and analyzing discrete event systems and are widely applied in scheduling, planning, queuing systems, deadlock control, stochastic processes, and performance evaluation in various resource allocation contexts [3, 4].

Max-plus algebra is a powerful framework for representing and analyzing discrete event systems, particularly those involving synchronization without concurrency [5, 6]. Built upon the max-plus semiring $\mathbb{R}_{\max} = \mathbb{R} \cup \{-\infty\}$ with operations $\oplus$ (maximum) and $\otimes$ (addition), it extends naturally to vectors and matrices [7]. Linear time-invariant systems can also be modeled within this algebraic structure. Eigenvalue and eigenvector problems in max-plus algebra are defined similarly to classical linear algebra but utilize max-plus operations, where $A \otimes v = \lambda \otimes v$ [8]. Combined with Petri nets, max-plus algebra effectively addresses discrete event system challenges. This study applies both approaches to real-world problems, specifically to determine train departure scheduling and rail transport procedures.

Research on max-plus algebra and Petri nets has been widely conducted to address real-world problems related to scheduling and queuing systems. Its applications include improving railway maintenance planning in the UK, analyzing student enrollment patterns, managing spare parts procurement for marine engines, and optimizing queuing systems in banks and healthcare facilities [9–12]. Other studies utilize Petri nets for cyber-physical systems, quantum annealing models, flexible manufacturing systems, railway delay simulations, business process error detection, and human-agent interaction planning [13–15]. These works demonstrate the effectiveness of combining Petri nets and max-plus algebra in improving efficiency, concurrency, and optimization across diverse domains.

Previous studies have explored the use of Petri nets in general contexts, but none have addressed entrance queues in train stations under current conditions involving both online and offline ticketing systems, nor have they focused on optimizing local train departure schedules in West Java, particularly for the Bandung Raya trains. This paper investigates public rail transportation scheduling using Petri net modeling and max-plus algebra. The Petri net models the complete passenger flow—from entering the station and purchasing tickets to boarding the train and departing. Max-plus algebra, using the Kleene star algorithm, is applied to calculate effective train departure time, with a case study on the Bandung Raya Ekonomi Train from Padalarang to Rancaekek. The study results include a Petri net model that accommodates both ticketing systems and an optimized train schedule that reduces passenger waiting time. This research aims to support the government and PT KAI in developing more efficient train schedules, ultimately enhancing the appeal and effectiveness of rail-based public transportation.

This study addresses a key problem in discrete event dynamic systems, which are a fundamental subset of nonlinear dynamical systems due to their event-driven, non-continuous behavior. The queuing and scheduling processes in railway systems inherently involve nonlinear interactions, particularly when modeling passenger flow and train departure synchronization. By employing Petri nets and max-plus algebra—both bee-

ing widely recognized tools in the analysis of nonlinear discrete systems, we provide a structured approach to model, simulate, and optimize the complex dynamics of train operations. The use of the Kleene star algorithm for computing train departure time further emphasizes the nonlinear temporal dependencies present in such systems. Thus, this research contributes to the nonlinear dynamics field by offering a mathematical and systems theoretical framework to address transport scheduling challenges, aligning with the focus on nonlinear systems and their applications.

2 Methodology

In this paper, train scheduling data from the Padalarang-Cicalengka route was retrieved using the KAI Access application, complemented by on-site observations at the nearest station. The research followed a structured flow: first, a Petri net was drawn to represent the ticket purchase and train entry process; then, this Petri net was tested and evaluated using the online tool at http://petri.hp102.ru/pnet.html. Based on the evaluation, a new Petri net was developed, which was then transformed into backward, forward, and incidence matrices. Using the incidence matrix, calculations were performed by analyzing enabled transitions. When these calculations returned to their initial form, an effective path through the Petri net was identified.

The eigenvalue and eigenvector calculation flow for a max-plus matrix involves several steps. First, compute the eigenvalues λ using the formula $\lambda = \bigotimes_{k=1}^{n} \left(\frac{1}{k} \operatorname{trace}\left(A^{\otimes k}\right)\right)$. Then, define $B = -\lambda \otimes A$. Next, calculate the star and plus closures of B, namely $B^* = E \oplus B \oplus \cdots \oplus B^{\otimes(n-1)}$ and $B^+ = B \otimes B^*$, where E is the max-plus identity matrix. The critical points of the associated graph $G(A)$ are identified by checking when the diagonal elements of B^+, i.e., $[B^+]_{vv}$, are equal to zero; such v indicates a critical node. The eigenvectors corresponding to the eigenvalue λ are then given by the v-th row of B^*. Finally, these eigenvalues and eigenvectors satisfy the max-plus eigen-equation $A \otimes v = \lambda \otimes v$, where A is the max-plus matrix, v is an eigenvector, and λ is the corresponding eigenvalue.

The train scheduling flow begins by calculating the eigenvalues and eigenvectors of the matrix that models the travel time between stations. These eigenvalues and eigenvectors are then used to determine a new train departure schedule, selecting a non-negative eigenvector since it corresponds to feasible scheduling. The departure time from each station is calculated using Eq. (1).

$$d(k) = d(0) \otimes \lambda^{\otimes k} = \begin{bmatrix} v_0 + k \cdot \lambda \\ v_1 + k \cdot \lambda \\ \vdots \\ v_{n-1} + k \cdot \lambda \end{bmatrix}, \tag{1}$$

where λ is an eigenvalue of the max-plus matrix A, and $v_0, v_1, \cdots, v_{n-1}$ are components of the corresponding eigenvector. The departure schedule is determined by substituting $k = 0$ for the first station, $k = 1$ for the second, and so on, up to $k = n - 1$ for the last station. This approach yields a new, optimized train schedule, incorporating assumptions about waiting time at each station along the route.

3 Results

3.1 Petri net from the flow of buying tickets

In both offline and online ticketing processes, passengers ultimately follow a similar journey to board the train, with the main difference being how the ticket is obtained. Offline ticketing requires passengers to visit the counter, present their KTP, and purchase a ticket directly from the counter keeper before proceeding to the station. In contrast, online ticketing allows passengers to buy tickets in advance via the KAI application. Upon arriving at the station in either case, a train scan officer verifies the ticket, after which passengers enter the waiting area and board the train when it arrives. Based on Figure 1, the flow of buying tickets until the passengers manage to get on the train is as follows.

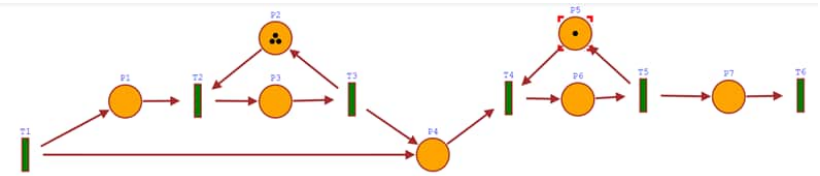

Figure 1: The Petri net from the flow of buying tickets to entering the train station.

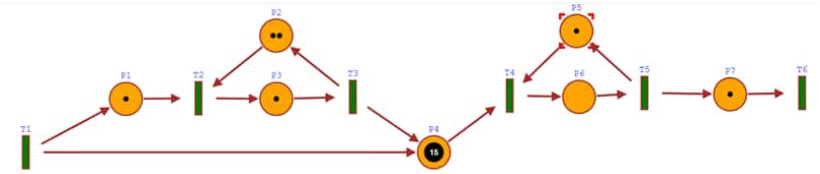

Figure 2: Evaluation of the Petri net.

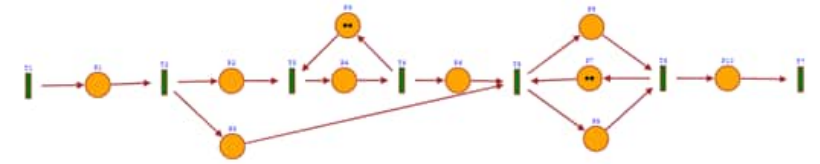

Figure 3: The new Petri net.

In Figure 1, the process begins at T1, when passengers arrive at the entrance counter (P1). At T2, they interact with the counterkeeper (P2) at the ticket sales transaction counter (P3) to purchase a ticket. After completing the transaction, T3 marks the point where passengers leave the counter and head toward the station entrance (P4). At T4, passengers move to the ticket scanning area (P6), where the scan officer (P5) verifies their tickets. Following this, at T5, passengers who have completed the scanning process proceed to the train departure station (P7). Finally, at T6, they board the train and depart from the station.

During the simulation, congestion occurred at the station entrance near the scanning area due to the formation of two separate queues—one for passengers with online tickets

and another for those with offline tickets — as illustrated in Figure 2. Based on this evaluation, it is recommended to add separate scanning points for online and offline tickets to reduce congestion, as shown in Figure 3.

The process begins at T1, when passengers arrive in the station area (P1).For offline ticket buyers, T2 marks their entry through the offline ticket purchase entrance (P2), followed by T3, where they interact with the counter officer (P5) at the ticket sales transaction counter (P4) to purchase a ticket. At T4, these passengers leave the counter and head toward the ticket scanning station (P6). For online ticket buyers, the entry is through the online ticket purchase entrance (P3), and both groups proceed to T5, the ticket scanning station (P6), where scanning is conducted by the ticket scanning officer (P7). Offline and online tickets are scanned separately at P8 and P9, respectively. After successful scanning at T6, passengers move to the train departure area, and at T7, they board the train and depart the station.

The new form of Petri net assumes that passengers using the online and offline ticket purchase methods must pass through the counter staff first. So, from the shape of the Petri net, the backward, forward, and incidence matrices will be obtained as follows:

$$\tilde{A}_f = \begin{array}{c} \\ P_1 \\ P_2 \\ P_3 \\ P_4 \\ P_5 \\ P_6 \\ P_7 \\ P_8 \\ P_9 \\ P_{10} \end{array} \begin{array}{c} \begin{array}{ccccccc} T_1 & T_2 & T_3 & T_4 & T_5 & T_6 & T_7 \end{array} \\ \begin{bmatrix} 1 & 0 & 0 & 0 & 0 & 0 & 0 \\ 0 & 1 & 0 & 0 & 0 & 0 & 0 \\ 0 & 1 & 0 & 0 & 0 & 0 & 0 \\ 0 & 0 & 1 & 0 & 0 & 0 & 0 \\ 0 & 0 & 0 & 1 & 0 & 0 & 0 \\ 0 & 0 & 0 & 1 & 0 & 0 & 0 \\ 0 & 0 & 0 & 0 & 0 & 1 & 0 \\ 0 & 0 & 0 & 0 & 1 & 0 & 0 \\ 0 & 0 & 0 & 0 & 1 & 0 & 0 \\ 0 & 0 & 0 & 0 & 0 & 1 & 0 \end{bmatrix} \end{array}, \tilde{A}_b = \begin{array}{c} \\ P_1 \\ P_2 \\ P_3 \\ P_4 \\ P_5 \\ P_6 \\ P_7 \\ P_8 \\ P_9 \\ P_{10} \end{array} \begin{array}{c} \begin{array}{ccccccc} T_1 & T_2 & T_3 & T_4 & T_5 & T_6 & T_7 \end{array} \\ \begin{bmatrix} 0 & 1 & 0 & 0 & 0 & 0 & 0 \\ 0 & 0 & 1 & 0 & 0 & 0 & 0 \\ 0 & 0 & 0 & 0 & 1 & 0 & 0 \\ 0 & 0 & 0 & 1 & 0 & 0 & 0 \\ 0 & 0 & 1 & 0 & 0 & 0 & 0 \\ 0 & 0 & 0 & 0 & 1 & 0 & 0 \\ 0 & 0 & 0 & 0 & 1 & 0 & 0 \\ 0 & 0 & 0 & 0 & 0 & 1 & 0 \\ 0 & 0 & 0 & 0 & 0 & 1 & 0 \\ 0 & 0 & 0 & 0 & 0 & 0 & 1 \end{bmatrix} \end{array},$$

$$\tilde{A} = \tilde{A}_f - \tilde{A}_b = \begin{array}{c} \\ P_1 \\ P_2 \\ P_3 \\ P_4 \\ P_5 \\ P_6 \\ P_7 \\ P_8 \\ P_9 \\ P_{10} \end{array} \begin{array}{c} \begin{array}{ccccccc} T_1 & T_2 & T_3 & T_4 & T_5 & T_6 & T_7 \end{array} \\ \begin{bmatrix} 1 & -1 & 0 & 0 & 0 & 0 & 0 \\ 0 & 1 & -1 & 0 & 0 & 0 & 0 \\ 0 & 1 & 0 & 0 & -1 & 0 & 0 \\ 0 & 0 & 1 & -1 & 0 & 0 & 0 \\ 0 & 0 & -1 & 1 & 0 & 0 & 0 \\ 0 & 0 & 0 & 1 & -1 & 0 & 0 \\ 0 & 0 & 0 & 0 & -1 & 1 & 0 \\ 0 & 0 & 0 & 0 & 1 & -1 & 0 \\ 0 & 0 & 0 & 0 & 1 & -1 & 0 \\ 0 & 0 & 0 & 0 & 0 & 1 & -1 \end{bmatrix} \end{array}.$$

The initial state of the Petri net is $x_0 = \begin{bmatrix}0 & 2 & 0 & 0 & 0 & 2 & 0 & 0\end{bmatrix}^T$. The possible firing sequences to return to the initial state are as follows:

$$1.\ x_2 = \begin{bmatrix}0\\1\\1\\0\\2\\0\\2\\0\\0\\0\end{bmatrix} \xrightarrow{t_3} \begin{bmatrix}0\\0\\1\\1\\1\\0\\2\\0\\0\\0\end{bmatrix} \xrightarrow{t_4} \begin{bmatrix}0\\0\\1\\0\\2\\1\\2\\0\\0\\0\end{bmatrix} \xrightarrow{t_5} \begin{bmatrix}0\\0\\0\\0\\2\\0\\1\\1\\1\\0\end{bmatrix} \xrightarrow{t_6} \begin{bmatrix}0\\0\\0\\0\\2\\0\\2\\0\\0\\1\end{bmatrix} \xrightarrow{t_7} \begin{bmatrix}0\\0\\0\\0\\2\\0\\2\\0\\0\\0\end{bmatrix} = x_1,$$

(passengers who buy tickets offline enter the scan area to enter the station)

$$2.\ x_2 = \begin{bmatrix}0\\1\\1\\0\\2\\0\\2\\0\\0\\0\end{bmatrix} \xrightarrow{t_5} \begin{bmatrix}0\\0\\0\\0\\2\\0\\1\\1\\1\\0\end{bmatrix} \xrightarrow{t_6} \begin{bmatrix}0\\0\\0\\0\\2\\0\\2\\0\\0\\1\end{bmatrix} \xrightarrow{t_7} \begin{bmatrix}0\\0\\0\\0\\2\\0\\2\\0\\0\\0\end{bmatrix} = x_1$$

(passengers who buy tickets online enter the scan area to enter the station).

Based on the calculation above, there are two critical paths in the Petri net, namely $t_1 \to t_2 \to t_3 \to t_4 \to t_5 \to t_6 \to t_7$, where the path is for passengers with offline ticket purchases, and $t_1 \to t_2 \to t_5 \to t_6 \to t_7 \to t_8$, where the path is for passengers with online ticket purchases. With the simulation conducted, it is found that the Petri net that has been made is an effective Petri net because there is no long queue when the officer scans the ticket.

3.2 Train departure scheduling using the Kleene star algorithm

In Figure 4, the stations included in the route are as follows: PDL refers to Padalarang Station, GK to Gadobangkong Station, CMI to Cimahi Station, CMD to Cimindi Station, CIR to Ciroyom Station, BD to Bandung Station, CTH to Cikudapateuh Station, KAC to Kiaracondong Station, CMK to Cimekar Station, RCK to Rancaekek Station, HRP to Haurpugur Station, and CCL to Cicalengka Station.

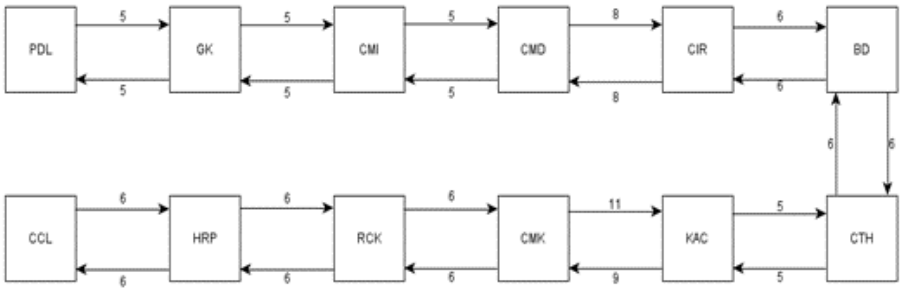

Figure 4: Graph of the Cicalengka Train Station - Padalarang Station route.

The model is based on several assumptions: there are two trains operating on the route; the travel time for each train between stations is fixed; arrival, passenger drop-off, boarding, and departure time are assumed to be zero; and each train's departure must wait for the arrival of the preceding train from the previous departure.

For example:
$x(k)$: The $k-th$ departure time of all trains
$d(k)$: Schedule of the $k-th$ departure of all trains
$x_1(k)$: The $k-th$ departure time from PDL station to GK station
$x_2(k)$: The $k-th$ departure time from GK station to CMI station
$x_3(k)$: The $k-th$ departure time from CMI station to CMD station
$\vdots$
$x_{22}(k)$: The $k-th$ departure time from GK station to PDL station.

So, from Figure 4, it can be modeled as follows :

$$\begin{aligned} x_1(k+1) &= (5 \otimes x_{22}(k)) \oplus d_1(k+1), \\ x_2(k+1) &= (5 \otimes x_1(k)) \oplus d_2(k+1), \\ x_3(k+1) &= (5 \otimes x_2(k)) \oplus d_3(k+1), \\ &\vdots \\ x_{22}(k+1) &= (5 \otimes x_{21}(k)) \oplus d_{22}(k+1). \end{aligned}$$

So, the matrix can be formed as

$$\begin{bmatrix} x_1(k+1) \\ x_2(k+1) \\ \vdots \\ x_{22}(k+1) \end{bmatrix} = \tilde{A} \otimes \begin{bmatrix} x_1(k) \\ x_2(k) \\ \vdots \\ x_{22}(k) \end{bmatrix} \oplus \vec{d}(k+1), \tag{2}$$

where

$$\tilde{A} = \begin{bmatrix}
\lambda & \lambda & \lambda & \lambda & \lambda & \lambda & \lambda & \lambda & \lambda & \lambda & \lambda & \lambda & \lambda & \lambda & \lambda & \lambda & \lambda & \lambda & \lambda & \lambda & 5 \\
5 & \lambda & \lambda & \lambda & \lambda & \lambda & \lambda & \lambda & \lambda & \lambda & \lambda & \lambda & \lambda & \lambda & \lambda & \lambda & \lambda & \lambda & \lambda & \lambda & \lambda \\
\lambda & 5 & \lambda & \lambda & \lambda & \lambda & \lambda & \lambda & \lambda & \lambda & \lambda & \lambda & \lambda & \lambda & \lambda & \lambda & \lambda & \lambda & \lambda & \lambda & \lambda \\
\lambda & \lambda & 5 & \lambda & \lambda & \lambda & \lambda & \lambda & \lambda & \lambda & \lambda & \lambda & \lambda & \lambda & \lambda & \lambda & \lambda & \lambda & \lambda & \lambda & \lambda \\
\lambda & \lambda & \lambda & 8 & \lambda & \lambda & \lambda & \lambda & \lambda & \lambda & \lambda & \lambda & \lambda & \lambda & \lambda & \lambda & \lambda & \lambda & \lambda & \lambda & \lambda \\
\lambda & \lambda & \lambda & \lambda & 6 & \lambda & \lambda & \lambda & \lambda & \lambda & \lambda & \lambda & \lambda & \lambda & \lambda & \lambda & \lambda & \lambda & \lambda & \lambda & \lambda \\
\lambda & \lambda & \lambda & \lambda & \lambda & 6 & \lambda & \lambda & \lambda & \lambda & \lambda & \lambda & \lambda & \lambda & \lambda & \lambda & \lambda & \lambda & \lambda & \lambda & \lambda \\
\lambda & \lambda & \lambda & \lambda & \lambda & \lambda & 5 & \lambda & \lambda & \lambda & \lambda & \lambda & \lambda & \lambda & \lambda & \lambda & \lambda & \lambda & \lambda & \lambda & \lambda \\
\lambda & \lambda & \lambda & \lambda & \lambda & \lambda & \lambda & 9 & \lambda & \lambda & \lambda & \lambda & \lambda & \lambda & \lambda & \lambda & \lambda & \lambda & \lambda & \lambda & \lambda \\
\lambda & \lambda & \lambda & \lambda & \lambda & \lambda & \lambda & \lambda & 6 & \lambda & \lambda & \lambda & \lambda & \lambda & \lambda & \lambda & \lambda & \lambda & \lambda & \lambda & \lambda \\
\lambda & \lambda & \lambda & \lambda & \lambda & \lambda & \lambda & \lambda & \lambda & 6 & \lambda & \lambda & \lambda & \lambda & \lambda & \lambda & \lambda & \lambda & \lambda & \lambda & \lambda \\
\lambda & \lambda & \lambda & \lambda & \lambda & \lambda & \lambda & \lambda & \lambda & \lambda & 6 & \lambda & \lambda & \lambda & \lambda & \lambda & \lambda & \lambda & \lambda & \lambda & \lambda \\
\lambda & \lambda & \lambda & \lambda & \lambda & \lambda & \lambda & \lambda & \lambda & \lambda & \lambda & 6 & \lambda & \lambda & \lambda & \lambda & \lambda & \lambda & \lambda & \lambda & \lambda \\
\lambda & \lambda & \lambda & \lambda & \lambda & \lambda & \lambda & \lambda & \lambda & \lambda & \lambda & \lambda & 6 & \lambda & \lambda & \lambda & \lambda & \lambda & \lambda & \lambda & \lambda \\
\lambda & \lambda & \lambda & \lambda & \lambda & \lambda & \lambda & \lambda & \lambda & \lambda & \lambda & \lambda & \lambda & 6 & \lambda & \lambda & \lambda & \lambda & \lambda & \lambda & \lambda \\
\lambda & \lambda & \lambda & \lambda & \lambda & \lambda & \lambda & \lambda & \lambda & \lambda & \lambda & \lambda & \lambda & \lambda & 11 & \lambda & \lambda & \lambda & \lambda & \lambda & \lambda \\
\lambda & \lambda & \lambda & \lambda & \lambda & \lambda & \lambda & \lambda & \lambda & \lambda & \lambda & \lambda & \lambda & \lambda & \lambda & 5 & \lambda & \lambda & \lambda & \lambda & \lambda \\
\lambda & \lambda & \lambda & \lambda & \lambda & \lambda & \lambda & \lambda & \lambda & \lambda & \lambda & \lambda & \lambda & \lambda & \lambda & \lambda & 6 & \lambda & \lambda & \lambda & \lambda \\
\lambda & \lambda & \lambda & \lambda & \lambda & \lambda & \lambda & \lambda & \lambda & \lambda & \lambda & \lambda & \lambda & \lambda & \lambda & \lambda & \lambda & 6 & \lambda & \lambda & \lambda \\
\lambda & \lambda & \lambda & \lambda & \lambda & \lambda & \lambda & \lambda & \lambda & \lambda & \lambda & \lambda & \lambda & \lambda & \lambda & \lambda & \lambda & \lambda & 8 & \lambda & \lambda \\
\lambda & \lambda & \lambda & \lambda & \lambda & \lambda & \lambda & \lambda & \lambda & \lambda & \lambda & \lambda & \lambda & \lambda & \lambda & \lambda & \lambda & \lambda & \lambda & 5 & \lambda \\
\lambda & \lambda & \lambda & \lambda & \lambda & \lambda & \lambda & \lambda & \lambda & \lambda & \lambda & \lambda & \lambda & \lambda & \lambda & \lambda & \lambda & \lambda & \lambda & \lambda & 5 & \lambda
\end{bmatrix}.$$

After doing calculations using Python, the eigenvalue is $\frac{68}{11} = 6.1818181818$, and the

$$\text{positive eigenvector is } \begin{bmatrix} 3.545454 \\ 2.363636 \\ 1.181818 \\ 0 \\ 1.818181 \\ 1.636363 \\ 1.454545 \\ 2.272727 \\ 3.090909 \\ 2.909090 \\ 2.727272 \\ 2.545454 \\ 2.363636 \\ 2.181818 \\ 2 \\ 6.818181 \\ 5.636363 \\ 5.454545 \\ 5.272727 \\ 7.090909 \\ 5.909090 \\ 4.727272 \end{bmatrix} = \begin{bmatrix} \frac{39}{11} \\ \frac{26}{11} \\ \frac{13}{11} \\ 0 \\ \frac{20}{11} \\ \frac{18}{11} \\ \frac{16}{11} \\ \frac{3}{11} \\ \frac{34}{11} \\ \frac{32}{11} \\ \frac{30}{11} \\ \frac{28}{11} \\ \frac{26}{11} \\ \frac{24}{11} \\ 2 \\ \frac{75}{11} \\ \frac{62}{11} \\ \frac{60}{11} \\ \frac{58}{11} \\ \frac{78}{11} \\ \frac{65}{11} \\ \frac{52}{11} \end{bmatrix} = \begin{bmatrix} 4 \\ 3 \\ 2 \\ 0 \\ 2 \\ 2 \\ 2 \\ 1 \\ 4 \\ 3 \\ 3 \\ 3 \\ 3 \\ 3 \\ 2 \\ 7 \\ 6 \\ 6 \\ 6 \\ 8 \\ 6 \\ 5 \end{bmatrix}.$$

After we got the eigenvalue and eigenvector, then the calculated train departure schedules from each station can be

$$d(k) = d(0) \otimes 6^{\otimes k} = \begin{bmatrix} v_0 + (6 \cdot \lambda) \\ v_1 + (6 \cdot \lambda) \\ \vdots \\ v_{22} + (6 \cdot \lambda) \end{bmatrix}. \tag{3}$$

Table 1 and Table 2 present the optimal departure schedules for Bandung Raya local trains at Padalarang Station and Cicalengka Station, respectively. These schedules were obtained through a mathematical optimization process aimed at minimizing delays and maximizing efficiency within the current railway operation framework. The schedules generated from this optimization model take into account various operational constraints

and objectives to ensure that train departures are well-coordinated.

Railway Station	Railway Schedule							
PDL	00.04	01.34	03.04	04.34	06.04	07.34	09.04	10.34
GD	00.10	01.40	03.10	04.40	06.10	07.40	09.10	10.40
CMI	00.16	01.46	03.16	04.46	06.16	07.46	09.16	10.46
CMD	00.21	01.51	03.21	04.51	06.21	07.51	09.21	10.51
CRM	00.30	02.00	03.30	05.00	06.30	08.00	09.30	11.00
BD	00.37	02.07	03.37	05.07	06.37	08.07	09.37	11.07
CKD	00.44	02.14	03.44	05.14	06.44	08.14	09.44	11.14
KAC	00.50	02.20	03.50	05.20	06.50	08.20	09.50	11.20
CMR	01.00	02.30	04.00	05.30	07.00	08.30	10.00	11.30
RCK	01.06	02.36	04.06	05.36	07.06	08.36	10.06	11.36
HPG	01.13	02.43	04.13	05.43	07.13	08.43	10.13	11.43
CCK	01.19	02.49	04.19	05.49	07.19	08.49	10.19	11.49
PDL	12.04	13.34	15.04	16.34	18.04	19.34	21.04	22.34
GD	12.10	13.40	15.10	16.40	18.10	19.40	21.10	22.40
CMI	12.16	13.46	15.16	16.46	18.16	19.46	21.16	22.46
CMD	12.21	13.51	15.21	16.51	18.21	19.51	21.21	22.51
CRM	12.30	14.00	15.30	17.00	18.30	20.00	21.30	23.00
BD	12.37	14.07	15.37	17.07	18.37	20.07	21.37	23.07
CKD	12.44	14.14	15.44	17.14	18.44	20.14	21.44	23.14
KAC	12.50	14.20	15.50	17.20	18.50	20.20	21.50	23.20
CMR	13.00	14.30	15.00	17.30	19.00	20.30	22.00	23.30
RCK	13.06	14.36	15.06	17.36	19.06	20.36	22.06	23.36
HPG	13.13	14.43	15.13	17.43	19.13	20.43	22.13	23.43
CCK	13.19	14.49	15.19	17.49	19.19	20.49	22.19	23.49

Table 1: The new train schedule from Padalarang to Cicalengka Station.

When compared with the existing schedules available through the KAI Access platform, the optimized results show only minor differences. This close alignment between the calculated and actual schedules indicates that the current operational departure times used by the railway operator are already functioning near an optimal level.Thus, the results validate the effectiveness of the existing train scheduling practices at both Padalarang and Cicalengka Stations.

Railway Station	Railway Schedule							
CCK	00.04	01.34	03.04	04.34	06.04	07.34	09.04	10.34
HPG	00.11	01.41	03.11	04.41	06.11	07.41	09.11	10.41
RCK	00.18	01.48	03.18	04.48	06.18	07.48	09.18	10.48
CMR	00.24	01.54	03.24	04.54	06.24	07.54	09.24	10.54
KAC	00.36	02.06	03.36	05.06	06.36	08.06	09.36	11.06
CKD	00.42	02.12	03.42	05.12	06.42	08.12	09.42	11.12
BD	00.49	02.19	03.49	05.19	06.49	08.19	09.49	11.19
CRM	00.56	02.26	03.56	05.26	06.56	08.26	09.56	11.26
CMD	01.05	02.35	04.05	05.35	07.05	08.35	10.05	11.35
CMI	01.10	02.40	04.10	05.40	07.10	08.40	10.10	11.40
GD	01.16	02.46	04.16	05.46	07.16	08.46	10.16	11.46
PDL	01.21	02.51	04.21	05.51	07.21	08.51	10.21	11.51
CCK	12.04	13.34	15.04	16.34	18.04	19.34	21.04	22.34
HPG	12.11	13.41	15.11	16.41	18.11	19.41	21.11	22.41
RCK	12.18	13.48	15.18	16.48	18.18	19.48	21.18	22.48
CMR	12.24	13.54	15.24	16.54	18.24	19.54	21.24	22.54
KAC	12.36	14.06	15.36	17.06	18.36	20.06	21.36	23.06
CKD	12.42	14.12	15.42	17.12	18.42	20.12	21.42	23.12
BD	12.49	14.19	15.49	17.19	18.49	20.19	21.49	23.19
CRM	12.56	14.26	15.56	17.26	18.56	20.26	21.56	23.26
CMD	13.05	14.35	15.05	17.35	19.05	20.35	22.05	23.35
CMI	13.10	14.40	15.10	17.40	19.10	20.40	22.10	23.40
GD	13.16	14.46	15.16	17.46	19.16	20.46	22.16	23.46
PDL	13.21	14.51	15.21	17.51	19.21	20.51	22.21	23.51

Table 2: The new train schedule from Cicalengka to Padalarang Station.

4 Discussion

The application of Petri nets in modeling the passenger entry flow at train stations provides an effective framework for visualizing and analyzing discrete event systems. In this study, the passenger process from ticket purchase to boarding was modeled using a Petri net that distinguishes between online and offline ticket buyers. Simulation results revealed congestion at the ticket scanning area, particularly due to the merging of online and offline passenger flows. By refining the Petri net to include separate scanning points, the revised model demonstrated reduced queuing, thus suggesting a more efficient station layout and process. These findings highlight the utility of Petri nets in optimizing station entry systems and guiding infrastructure improvements.

The use of the Kleene Star algorithm and Max-Plus Algebra provided a mathematical basis for calculating an optimal train departure schedule. By modeling travel time between stations using a max-plus matrix, the eigenvalues and eigenvectors were computed to determine departure intervals that minimize delays and maximize efficiency. The new

schedule, compared against real data from KAI Access, showed a high level of alignment with current operational times, reinforcing the accuracy of the model. This not only validates the Kleene Star approach but also confirms its practical potential for supporting real-world railway scheduling systems.

Furthermore, the integration of Petri nets and max-plus algebra reveals a promising interdisciplinary methodology for transport systems analysis. The Petri net effectively captures system behavior and interaction among components, while the max-plus algebra offers a structured approach for computing optimal timing. This combination enables the modeling of complex queuing behavior and time synchronization, which are critical in public transport environments. As demonstrated in the case of the Bandung Raya local train line, this approach can be tailored to other routes and regions with similar scheduling constraints and commuter behaviors.

The proposed models also offer policy implications for PT KAI and local government transportation agencies. By identifying critical points of congestion and providing data-driven departure scheduling, the methods in this study can be used to enhance commuter satisfaction and system efficiency. In particular, separating the service flow between online and offline ticket users may be a low-cost intervention with significant impact. Future work may include implementing real-time data and machine learning integration to further refine the models and adapt them dynamically based on daily traffic fluctuations or unexpected delays.

5 Conclusion

In this paper, we have used a combined modeling framework that integrates Petri nets for station entry flow and the Kleene star algorithm within max-plus algebra for train departure scheduling—an approach that, to our knowledge, has not been applied in previous studies of railway systems. The novelty also lies in the modeling of parallel online and offline ticketing flows as distinct Petri net structures, which reflect operational conditions and directly inform infrastructure improvements. Furthermore, the derived train schedule aligns with existing KAI departure data, indicating that the model is both theoretically rigorous and practically applicable. These contributions offer a new methodology for optimizing discrete-event transportation systems within the field of nonlinear dynamics.

Acknowledgment

This study is supported by Riset Kompetensi Dosen Unpad (RKDU) with the contract number 1549/UN6.3.1/PT.00/2023, and we also acknowledge the Academic Leadership Grant (ALG) Scheme of Padjadjaran University for the completion of the manuscript with the contract number 1418/UN6.3.1/PT.00/2024.

References

[1] Y. Lei and H. Mu. Analysis and optimization of a stochastic Petri net for air–rail intermodal transportation. *PLOS One* **19** (7) (2024) e0307647.

[2] I. Kabashkin and Z. Sansyzbayeva. Methodological framework for sustainable transport corridor modeling using Petri nets. *Sustainability* **16** (2) (2024) 489.

[3] A. Boukoftane, M. A. Kalwar, N. Oukid, K. Zennir, M. S. Memon and M. A. Khan. Application of discrete event simulation and system dynamics modeling in optimizing the perfor-

mance of outpatient department. *Nonlinear Dynamics and Systems Theory* **24** (4) (2024) 354–365.

[4] A. Chahad, M. Bassoudi and Z. C. Elmezouar. Spectral density estimation in time series analysis for dynamical systems. *Nonlinear Dynamics and Systems Theory* **25** (2) (2025) 128–143.

[5] A. Sambas, X. Zhang, I. A. Moghrabi, S. Vaidyanathan, K. Benkouider, M. Alçın, M. Tuna and M. D. Johansyah. ANN-based chaotic PRNG in the novel jerk chaotic system and its application for image encryption via 2-D Hilbert curve. *Scientific Reports* **14** (1) (2024) 29602.

[6] A. Sambas, M. Miroslav, S. Vaidyanathan, B. Ovilla-Martínez, E. Tlelo-Cuautle, A. A. Abd El-Latif and T. Bonny. A new hyperjerk system with a half line equilibrium: multistability, period-doubling reversals, antimonotonicity, electronic circuit, FPGA design, and an application to image encryption. *IEEE Access* **12** (2024) 9177–9194.

[7] S. Gaubert and S. Sergeev. The level set method for the two-sided max-plus eigenproblem. *Discrete Event Dynamic Systems* **23** (2) (2013) 105–134.

[8] M. Umer, U. Hayat, F. Abbas, A. Agarwal and P. Kitanov. An efficient algorithm for eigenvalue problem of Latin squares in a bipartite min-max-plus system. *Symmetry* **12** (2) (2020) 311.

[9] N. Gkonou, E. Nisyrios and K. Gkiotsalitis. Combined optimization of maintenance works and crews in railway networks. *Applied Sciences* **13** (18) (2023) 10503.

[10] M. Raji, J. Duggan, B. DeCotes, J. Huang and B. Vander Zanden. Modeling and visualizing student flow. *IEEE Transactions on Big Data* **7** (3) (2018) 510–523.

[11] F. Azizah and S. Subiono. Max-plus algebra and Petri net application on scheduling of ship engine component's spare part ordering. *International Journal of Computing Science and Applied Mathematics* **4** (1) (2018) 1–9.

[12] T. Gonsalves and K. Itoh. Service optimization with patient satisfaction in healthcare systems. *Journal of Simulation* **3** (3) (2009) 150–162.

[13] H. Orojloo and M. A. Azgomi. Modelling and evaluation of the security of cyber-physical systems using stochastic Petri nets. *IET Cyber-Physical Systems: Theory & Applications* **4** (1) (2019) 50–57.

[14] M. Nakamura, K. Kaneshima and T. Yoshida. Petri net modeling for Ising model formulation in quantum annealing. *Applied Sciences* **11** (16) (2021) 7574.

[15] Y. Yang, J. Yang, N. Liang and C. Zhong. Control law for two-process flexible manufacturing systems modeled using Petri nets. *Mathematics* **13** (4) (2025) 611.

Nonlinear Dynamics and Systems Theory, **26** (1) (2026) 14–28

Analysis of Novel Smart MPPT Approaches Based on M5-Pruned and REPTree Algorithms for Photovoltaic Systems

Z. Ettahri [1], M. Zegrar [1], A. Moualdia [2*] and F. Z. Zerhouni [1]

[1] *Microsystems and Embedded Systems Laboratory (LMSE), Department of Electronics, University of Sciences and Technology of Oran Mohamed BOUDIAf (USTO-MB), Oran, Algeria.*

[2] *Research Laboratory of Electrical Engineering & Automatic (LREA), Department of Electrical Engineering University of Medea, Medea, Algeria.*

Received: September 21, 2025; Revised: February 15, 2026

Abstract: This paper presents three novel smart MPPT methods that combine a decision tree with a modified incremental conductance and a perturb-and-observe technique to improve the efficiency of solar photovoltaic systems while reducing power ripples in both the photovoltaic system and the associated boost converter during fluctuations in the weather, especially changes in solar irradiation and temperature. Initially, we constructed a mathematical model for solar panels. Subsequently, we developed three innovative smart MPPT techniques utilizing M5-Pruned and REP-Tree through Weka software, conducted simulations by using MATLAB/SIMULINK, and compared the outcomes with those derived from modified incremental conductance (MINC) and perturb and observe (P&O) MPPT approaches. The simulation results under various conditions indicated that the three innovative smart methods, which utilize M5-Pruned and REPTree, effectively track the maximum power point (MPPT), reduce power ripples in photovoltaic systems and the output ripple of the associated boost converter to it, and enhance the efficiency of solar systems compared to MINC and P&O. Novel approaches exhibit efficiency above 99.77% in comparison to MINC and P&O methods, with an efficiency of 98.88% and 98.83%, respectively. These methods exemplify robust artificial intelligence algorithms for maximum power point tracking (MPPT) due to their efficacy, simplicity in learning and design, and low complexity.

Keywords: *photovoltaic panel; boost converter; modified incremental conductance; M5-Pruned; REPTree.*

Mathematics Subject Classification (2020): 03B52, 93C42, 94D05.

* Corresponding author: mailto:amoualdia@gmail.com

© 2026 InforMath Publishing Group/1562-8353 (print)/1813-7385 (online)/http://e-ndst.kiev.ua

List of Abbreviations

MPPT	Maximum Power Point Tracking
MINC	Modified Incremental Conductance
P&O	Perturb and Observe
PV	Photovoltaic
M5P	M5-Pruned
REPTree	Reduced Error Pruning Tree
PSO	Particle Swarm Optimization
FLC	Fuzzy Logic Control
ACO	Ant Colony Optimization
ANN	Artificial Neural Network
ANFIS	Adaptive Neuro-Fuzzy Inference System
CS	Cuckoo Search
ABC	Artificial Bee Colony
GWO-INC	Grey Wolf Optimization – Incremental Conductance
PSO-INC	Particle Swarm Optimization – Incremental Conductance
GWO-P&O	Grey Wolf Optimization – Perturb and Observe
INC	Incremental Conductance
HC	Hill Climbing
FOCV	Fractional Open Circuit Voltage
FSCC	Fractional Short Circuit Current
VSSP&O	Improved Variable Step Size Perturb and Observe
THD	Total Harmonic Distortion
M5P-MINC	M5-Pruned – Modified Incremental Conductance
DC–DC	Direct Current to Direct Current

1 Introduction

The photovoltaic solar system is a complicated nonlinear dynamical system, with its output exhibiting nonlinear behavior greatly influenced by external factors such as irradiance levels (G) and temperature (T), as illustrated in Figures 3-4 and equation 1. This nonlinearity engenders a complex, frequently multimodal, non-convex power surface, particularly under partial shade, while the rapidly fluctuating levels of solar irradiation and temperature pose a substantial control and tracking issue within the context of systems theory. Selecting the ideal Maximum Power Point Tracking (MPPT) controller is essential for optimizing power extraction and reducing power loss from the solar panel to DC-DC converters. The MPPT technique's effectiveness is evaluated based on its ability to maintain stability, withstand parametric uncertainty, and achieve rapid convergence — all essential criteria in nonlinear control theory.

Thus, the execution of artificial intelligence (AI) in this field is essential, as conventional MPPT methods often fail to efficiently handle the complex dynamic landscape of the PV system. Papers [1–6] delineate various strategies of AI-based MPPT for optimizing power extraction under both uniform irradiation and partial shading conditions. These methods include the Particle Swarm Optimization (PSO) algorithm, Fuzzy Logic Control (FLC), Ant Colony Optimization (ACO), ANN algorithm [1], Adaptive Neuro-Fuzzy Inference System (ANFIS) algorithm [2], Cuckoo Search Colony (ABC) [3], the Grey Wolf Optimization and Incremental Conductance-Based Hybrid MPPT method

(GWO-INC) [4], Hybrid PSO-INC MPPT [5], GWO-P&O algorithm, and other methods based on M5-Purbed [6].

These methods efficiently extract MPPT and minimize power loss during the adaptation phase, however, they are complex and costly to design and implement in practice. Consequently, this has led to enhancements in certain conventional techniques such as the Perturb and Observe (P&O) method, the Incremental Conductance (INC), and Hill Climbing (HC), which are commonly used. Techniques such as Fractional Open Circuit Voltage (FOCV) [8] and Fractional Short Circuit Current (FSCC), and improved Variable Step Size Perturb and Observe (VSSP&O) and modified incremental conductance [9] are used for their simplicity and efficiency in extracting the MPPT under different conditions. Abdelkhalek Chellakhi and his team [9] proposed a unique upgraded Perturb and Observe (P&O) algorithm that integrates an adjustable step-size mechanism, which was implemented using an Arduino board. The new method demonstrates superior performance compared to PSO, FLC, ZV, and traditional P&O algorithms.

M. Sacid Endiz [20] exhibited the effectiveness of the modified incremental conductance method for MPPT extraction using both simulation and empirical findings. The suggested incremental conductance method more accurately identifies the maximum power point and provides optimal power for battery charging under fluctuating solar irradiation conditions, unlike the traditional incremental conductance method. The proposed system can function as a charging infrastructure solution for low-powered electric devices. A. Bouhouta and his team [10] developed a mixed control strategy using pruned model tree (M5P) and fuzzy logic controller datasets. The system effectively detects harmonic currents in active power filter systems, achieving a power factor of 0.99, a minimal THD of 3.07%, and a rapid response time of 100 ms. see [6, 10, 11, 16]. We have conducted extensive research on decision tree-based approaches. We have noticed that these approaches give better results than other methods, and display efficiency across various sectors including electrical, biomedical, and photovoltaic systems, wind energy, agronomy, and the identification of DDoS attacks in software-defined networks. Remaining with this aim to enhance the maximum power point tracking system (Figure 1), we proposed three unique mixed control strategies employing the pruned model tree (M5P), REPTree, and collected datasets from a modified incremental conductance controller and perturb and observe methods.

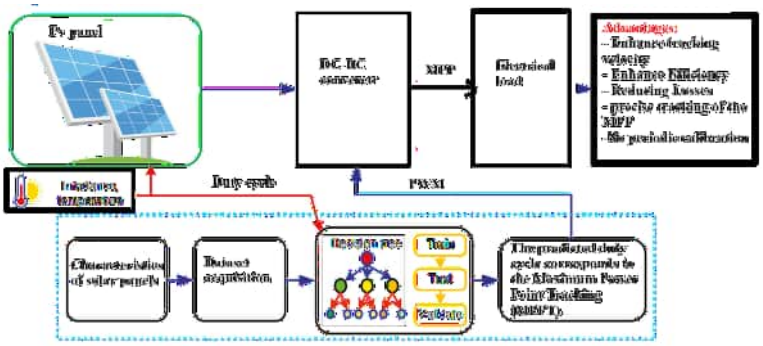

Figure 1: PV panel connected with MPPT [9].

The first approach is M5P-MINC, the second is M5P-P&O, and the third is REPTree-

MINC. This combination aims to leverage the rapid decision-making capabilities of decision trees in conjunction with the advantages of the modified incremental conductance and perturb and observe methods in fluctuating weather conditions such as rapid variations in solar irradiance and temperature. The simulation using MATLAB/SIMULINK under various dynamic settings demonstrated the effectiveness of this combination.

This paper is structured as follows. Section 2 offers a comprehensive explanation of the modeling of the photovoltaic panel and boost converter, whereas Section 3 delineates the proposed methodologies. Section 4 subsequently shows the simulation findings. In conclusion, Section 5 finalizes the paper.

2 Pv Panel, Boost Converter Modelling

2.1 Pv panel modelling

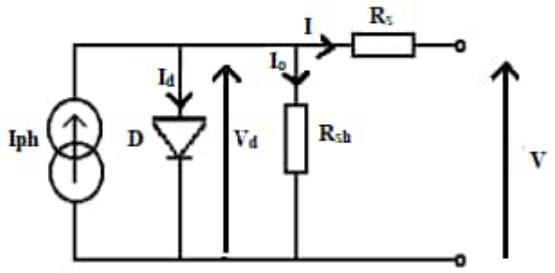

Figure 2: Equivalent electrical circuit to a photovoltaic cell [21].

A solar photovoltaic panel comprises several cells linked in series, parallel, or mixed. Each cell (panel) can be shown by an equivalent circuit, see Figure 2, which consists of a current source (Iph), a single diode (D), a series resistance (Rs), and a parallel resistance (Rp). The correlation between voltage V and current I in a solar cell is articulated by the equation (1):

$$I = I_{ph} - I_0 \left[\exp\left(\frac{V + R_s \cdot I}{U_T \cdot A} \right) - 1 \right] - \frac{V + R_s \cdot I}{R_{sh}}. \tag{1}$$

UT signifies the thermal voltage of the panel, whereas A indicates the diode ideality index. Figures 3-4 illustrate the distinct characteristic P-V and I-V curves of the solar panel utilized in this study.

2.2 DC-DC boost converter

The employed DC-DC converter is a boost converter. The principal function is to modify the voltage or current levels from an input source to a specified output. This type of switched-mode power supply has two semiconductor components (transistors and diodes) in conjunction with an energy storage element. To ensure a more stable voltage, it is customary to incorporate capacitor-based filters at the input and output terminals of the converter. Figure 5 illustrates the fundamental architecture of the boost converter. The output voltage is elevated with respect to the input voltage. The input power (P_{in})

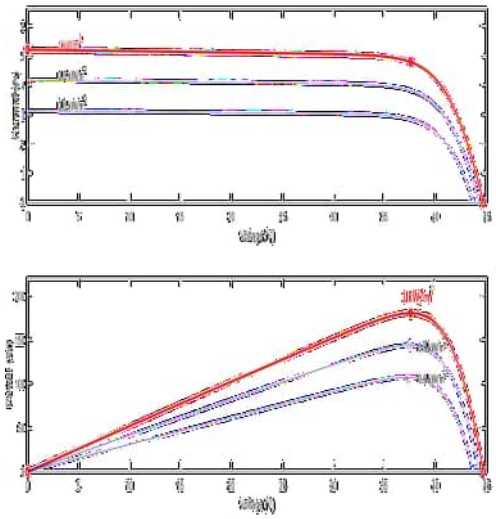

Figure 3: P-V and I-V curves with T constant and G variable.

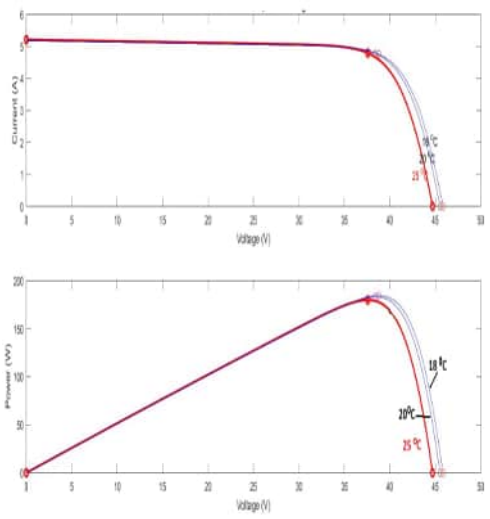

Figure 4: P-V and I-V curves when T is variable and G is fixed.

and output power (P_{out}) are commensurate in accordance with the principle of energy conservation [17],

$$P_{in} = P_{out}. \tag{2}$$

The relation between the input and output voltage is represented by

$$V_{out} = \frac{V}{1-\alpha}, \tag{3}$$

where V_{out} and V represent the output voltage and input voltage, respectively, while α represents the duty cycle.

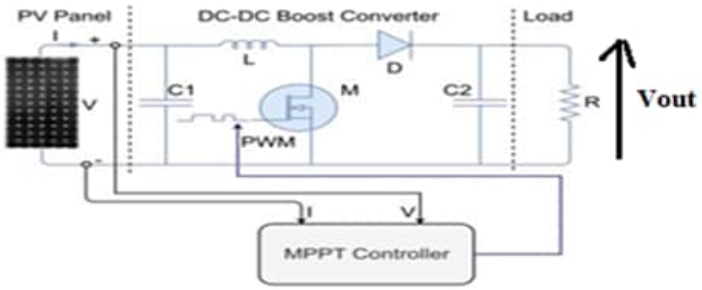

Figure 5: Electrical circuit of boost converter [18].

3 MPPT Approaches

3.1 M5P decision tree

Decision tree algorithms are regarded as the most robust and effective supervised machine learning methods in control applications. Its swift modelling techniques are useful across several engineering domains for regression and classification objectives. DT employs a statistical methodology to classify input data, referred to as "attributes", into several segments via a tree structure. Pruned M5 (M5P) is an improved variant of the M5 tree [19]. The pruned M5P model tree algorithm partitions training data into subsets, combining traditional model trees with linear regression, resulting in intuitive, comprehensible, and interpretable tree models for accurate class label prediction. R. Quinlan [10] improved the original M5 model by creating an extended version that facilitates tree generation without requiring alterations to system parameters or domain expertise. Numerous studies indicate that the M5P approach is remarkably stable and achieves prediction accuracy akin to that of an artificial neural network (ANN) when utilizing identical data sets. The integration of fuzzy logic with decision tree algorithms can yield improved efficiency.

3.2 REPTree decision tree

REPTree generates several trees across various iterations employing the regression tree framework. The REPTree function constructs a decision tree using a specified data set. It is considered an extension of C45 because it employs Reduced Error Pruning (REP) to improve the pruning process. The C4.5 algorithm is a proficient decision tree learner that generates classification trees for discrete results and regression trees for continuous results. Reduced-error pruning, which includes backfitting, is utilized to determine the requisite pruning cuts following the development of a regression or decision tree utilizing information gain or variance.

3.3 Description of MPPT methods

3.3.1 Perturb and Observe MPPT method

This is the primary method employed in commercial applications. P&O is the favored choice for most practical photovoltaic systems because of their remarkable reliability, simplicity, and efficiency. The process is essentially one of experimentation and correction. This method depends on determining the power output of the photovoltaic (PV) system and the fluctuations in power by quantifying the current and voltage of the photovoltaic array. It functions by adjusting the PV array voltage upward or downward. Assume that a specific disturbance causes a fluctuation in PV power levels. The duty ratio of the boost converter is continually modified and repeated until the MPPT is achieved. A subsequent disturbance should be produced in a comparable or contrasting manner. The oscillations can be diminished by decreasing the intensity of the perturbation step. However, the principal disadvantage of this approach is its effect on the speed of the MPP tracking in smaller increments while the system functions at peak power [8], for a simple implementation, see Figure 6.

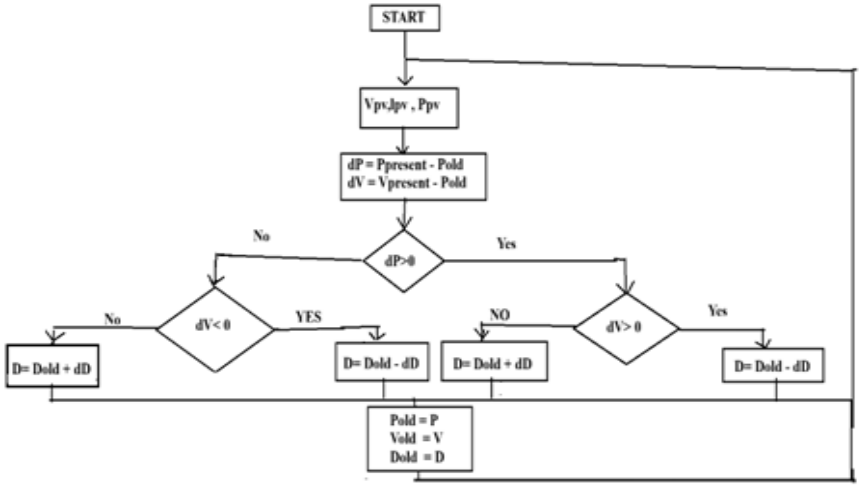

Figure 6: Flowchart of P&O algorithm.

3.3.2 Modified Incremental Conductance (MINC)

The Modified Incremental Conductance technique (MINC) provides enhanced tracking efficiency and usability compared to traditional Incremental Conductance (INC). It employs an optimized computational method to calculate the sum of 'I/V' and 'dI/dV' values to sustain the solar module at the Maximum Power Point (MPP). The MINC employs fewer decision blocks and reduced code, leading to improved algorithm efficacy [19].

3.3.3 Smart MPPT proposed

A distinctive combination of decision trees, M5P and REPTree, together with modified incremental conductance (MINC) and perturb and observe (P&O) methods, is proposed for maximum power point tracking (MPPT). The first method, M5P-MINC, the second, REPTree-MINC, and the third, M5P-P&O, demonstrate swift and dependable tracking skills. The suggested non-parametric MPPT model is developed using input and output data derived from MINC and P&O MPPT approaches. A dataset has been methodically created for the MINC and P&O techniques, leveraging simulated data collected over 100 milliseconds. The chosen MINC and P&O input and output characteristics pertain to the voltage of the solar panel (Vpv), the current of the photovoltaic panel (Ipv), and the outputs of MINC and P&O, which represent the duty cycle, are enumerated accordingly. A data set of 100,000 samples is employed to develop the proposed M5P and REPTree model-tree-based MPPT, with 66% allocated for training and the remaining portion for testing. Figure 8 succinctly illustrates the data acquisition and training methodologies. Figure 9 delineates a comprehensive analysis of data flow, incorporating WEKA and simulation specifics, and elucidates the principal phases in the formulation of three proposed methodologies.

1. Data collection: The initial phase entails gathering data from the solar panel's Vpv and Ipv voltage sensors, along with the modifier incremental conductance controller

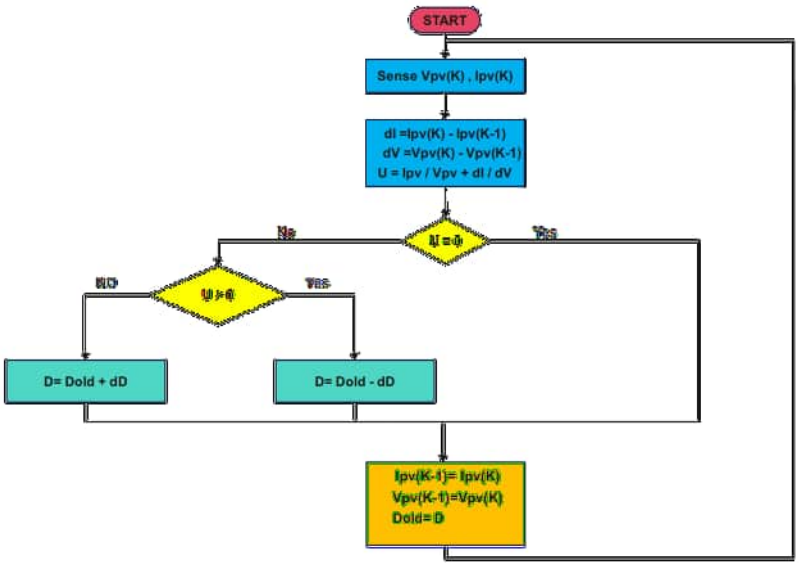

Figure 7: Flow chart of modified incremental conductance.

(MINC) and perturb and observe (P&O), to acquire accurate readings for analysis and regulation.

2. Preprocessing: The step encompasses normalization, data imputation, or filtering approaches to ensure data is organized and prepared for feature extraction and modelling, removing noise, and missing values.

3. Feature extraction (WEKA): During this step, WEKA, a machine learning tool, is utilised to extract some of the pertinent features from the previously processed data. This process entails the selection or modification of the most pertinent variables for the development of the M5-Pruned and REPTree models. This step seeks to diminish data dimensionality and concentrate on critical inputs that affect the system's performance.

4. M5-Pruned and REPTree model training (WEKA): WEKA employs the extracted features to train the M5-Pruned and REPTree algorithms. These methods create a decision tree, where the leaves represent linear regression models that forecast output variables. The predictive model enables immediate decision-making within the control system.

4 Results and Discussion

Figure 13 depicts the model employed for simulation. This system has five solar panels (Zytech 180s type), linked with boost converters that are controlled by various MPPT algorithms. Figure 14 illustrates the multiple conditions implemented for the validation and assessment of the efficacy of the proposed approaches. The simulation duration

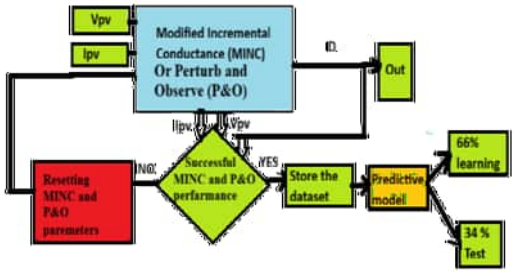

Figure 8: Dataset extraction methodology via MINC and P&O.

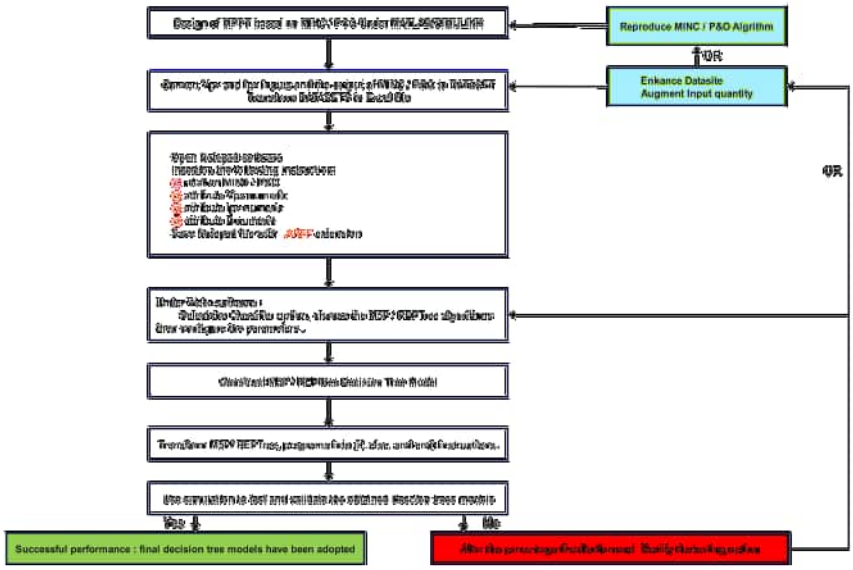

Figure 9: Dataset management process.

in this study was set at 100 milliseconds (ms). During the interval from 0 ms to 30 ms, the temperature and solar irradiation levels are 20◦ and 800 W m^{-2}, respectively. In the subsequent interval from 30 ms to 40 ms, the temperature and solar irradiation decline to 18◦ and 600 W m^{-2}, respectively. Subsequently, between 40 ms and 53 ms, the temperature and solar irradiation levels are recorded at 18◦ and 600 W m^{-2}, respectively. During the ensuing interval from 53 ms to 70 ms, these levels rise to 25◦ and 1000 W m^{-2}, respectively. In the span of 70 ms to 100 ms, the temperature is 25◦ and the solar irradiation is 1000 W m^{-2}.

Figures 15 and 16 depict the simulation outcomes for the power delivered by the solar photovoltaic system and the output power of the boost converter linked to the photovoltaic panel (Pload), regulated by various MPPT methodologies, all inside the simulation framework. Table 4 presents a summary of these findings.

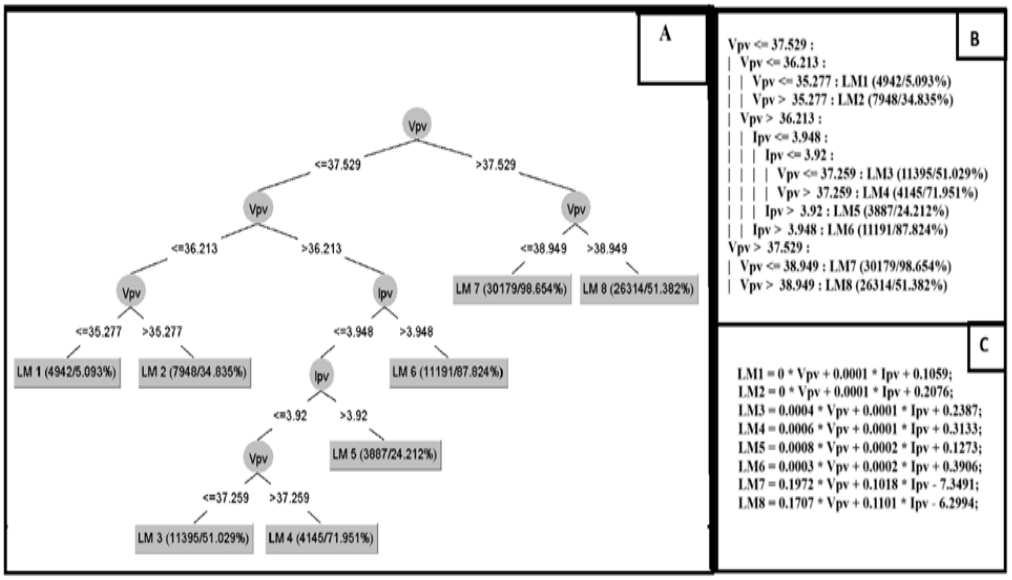

Figure 10: Results of Training Process of M5P-MINC Control via WEKA Software. (A) : Prunted flowchart of the M5P-MINC Decision Tree. (B): Predictive Rules of Decision Tree. (C): Attribute Target Weights.

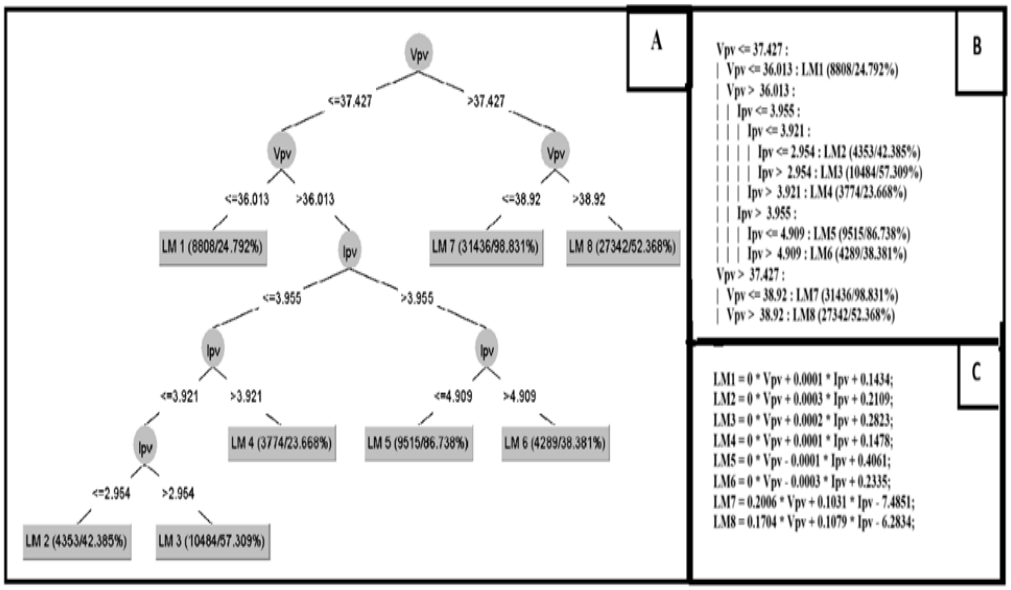

Figure 11: Results of Training Process of M5P-P&O Control via WEKA Software. (A) : Prunted flowchart of the M5P-P&O Decision Tree. (B): Predictive Rules of Decision Tree. (C): Attribute Target Weights.

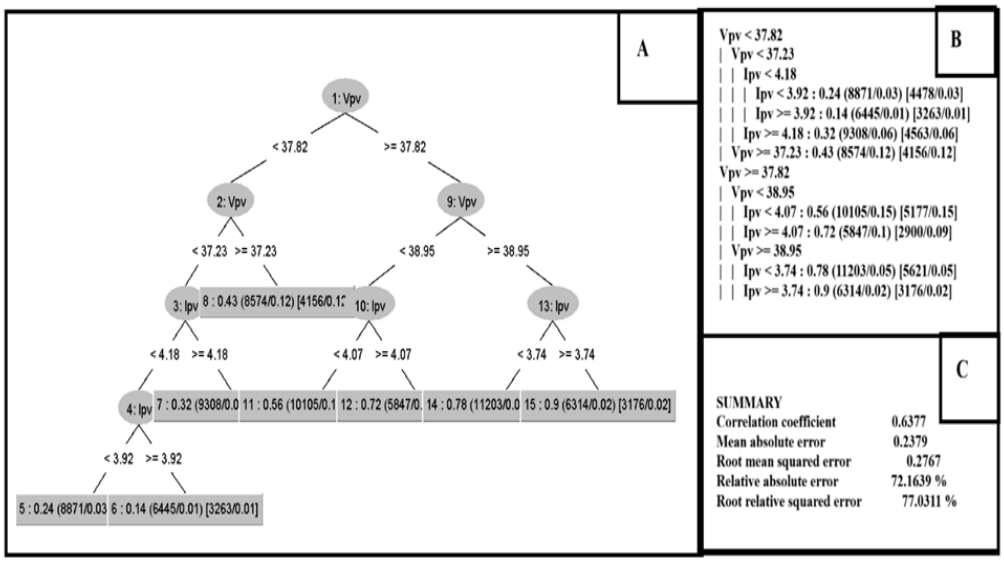

Figure 12: Results of Training Process of REPTree-MINC Control via WEKA Software. (A) : Prunted flowchart of the REPTree-MINC Decision Tree. (B): Predictive Rules of Decision Tree. (C): Summary of Process.

The effectiveness of the innovative methods, which combine decision tree (DT) algorithms with modified incremental conductance and perturb and observe, was evaluated under variable weather circumstances. The initial method is M5P-MINC, the subsequent method is REPTree-MINC, and the final method is M5P-P&O. These methods are compared to the MINC and P&O methods. The assessment focused on the accuracy of MPPT tracking, the speed of tracking to MPPT, and the power ripples of both the PV panel and the Pload, in addition to the overall conversion efficiency and the efficiency of MPPT, utilizing MATLAB/SIMULINK.

All evaluated methods effectively extract the MPP and demonstrate swift convergence to the MPPT under various fluctuation conditions. However, as concerning the reduction of the ripple of power for photovoltaic systems and the output ripple of the boost converter linked to the photovoltaic system, the proposed smart algorithms attain minimal ripple levels in contrast to the modified incremental conductance and perturb and observe approaches, which exhibit elevated ripples. The proposed methods demonstrate superior efficiency in the tracking of the maximum power point compared to MINC and P&O, achieving an efficiency exceeding 99.77% versus to 98.88% and 98.83% for MINC and P&O, respectively. Furthermore, the overall conversion efficiency surpasses 88.3% for smart approaches, in contrast to that of MINC and P&O, which is equal to 85.61% and 85.72%, respectively, while the proposed approaches exhibit reduced computational complexity.

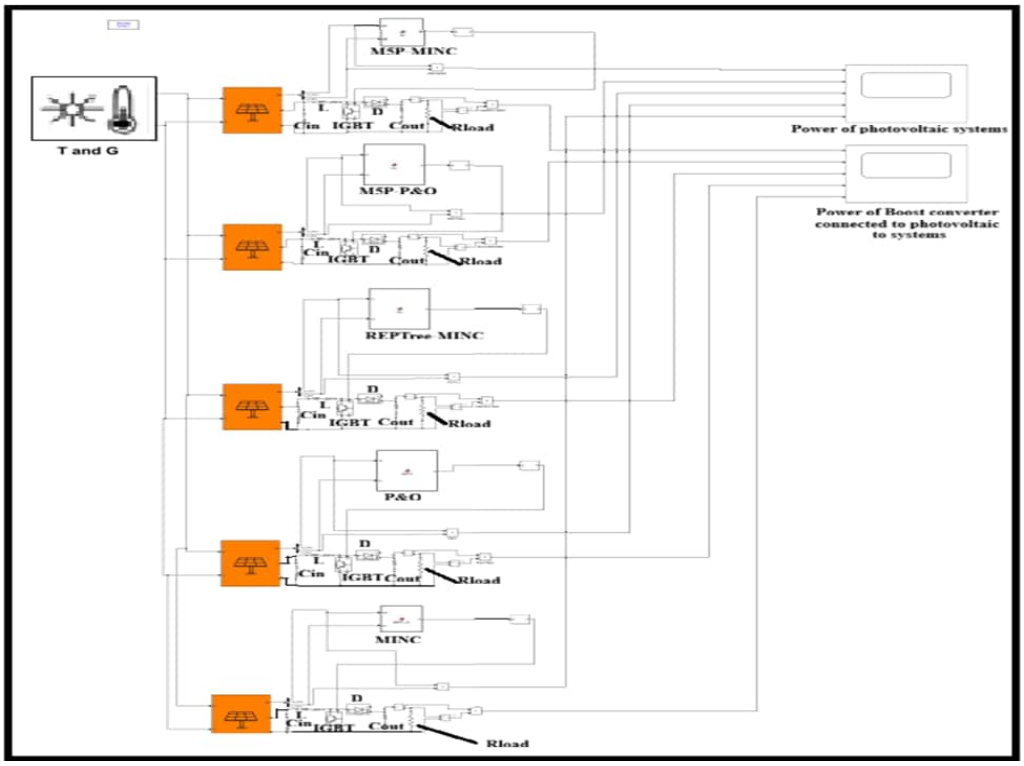

Figure 13: Simulation Model.

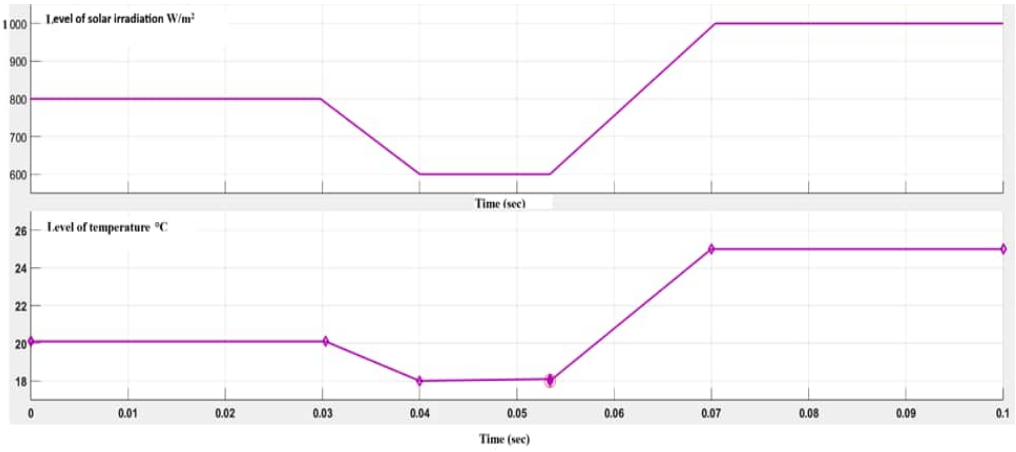

Figure 14: The variation of temperature and solar irradiation over time.

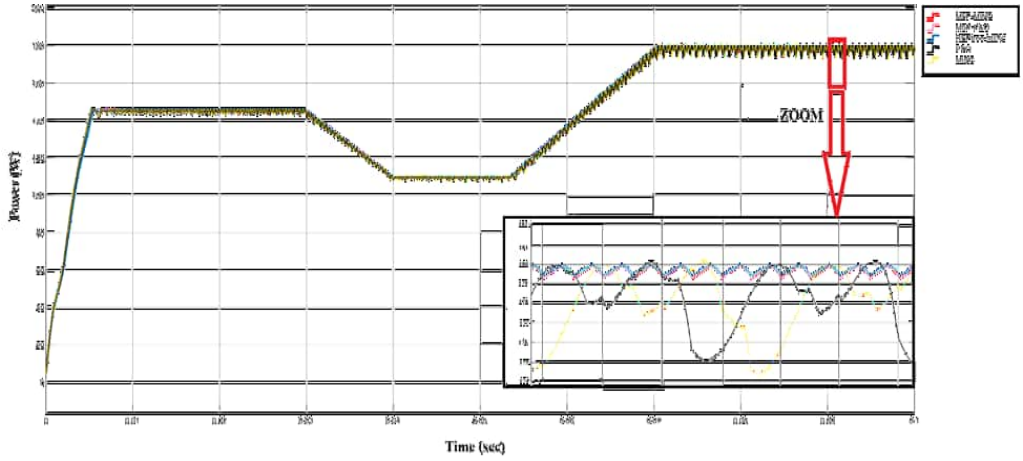

Figure 15: The simulation outcomes for the power delivered by Photovoltaic panel by using the various MPPT approaches.

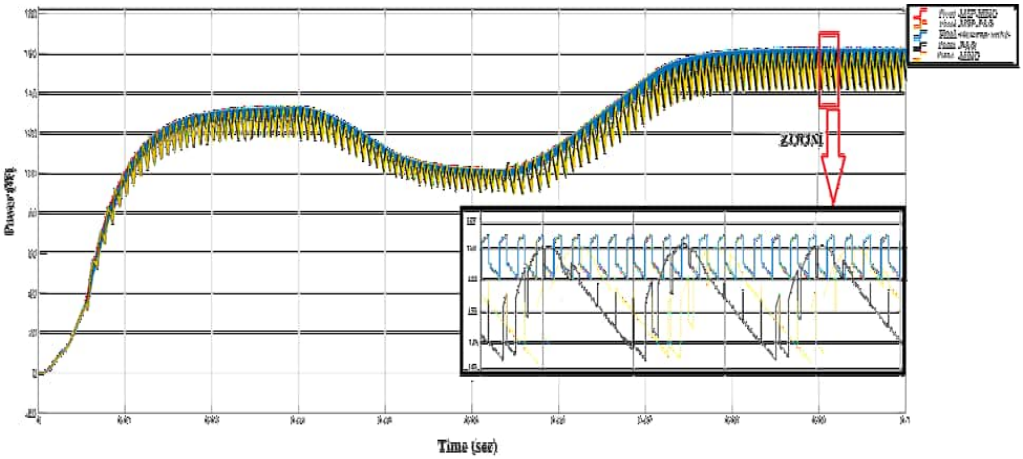

Figure 16: The simulation outcomes for the power of the boost converter connected to the Photovoltaic panel by using the various MPPT approaches.

	Tracking of MPPT	Fast of conversion to MPPT	Ripple of power of PV panel	Ripple of output Boost	Efficiency of tracking MPPT $\left(\frac{P_{simulation}}{P_{theorique}}\right)$	Complexity	Efficiency of conversion $\left(\frac{P_{out}}{P_{pv}}\right)$
MINC	YES	HIGH	HIGH (3.68%)	HIGH (12.51%)	98.88%	LOW	Medium (85.61%)
P&O	YES	HIGH	HIGH (3.63%)	HIGH (12.48%)	98.83%	LOW	Medium (85.72%)
M5P-MINC	YES	HIGH	Small (0.39%)	Small (4.36%)	99.77%	LOW	HIGH (88.3%)
M5P-P&O	YES	HIGH	Small (0.40%)	Small (4.37%)	99.77%	LOW	HIGH (88.3%)
REPTree-MINC	YES	HIGH	Small (0.33%)	Small (4.37%)	99.83%	LOW	HIGH (88.31%)

Table 1: The Simulation Results.

5 Conclusion

This paper evaluates three distinct artificial intelligence-based maximum power point tracking (MPPT) methods that combine a modified incremental conductance (MINC)

and perturb and observe (P&O) strategies with M5-Pruned (M5P) and REPTree decision tree techniques. The effectiveness of the proposed techniques was assessed in various dynamic conditions, specifically with variations in temperature and solar radiation levels. The aim is to evaluate the suggested M5P-MINC, REPTree-MINC, and M5P-P&O methodologies against the MINC and P&O methods. Comparative simulations were performed. The main factors for comparison included MPPT efficiency, convergence speed, power ripple reduction in the photovoltaic (PV) system and its corresponding boost converter, as well as the overall conversion efficiency. All assessed approaches efficiently extract the MPP and exhibit rapid convergence to the MPPT over diverse fluctuation situations. However, in terms of the attenuation of power ripple in photovoltaic systems and the output ripple of the boost converter associated with the solar system, the suggested smart algorithms achieve minimal ripple levels compared to the modified incremental conductance and perturb and observe methods, which display higher ripples. The proposed methods exhibit greater efficiency in maximum power point tracking than MINC and P&O, attaining an efficiency of over 99.77% compared to 98.88% and 98.83% for MINC and P&O, respectively. The overall conversion efficiency surpasses 88.3% for the proposed smart approaches, whereas that of MINC and P&O is 85.61% and 85.72%, respectively. The proposed methods exhibit reduced computational complexity. Our findings indicate that the proposed strategies are efficacious for MPPT and ripple reduction in solar systems. These methodologies provide a pragmatic and efficient AI-driven solution, enabling seamless data collection, adaptive system learning, and real-time implementation with little cost.

Acknowledgment

This research is supported by the General Directorate for Scientific Research and Technological Development (DGRSDT).

References

[1] M. T. Hussain, A. Sarwar, M. Tariq, S. Urooj, A. BaQais and M. A. Hossain. an evaluation of ANN algorithm performance for MPPT energy harvesting in solar PV systems, *Sustainability* **15** (14) (2023) 11–144. doi:10.3390/su151411144.

[2] S. Kumar, R. Raunak Jangid and K. Parikh. Comparative performance analysis of ANFIS & ANN algorithms based MPPT energy harvesting in solar PV system. *Int. J. Tech. Res. Sci.* **8** (3) (2023) 1–8. doi:10.30780/ijtrs.v08.i03.001.

[3] C. Gonzalez-Castano, C. Restrepo, S. Kouro and J. Rodriguez. MPPT algorithm based on Artificial Bee Colony for PV system. *IEEE Access* **9** (2021) 43121–43133. doi:10.1109/ACCESS.2021.3066281.

[4] D. Shetty and J. N. Sabhahit. Grey wolf optimization and incremental conductance based hybrid MPPT technique for solar powered induction motor driven water pump. *Int. J. Renew. Energy Dev.* **13** (1) (2024) 52–61. doi:10.14710/ijred.2024.57096.

[5] A. M. Leopoldino, C. M. Freitas, and L. C. Monteiro. Analysis of the hybrid PSO-InC MPPT for different partial shading conditions. *Adv. Electr. Comput. Eng.* **22** (2) (2022) 29–36. doi:10.4316/AECE.2022.02004.

[6] S. A. Blaifi, S. Moulahoum, R. Benkercha, B. Taghezouit and A. Saim. M5P model tree based fast fuzzy maximum power point tracker. *Solar Energy* **163** (2018) 405–424. doi:10.1016/j.solener.2018.01.071.

[7] A. Ali, et al. Investigation of MPPT techniques under uniform and non-uniform solar irradiation condition – A retrospection. *IEEE Access* **8** (2020) 127368–127392. doi:10.1109/ACCESS.2020.3007710.

[8] N. Ishaq, F. Altaf, Z. A. Afridi and N. Arbab. Performance analysis of Perturb and Observe and open circuit voltage algorithms for MPPT tracking at different environmental conditions.*Int. J. Eng. Work.*, **8** (4) (2021) 143–148. doi:10.34259/ijew.21.804143148.

[9] A. Chellakhi, S. El Beid, M. El Marghichi, E. M. Bouabdalli, A. Harrison and H. Abouobaida. Implementation of a low-cost current perturbation-based improved P and O MPPT approach using Arduino board for photovoltaic systems. *e-Prime – Advances in Electrical Engineering, Electronics and Energy* **10** (2024) 100807. doi:10.1016/j.prime.2024.100807.

[10] A. Bouhouta, S. Moulahoum and N. Kabache. Efficient learning approach using new combined fuzzy-M5P model tree: experimental investigation of active power filters. *J. Power Electron.* **22** (2022) 981–990. doi:10.1007/s43236-022-00434-w.

[11] A. F. Kasse, N. Kabeche and S. Moulahoum. Separate integration of solar PVs into the low-voltage DC link of a solid-state transformer based on a modular multilevel converter. *Rev. Roum. Sci. Tech. Ser. Electrotech. Energ.* **70** (1) (2025) 33–38. doi:10.59277/RRST-EE.2025.1.6.

[12] S. Boulkhrachef, A. Moualdia, Dj. Boudana and P. Wira. Higher-order sliding mode control of a wind energy conversion system. *Nonlinear Dynamics and System Theory* **19** (4) (2019) 486–496.

[13] T. Djellouli, S. Moulahoum, A. Moualdia, M. S. Bouchrit and P. Wira. Speed Sensorless Direct Torque Control Strategy of a Doubly Fed Induction Motor Using an ANN and an EKF. *Nonlinear Dynamics and System Theory* **20**(4) (2020) 374–387.

[14] Y. Chedni, D.J. Boudana, A. Moualdia, L. Nezli and P. Wira. Sensorless Two Series Connected Quasi Six-Phase IM Based Direct Torque Control for Torque Ripples Minimization. *Nonlinear Dynamics and System Theory* **20** (2) (2020) 153–167.

[15] H. Mujammal Ahmed, A. Moualdia, Dj. Boudana, P. Wira and A. Cherifi. Implementation of smart direct power control strategy based on M5-Pruned algorithm for three-phase pulse width modulation rectifier.*Energy* **315**(2025) 134417.doi:10.1016/j.energy.2025.134417

[16] T. Tundo and S. Uyun. Perbandingan Decision Tree J48, REPTREE, dan Random Tree dalam menentukan prediksi produksi minyak kelapa sawit menggunakan Fuzzy Tsukamoto. *J. Teknol. Inf. dan Ilmu Komput.* **8** (3) (2021) 473. doi:10.25126/jtiik.2021833108.

[17] J. Mishra, S. Das, D. Kumar and M. Pattnaik. A novel auto-tuned adaptive frequency and adaptive step-size incremental conductance MPPT algorithm for photovoltaic system. *Int. Trans. Electr. Energy Syst.* **31** (10) (2021) 1–14. doi:10.1002/2050-7038.12813.

[18] D. Ounnas, D. Guiza, Y. Soufi and M. Maamri. Design and hardware implementation of modified incremental conductance algorithm for photovoltaic system.*Adv. Electr. Electron. Eng.* **19**(2) (2021) 100–111. doi:10.15598/aeee.v19i2.3881.

[19] A. Bouhouta, S. Moulahoum, and N. Kabache. A novel combined fuzzy-M5P model tree control applied to grid-tied PV system with power quality consideration. *Energy Sources, Part A: Recovery, Utilization and Environmental Effects* **44** (2) (2022) 3125–3147. doi:10.1080/15567036.2022.2060380.

[20] M. S. Endiz. Design and implementation of microcontroller-based solar charge controller using modified incremental conductance MPPT algorithm. *J. Radiat. Res. Appl. Sci.* **17** (2) (2024) 100938. doi:10.1016/j.jrras.2024.100938.

[21] F. Z. Zerhouni, M. H. Zerhouni, M. Zegrar, M. T. Benmessaoud, A. Tilmatine and A. B. Stambouli. Modelling polycrystalline photovoltaic cells using design of experiments. *Scientia Iranica* **21** (6) (2014) 2273–2287.

Nonlinear Dynamics and Systems Theory, **26** (1) (2026) 29–40

A Taylor Collocation Approach for Solving Systems of Two-Dimensional Volterra Integral Equations

C. Hennous [1] and H. Laib [1,2*]

[1] *Laboratory of Mathematics and Its Interactions, Abdelhafid Boussouf University, Mila, Algeria.*
[2] *Ecole Normale Supérieure Echeikh Mohamed Elbachir Elibrahimi, Algiers, Algeria.*

Received: December 20, 2024; Revised: January 15, 2026

Abstract: This work presents a numerical approach for solving systems of linear two-dimensional Volterra integral equations (2D-VIEs), which frequently arise in modeling dynamical systems with memory effects, including applications in control theory, population dynamics, and epidemic modeling. An algorithm based on Taylor polynomials is developed to construct a collocation solution for these systems. The convergence of the proposed method is established, ensuring accurate and efficient approximations while preserving the integral structure of the system. Numerical examples are provided to illustrate the accuracy and applicability of the method in solving problems relevant to systems theory.

Keywords: *system of two-dimensional Volterra integral equations; spline approximation; power series; error analysis.*

Mathematics Subject Classification (2020): 41A15, 45D05, 45L05, 65R20, 37N25.

1 Introduction

The numerical solution of integral equations, particularly systems of Volterra integral equations (VIEs), is crucial for modeling and solving complex problems in science and engineering. Such equations frequently arise in fluid dynamics, signal processing, control theory, mathematical biology, and various other areas of nonlinear dynamics and systems theory. For instance, in nonlinear dynamical systems, VIEs are used to describe systems with memory effects, such as in population dynamics, where the interaction between

* Corresponding author: mailto:hafida.laib@gmail.com

© 2026 InforMath Publishing Group/1562-8353 (print)/1813-7385 (online)/http://e-ndst.kiev.ua

species or components is influenced. Similarly, in systems theory, VIEs provide a framework for modeling the evolution of systems under nonlinear influences, such as in control theory, where the system's behavior over time is influenced by feedback mechanisms that are inherently memory-dependent.

Numerous numerical methods have been developed for one-dimensional cases, including the modified homotopy perturbation method [5], the semi-orthogonal B-spline collocation method [11], and the Hybrid Legendre Block-Pulse functions method [12]. Research on computational methods for solving systems of two-dimensional integral equations (2D-IEs) remains limited.

This paper further develops the Taylor collocation method (TCM), as introduced in [1–3, 6], to solve (1). The TCM provides a direct and reliable framework for addressing such systems. Unlike traditional techniques that transform equations into algebraic systems, the TCM leverages Taylor series expansions to approximate solutions directly in their integral form. By exploiting the inherent smoothness and flexibility of Taylor series, the method ensures accurate approximations while preserving the structure of the original system.

The structure of the paper is as follows. Section 2 introduces the approximation of solutions for 2D VIEs using the polynomial spline space $S^{(-1)}_{p-1,p-1}$ in conjunction with Taylor polynomials. Section 3 provides a detailed convergence analysis. Section 4 presents numerical examples to validate and illustrate the theoretical findings. Finally, the paper concludes with a summary of the research findings and directions for future work.

2 Description of the Method

We aim to solve a linear system of two-dimensional Volterra integral equations (2D VIEs) of the form

$$\begin{cases} u_1(x,y) = g_1(x,y) + \int_0^x \int_0^y \left[K_{1,1}(x,y,t,s)u_1(t,s) + K_{1,2}(x,y,t,s)u_2(t,s)\right] dsdt, \\ u_2(x,y) = g_2(x,y) + \int_0^x \int_0^y \left[K_{2,1}(x,y,t,s)u_1(t,s) + K_{2,2}(x,y,t,s)u_2(t,s)\right] dsdt, \end{cases} \tag{1}$$

where $(x,y) \in D$, and the functions g_d and $K_{d,\delta}$, with $d,\delta = 1,2$, are given continuous real-valued functions defined on $D = [0,a] \times [0,b] \subset \mathbb{R}^2$, $S = \{(x,y,t,s) : 0 \le t \le x \le a, 0 \le s \le y \le b\}$.

The existence and uniqueness of solutions for systems of 2D VIEs have been established in [10, 13].

To numerically solve these equations, let $\Pi_N = \{x_i = ih, i = 0,1,\ldots,N\}$ and $\Pi_M = \{y_j = jk, j = 0,1,\ldots,M\}$ represent uniform partitions of the intervals $[0,a]$ and $[0,b]$, with step sizes $h = \frac{a}{N}$ and $k = \frac{b}{M}$. These partitions form a grid for D given by

$$\Pi_{N,M} = \Pi_N \times \Pi_M = \{(x_n, y_m) : 0 \le n \le N, 0 \le m \le M\}.$$

Define the subintervals

$$\begin{aligned} &\sigma_n = [x_n, x_{n+1}), \quad n = 0,1,\ldots,N-2; \quad \sigma_{N-1} = [x_{N-1}, x_N], \\ &\delta_m = [y_m, y_{m+1}), \quad m = 0,1,\ldots,M-2; \quad \delta_{M-1} = [y_{M-1}, y_M], \end{aligned}$$

and the rectangular regions

$$D_{n,m} := \sigma_n \times \delta_m, \quad n = 0,\ldots,N-1; \quad m = 0,\ldots,M-1.$$

Additionally, let $\pi_{p-1,p-1}$ denote the set of all real polynomials of degree at most $p-1$ in both x and y. The polynomial spline space of degree $p-1$ in x and y is defined as

$$S^{(-1)}_{p-1,p-1}(\Pi_{N,M}) = \{(v_1, v_2)^t : (v_{1,n,m}, v_{2,n,m})^t = (v_1, v_2)^t|_{D_{n,m}} \in \pi_{p-1,p-1}, \\ n = 0, \dots, N-1;\ m = 0, \dots, M-1\}.$$

This space consists of bivariate polynomial spline functions of degree at most $p-1$ in x and y. It has dimension $2NMp^2$, equal to the total number of coefficients of the polynomials $v_{1,n,m}$ and $v_{2,n,m}$. To determine these coefficients, we use Taylor polynomials on each rectangular region $D_{n,m}$.

The solution u of (1) is known along part of the boundary of D

$$u(x,y) = g(x,0), \quad \text{for } 0 \le x \le a \text{ and } y = 0,$$
$$u(x,y) = g(0,y), \quad \text{for } 0 \le y \le b \text{ and } x = 0.$$

First, we approximate u in the rectangle $D_{0,0}$ by the polynomials

$$v_{d,0,0}(x,y) = \sum_{i+j=0}^{p-1} \frac{1}{i!j!} \frac{\partial^{i+j} u_d(0,0)}{\partial x^i \partial y^j} x^i y^j \ ; \quad (x,y) \in D_{0,0}, d = 1,2, \tag{2}$$

where $\dfrac{\partial^{i+j} u_d(0,0)}{\partial x^i \partial y^j}$ is the exact value of $\dfrac{\partial^{i+j} u_d}{\partial x^i \partial y^j}$ at point $(0,0)$.

To find $\dfrac{\partial^{i+j} u_1(x,y)}{\partial y^j}$ and $\dfrac{\partial^{i+j} u_2(x,y)}{\partial y^j}$, we differentiate (1) j times with respect to y, then i times with respect to x, we obtain

$$\begin{aligned}
\frac{\partial^{i+j} u_d(x,y)}{\partial x^i \partial y^j} &= \partial_1^{(i)} \partial_2^{(j)} g_d(x,y) + \sum_{r=0}^{j-1} \sum_{l=0}^{r} \sum_{q=0}^{i-1} \sum_{\eta=0}^{q} \binom{r}{l} \binom{q}{\eta} \times \\
&\frac{\partial^{q-\eta}}{\partial x^{q-\eta}} \left[\frac{\partial^{i-1-q}}{\partial x^{i-1-q}} \bigg|_{t=x} \left(\frac{\partial^{r-l}}{\partial y^{r-l}} \left[\partial_2^{(j-1-r)} K_{d,1}(x,y,t,y) \right] \right) \right] \frac{\partial^{\eta+l} u_1(x,y)}{\partial x^\eta \partial y^l} \\
&+ \frac{\partial^{q-\eta}}{\partial x^{q-\eta}} \left[\frac{\partial^{i-1-q}}{\partial x^{i-1-q}} \bigg|_{t=x} \left(\frac{\partial^{r-l}}{\partial y^{r-l}} \left[\partial_2^{(j-1-r)} K_{d,2}(x,y,t,y) \right] \right) \right] \frac{\partial^{\eta+l} u_2(x,y)}{\partial x^\eta \partial y^l} \\
&+ \sum_{r=0}^{j-1} \sum_{l=0}^{r} \binom{r}{l} \int_0^x \frac{\partial^i}{\partial x^i} \left[\frac{\partial^{r-l}}{\partial y^{r-l}} [\partial_2^{(j-1-r)} K_{d,1}(x,y,t,y)] \right] \frac{\partial^l u_1(t,y)}{\partial y^l} \\
&+ \frac{\partial^i}{\partial x^i} \left[\frac{\partial^{r-l}}{\partial y^{r-l}} [\partial_2^{(j-1-r)} K_{d,2}(x,y,t,y)] \right] \frac{\partial^l u_2(t,y)}{\partial y^l} dt \\
&+ \sum_{q=0}^{i-1} \sum_{\eta=0}^{q} \binom{q}{\eta} \int_0^y \frac{\partial^{q-\eta}}{\partial x^{q-\eta}} \left[\partial_1^{(i-1-q)} \partial_2^{(j)} K_{d,1}(x,y,x,s) \right] \frac{\partial^\eta u_1(x,s)}{\partial x^\eta} \\
&+ \frac{\partial^{q-\eta}}{\partial x^{q-\eta}} \left[\partial_1^{(i-1-q)} \partial_2^{(j)} K_{d,2}(x,y,x,s) \right] \frac{\partial^\eta u_2(x,s)}{\partial x^\eta} ds \\
&+ \int_0^x \int_0^y \partial_1^{(i)} \partial_2^{(j)} K_{d,1}(x,y,t,s) u_1(t,s) + \partial_1^{(i)} \partial_2^{(j)} K_{d,2}(x,y,t,s) u_2(t,s) ds dt.
\end{aligned}$$

Second, we approximate u in the rectangles $D_{n,0}, n = 1, ..., N-1$, by the polynomials

$$v_{d,n,0}(x,y) = \sum_{i+j=0}^{p-1} \frac{1}{i!j!} \frac{\partial^{i+j} \hat{v}_{d,n,0}(x_n,0)}{\partial x^i \partial y^j} (x-x_n)^i y^j \ ; \quad d = 1,2; (x,y) \in D_{n,0}, \tag{3}$$

where $\hat{v}_{d,n,0}$, $d = 1, 2$ is the exact solution of the system

$$\begin{aligned} \hat{v}_{d,n,0}(x,y) &= g_d(x,y) \\ &+ \sum_{\xi=0}^{n-1} \int_{x_\xi}^{x_{\xi+1}} \int_0^y K_{d,1}(x,y,t,s) v_{1,\xi,0}(t,s) + K_{d,2}(x,y,t,s) v_{2,\xi,0}(t,s) ds dt \\ &+ \int_{x_n}^{x} \int_0^y K_{d,1}(x,y,t,s) \hat{v}_{1,n,0}(t,s) + K_{d,2}(x,y,t,s) \hat{v}_{2,n,0}(t,s) ds dt. \end{aligned} \tag{4}$$

To find $\dfrac{\partial^{i+j} \hat{v}_{d,n,0}(x,y)}{\partial y^j}$, we differentiate (4) j times with respect to y, then i times with respect to x, we obtain

$$\begin{aligned} &\frac{\partial^{i+j} \hat{v}_{d,n,0}(x,y)}{\partial x^i \partial y^j} = \partial_1^{(i)} \partial_2^{(j)} g_d(x,y) \\ &+ \sum_{\xi=0}^{n-1} \sum_{r=0}^{j-1} \sum_{l=0}^{r} \binom{r}{l} \int_{x_\xi}^{x_{\xi+1}} \frac{\partial^i}{\partial x^i} \left[\frac{\partial^{r-l}}{\partial y^{r-l}} [\partial_2^{(j-1-r)} K_{d,1}(x,y,t,y)] \right] \frac{\partial^l v_{1,\xi,0}(t,y)}{\partial y^l} \\ &+ \frac{\partial^i}{\partial x^i} \left[\frac{\partial^{r-l}}{\partial y^{r-l}} [\partial_2^{(j-1-r)} K_{d,2}(x,y,t,y)] \right] \frac{\partial^l v_{2,\xi,0}(t,y)}{\partial y^l} dt \\ &+ \sum_{\xi=0}^{n-1} \int_{x_\xi}^{x_{\xi+1}} \int_0^y \partial_1^{(i)} \partial_2^{(j)} K_{d,1}(x,y,t,s) v_{1,\xi,0}(t,s) + \partial_1^{(i)} \partial_2^{(j)} K_{d,2}(x,y,t,s) v_{2,\xi,0}(t,s) ds dt \\ &+ \sum_{r=0}^{j-1} \sum_{l=0}^{r} \sum_{q=0}^{i-1} \sum_{\eta=0}^{q} \binom{r}{l} \binom{q}{\eta} \times \\ &\frac{\partial^{q-\eta}}{\partial x^{q-\eta}} \left[\frac{\partial^{i-1-q}}{\partial x^{i-1-q}} \bigg|_{t=x} \left(\frac{\partial^{r-l}}{\partial y^{r-l}} \left[\partial_2^{(j-1-r)} K_{d,1}(x,y,t,y) \right] \right) \right] \frac{\partial^{\eta+l} \hat{v}_{1,n,0}(x,y)}{\partial x^\eta \partial y^l} \\ &+ \frac{\partial^{q-\eta}}{\partial x^{q-\eta}} \left[\frac{\partial^{i-1-q}}{\partial x^{i-1-q}} \bigg|_{t=x} \left(\frac{\partial^{r-l}}{\partial y^{r-l}} \left[\partial_2^{(j-1-r)} K_{d,2}(x,y,t,y) \right] \right) \right] \frac{\partial^{\eta+l} \hat{v}_{2,n,0}(x,y)}{\partial x^\eta \partial y^l} \\ &+ \sum_{r=0}^{j-1} \sum_{l=0}^{r} \binom{r}{l} \int_{x_n}^{x} \frac{\partial^i}{\partial x^i} \left[\frac{\partial^{r-l}}{\partial y^{r-l}} [\partial_2^{(j-1-r)} K_{d,1}(x,y,t,y)] \right] \frac{\partial^l \hat{v}_{1,n,0}(t,y)}{\partial y^l} \\ &+ \frac{\partial^i}{\partial x^i} \left[\frac{\partial^{r-l}}{\partial y^{r-l}} [\partial_2^{(j-1-r)} K_{d,2}(x,y,t,y)] \right] \frac{\partial^l \hat{v}_{2,n,0}(t,y)}{\partial y^l} dt \\ &+ \sum_{q=0}^{i-1} \sum_{\eta=0}^{q} \binom{q}{\eta} \int_0^y \frac{\partial^{q-\eta}}{\partial x^{q-\eta}} \left[\partial_1^{(i-1-q)} \partial_2^{(j)} K_{d,1}(x,y,x,s) \right] \frac{\partial^\eta \hat{v}_{1,n,0}(x,s)}{\partial x^\eta} \\ &+ \frac{\partial^{q-\eta}}{\partial x^{q-\eta}} \left[\partial_1^{(i-1-q)} \partial_2^{(j)} K_{d,2}(x,y,x,s) \right] \frac{\partial^\eta \hat{v}_{2,n,0}(x,s)}{\partial x^\eta} ds \\ &+ \int_{x_n}^{x} \int_0^y \partial_1^{(i)} \partial_2^{(j)} K_{d,1}(x,y,t,s) \hat{v}_{1,n,0}(t,s) + \partial_1^{(i)} \partial_2^{(j)} K_{d,2}(x,y,t,s) \hat{v}_{2,n,0}(t,s) ds dt. \end{aligned}$$

Third, we approximate u in the rectangle $D_{n,m}, n = 0, ..., N-1$ and $m = 1, ..., M-1$ by, the polynomials

$$v_{d,n,m}(x,y) = \sum_{i+j=0}^{p-1} \frac{1}{i!j!} \frac{\partial^{i+j} \hat{v}_{d,n,m}(x_n, y_m)}{\partial x^i \partial y^j} (x - x_n)^i (y - y_m)^j \ ; \quad d = 1, 2; (x,y) \in D_{n,m}, \tag{5}$$

where $\hat{v}_{d,n,m}$, $d = 1, 2$, is the exact solution of the system

$$\begin{aligned}
&\hat{v}_{d,n,m}(x,y) = g_d(x,y) \\
&+ \sum_{\xi=0}^{n-1} \sum_{\rho=0}^{m-1} \int_{x_\xi}^{x_{\xi+1}} \int_{y_\rho}^{y_{\rho+1}} K_{d,1}(x,y,t,s) v_{1,\xi,\rho}(t,s) + K_{d,2}(x,y,t,s) v_{2,\xi,\rho}(t,s) ds dt \\
&+ \sum_{\xi=0}^{n-1} \int_{x_\xi}^{x_{\xi+1}} \int_{y_m}^{y} K_{d,1}(x,y,t,s) v_{1,\xi,m}(t,s) + K_{d,2}(x,y,t,s) v_{2,\xi,m}(t,s) ds dt \\
&+ \sum_{\rho=0}^{m-1} \int_{x_n}^{x} \int_{y_\rho}^{y_{\rho+1}} K_{d,1}(x,y,t,s) v_{1,n,\rho}(t,s) + K_{d,2}(x,y,t,s) v_{2,n,\rho}(t,s) ds dt \\
&+ \int_{x_n}^{x} \int_{y_m}^{y} K_{d,1}(x,y,t,s) \hat{v}_{1,n,m}(t,s) + K_{d,2}(x,y,t,s) \hat{v}_{2,n,m}(t,s) ds dt.
\end{aligned} \tag{6}$$

To find $\dfrac{\partial^{i+j} \hat{v}_{d,n,m}(x,y)}{\partial y^j}$, we differentiate (6) j times with respect to y, then i times with respect to x, we obtain

$$\begin{aligned}
&\frac{\partial^{i+j} \hat{v}_{d,n,m}(x,y)}{\partial x^i \partial y^j} = \partial_1^{(i)} \partial_2^{(j)} g_d(x,y) \\
&+ \sum_{\xi=0}^{n-1} \sum_{\rho=0}^{m-1} \int_{x_\xi}^{x_{\xi+1}} \int_{y_\rho}^{y_{\rho+1}} \partial_1^{(i)} \partial_2^{(j)} \left(K_{d,1}(x,y,t,s) v_{1,\xi,\rho}(t,s) + K_{d,2}(x,y,t,s) v_{2,\xi,\rho}(t,s) \right) ds dt \\
&+ \sum_{\xi=0}^{n-1} \sum_{r=0}^{j-1} \sum_{l=0}^{r} \binom{r}{l} \int_{x_\xi}^{x_{\xi+1}} \frac{\partial^i}{\partial x^i} \left[\frac{\partial^{r-l}}{\partial y^{r-l}} [\partial_2^{(j-1-r)} K_{d,1}(x,y,t,y)] \right] \frac{\partial^l v_{1,\xi,m}(t,y)}{\partial y^l} \\
&+ \frac{\partial^i}{\partial x^i} \left[\frac{\partial^{r-l}}{\partial y^{r-l}} [\partial_2^{(j-1-r)} K_{d,2}(x,y,t,y)] \right] \frac{\partial^l v_{2,\xi,m}(t,y)}{\partial y^l} dt \\
&+ \sum_{\xi=0}^{n-1} \int_{x_\xi}^{x_{\xi+1}} \int_{y_m}^{y} \partial_1^{(i)} \partial_2^{(j)} K_{d,1}(x,y,t,s) v_{1,\xi,m}(t,s) + \partial_1^{(i)} \partial_2^{(j)} K_{d,2}(x,y,t,s) v_{2,\xi,m}(t,s) ds dt \\
&+ \sum_{\rho=0}^{m-1} \sum_{q=0}^{i-1} \sum_{\eta=0}^{q} \binom{q}{\eta} \int_{y_\rho}^{y_{\rho+1}} \frac{\partial^{q-\eta}}{\partial x^{q-\eta}} \left[\partial_1^{(i-1-q)} \partial_2^{(j)} K_{d,1}(x,y,x,s) \right] \frac{\partial^\eta v_{1,n,\rho}(x,s)}{\partial x^\eta} \\
&+ \frac{\partial^{q-\eta}}{\partial x^{q-\eta}} \left[\partial_1^{(i-1-q)} \partial_2^{(j)} K_{d,2}(x,y,x,s) \right] \frac{\partial^\eta v_{2,n,\rho}(x,s)}{\partial x^\eta} ds \\
&+ \sum_{\rho=0}^{m-1} \int_{x_n}^{x} \int_{y_\rho}^{y_{\rho+1}} \partial_1^{(i)} \partial_2^{(j)} K_{d,1}(x,y,t,s) v_{1,n,\rho}(t,s) + \partial_1^{(i)} \partial_2^{(j)} K_{d,2}(x,y,t,s) v_{2,n,\rho}(t,s) ds dt
\end{aligned}$$

$$+\sum_{r=0}^{j-1}\sum_{l=0}^{r}\sum_{q=0}^{i-1}\sum_{\eta=0}^{q}\binom{r}{l}\binom{q}{\eta}\times$$
$$\frac{\partial^{q-\eta}}{\partial x^{q-\eta}}\left[\left.\frac{\partial^{i-1-q}}{\partial x^{i-1-q}}\right|_{t=x}\left(\frac{\partial^{r-l}}{\partial y^{r-l}}\left[\partial_2^{(j-1-r)}K_{d,1}(x,y,t,y)\right]\right)\right]\frac{\partial^{\eta+l}\hat{v}_{1,n,m}(x,y)}{\partial x^{\eta}\partial y^{l}}$$
$$+\frac{\partial^{q-\eta}}{\partial x^{q-\eta}}\left[\left.\frac{\partial^{i-1-q}}{\partial x^{i-1-q}}\right|_{t=x}\left(\frac{\partial^{r-l}}{\partial y^{r-l}}\left[\partial_2^{(j-1-r)}K_{d,2}(x,y,t,y)\right]\right)\right]\frac{\partial^{\eta+l}\hat{v}_{2,n,m}(x,y)}{\partial x^{\eta}\partial y^{l}}$$
$$+\sum_{r=0}^{j-1}\sum_{l=0}^{r}\binom{r}{l}\int_{x_n}^{x}\frac{\partial^{i}}{\partial x^{i}}\left[\frac{\partial^{r-l}}{\partial y^{r-l}}[\partial_2^{(j-1-r)}K_{d,1}(x,y,t,y)]\right]\frac{\partial^{l}\hat{v}_{1,n,m}(t,y)}{\partial y^{l}}$$
$$+\frac{\partial^{i}}{\partial x^{i}}\left[\frac{\partial^{r-l}}{\partial y^{r-l}}[\partial_2^{(j-1-r)}K_{d,2}(x,y,t,y)]\right]\frac{\partial^{l}\hat{v}_{2,n,m}(t,y)}{\partial y^{l}}dt$$
$$+\sum_{q=0}^{i-1}\sum_{\eta=0}^{q}\binom{q}{\eta}\int_{y_m}^{y}\frac{\partial^{q-\eta}}{\partial x^{q-\eta}}\left[\partial_1^{(i-1-q)}\partial_2^{(j)}K_{d,1}(x,y,x,s)\right]\frac{\partial^{\eta}\hat{v}_{1,n,m}(x,s)}{\partial x^{\eta}}$$
$$+\frac{\partial^{q-\eta}}{\partial x^{q-\eta}}\left[\partial_1^{(i-1-q)}\partial_2^{(j)}K_{d,2}(x,y,x,s)\right]\frac{\partial^{\eta}\hat{v}_{2,n,m}(x,s)}{\partial x^{\eta}}ds$$
$$+\int_{x_n}^{x}\int_{y_m}^{y}\partial_1^{(i)}\partial_2^{(j)}K_{d,1}(x,y,t,s)\hat{v}_{1,n,m}(t,s)+\partial_1^{(i)}\partial_2^{(j)}K_{d,2}(x,y,t,s)\hat{v}_{2,n,m}(t,s)dsdt.$$

3 Analysis of Convergence and Numerical Error

We consider the space $L^{\infty}(D)$ with the norm

$$\|\varphi\| = \inf\{C\in\mathbb{R} : |\varphi(\tau,z)|\le C \ \text{ for a.e. } (\tau,z)\in D\} < \infty.$$

The following lemmas will be used in proving the convergence of the presented method.

Lemma 3.1 (*Discrete Gronwall type inequality [4]*) *Let $\{k_j\}_{j=0}^{n}$ be a given non negative sequence and the sequence $\{\varepsilon_n\}$ satisfies $\varepsilon_0 \le p_0$ and*

$$\varepsilon_n \le p_0 + \sum_{i=0}^{n-1} k_i\varepsilon_i, \quad n\ge 1,$$

with $p_0 \ge 0$. Then ε_n can be bounded by

$$\varepsilon_n \le p_0 \exp\left(\sum_{j=0}^{n-1} k_j\right), \quad n\ge 1.$$

Lemma 3.2 (*Discrete Gronwall type inequality of two variables [8]) Let $u_{n,m}$ be a given non negative sequence, and let $K_i, (i=1,2,3)$ and Δ be strictly positive. If the sequence $u_{n,m}$ satisfies, for all $n=0,1,...,N, m=0,1,...,M$,*

$$u_{n,m} \le hK_1\sum_{\xi=0}^{n-1}u_{\xi,m} + kK_2\sum_{\rho=0}^{m-1}u_{n,\rho} + hkK_3\sum_{\xi=0}^{n-1}\sum_{\rho=0}^{m-1}u_{\xi,\rho} + \Delta,$$

then $u_{n,m} \le \Delta exp(\gamma(Nh+Mk))$, where $\gamma = \frac{1}{2}\left(K_1+K_2+\sqrt{(K_1+K_2)^2+4K_3}\right)$.

Lemma 3.3 (*Wendroff's inequality [14]*) *Let f and u be continuous and non negative functions defined on $[a,b]\times[c,d]$, and let g be non negative and twice continuously differentiable function on $[a,b]\times[c,d]\times[a,b]\times[c,d]$. Then the inequality*

$$u(x,y)\leq f(x,y)+\int_a^x\int_c^y g(x,y,t,s)u(t,s)dsdt,\quad (x,y)\in[a,b]\times[c,d],$$

implies that

$$u(x,y)\leq f(x,y)\exp\left(\int_a^x\int_c^y R(t,s)dsdt\right),\quad (x,y)\in[a,b]\times[c,d],$$

where

$$\begin{aligned}R(x,y)=&g(x,y,x,y)+\int_a^x\partial_1 g(x,y,t,y)dt\\&+\int_b^y\partial_2 g(x,y,x,s)ds+\int_a^x\int_c^y\partial_2\partial_1 g(x,y,t,s)dsdt.\end{aligned}$$

Theorem 3.1 (*Taylor's Theorem for functions of two independent variables [9]*) *Let f be p times continuously differentiable on $D=[a,b]\times[c,d]$ and let $(x_0,y_0)\in D$. Then for all $(x,y)\in D$, we have*

$$f(x,y)=\sum_{i+j=0}^{p-1}\frac{1}{i!j!}\frac{\partial^{i+j}f(x_0,y_0)}{\partial x^i\partial y^j}(x-x_0)^i(y-y_0)^j+\sum_{i+j=p}\frac{1}{i!j!}\frac{\partial^{i+j}f(x_1,y_1)}{\partial x^i\partial y^j}(x-x_0)^i(y-y_0)^j,$$

where

$$\begin{cases}x_1=\theta x+(1-\theta)x_0\in[a,b],\\ y_1=\theta y+(1-\theta)y_0\in[c,d],\end{cases}\qquad\theta\in(0,1).$$

In the following, for a given function $\varphi\in C(D,\mathbb{R}^2)$, we define the norm $\|\varphi\|$ by

$$\|\varphi\|=\max\{\ |\varphi_d(x,y)|,\quad (x,y)\in D,\quad d=1,2\}.$$

Theorem 3.2 *Let g and K be p times continuously differentiable on their respective domains. Then equations (2),(3),(5) define a unique approximation $v\in(S^{(-1)}_{p-1,p-1}(\Pi_{N,M}))^2$, and the resulting error function $e(x,y)=u(x,y)-v(x,y)$ satisfies*

$$\|e\|\leq C(h+k)^p,$$

where C is a finite constant independent of h, k.

Proof. The proof is split into three steps.
Claim 1. Define the error $e_0=e|_{D_{0,0}}$ by $e_{d,0,0}(x,y)=u_d(x,y)-v_{d,0,0}(x,y)$, for $d=1,2$. There exists a constant C_1 independent of h and k such that $\|e_0\|\leq C_1(h+k)^p$.

Let $(x,y)\in D_{0,0}$, by using Taylor's theorem, we obtain from (2)

$$|e_{d,0,0}(x,y)|\leq\sum_{i+j=p}\frac{1}{i!j!}\left\|\frac{\partial^{i+j}u_d}{\partial x^i\partial y^j}\right\|h^ik^j,\qquad d=1,2.$$

When employing a more direct generalization of the methods used in Lemma 5 of [2], there exists a positive constant $\alpha(p)$ such that for all $n = 0, \dots, N-1$, $m = 0, \dots, M-1$, $d = 1, 2$, and $i + j = 0, 1, \dots, p$, the following inequality holds:

$$\left\| \frac{\partial^{i+j} \hat{v}_{d,n,m}}{\partial x^i \partial y^j} \right\|_{L^\infty(D_{n,m})} \leq \alpha(p).$$

Hence, we have

$$|e_{d,0,0}(x,y)| \leq \alpha(p) \sum_{i+j=p} \frac{1}{i!j!} h^i k^j = \underbrace{\frac{\alpha(p)}{p!}}_{C_1} (h+k)^p, \qquad d = 1, 2.$$

Claim 2. Define the error $e_n = e|_{D_{n,0}}$ by $e_{d,n,0}(x,y) = u_d(x,y) - v_{d,n,0}(x,y)$ for all $n \in \{0, \dots, N-1\}$ and $d = 1, 2$.
There exists a constant C_2 independent of h and k such that $\|e_n\| \leq C_2(h+k)^p$ for all $n = 1, \dots, N-1$. Let $(x,y) \in D_{n,0}$, we have from (4)

$$u_d(x,y) - \hat{v}_{d,n,0}(x,y) = \sum_{\xi=0}^{n-1} \int_{x_\xi}^{x_{\xi+1}} \int_0^y (K_{d,1}(x,y,t,s)(u_1(t,s) - v_{1,\xi,0}(t,s))$$
$$+ K_{d,2}(x,y,t,s)(u_2(t,s) - v_{2,\xi,0}(t,s)))dsdt + \int_{x_n}^x \int_0^y (K_{d,1}(x,y,t,s)(u_1(t,s) - \hat{v}_{1,\xi,0}(t,s))$$
$$+ K_{d,2}(x,y,t,s)(u_2(t,s) - \hat{v}_{2,\xi,0}(t,s)))dsdt,$$

hence,

$$|u_d(x,y) - \hat{v}_{d,n,0}(x,y)| \leq \sum_{\xi=0}^{n-1} hk\overline{K}_d \|e\|$$
$$+ \overline{K}_d \int_{x_n}^x \int_0^y |u_1(t,s) - \hat{v}_{1,n,0}(t,s)| + |u_2(t,s) - \hat{v}_{2,n,0}(t,s)|dsdt,$$

where $\overline{K}_d = \|K_{d,1}\| + \|K_{d,2}\|$, $d = 1, 2$. By adding the two inequalities, we have

$$|u_1(x,y) - \hat{v}_{1,n,0}(x,y)| + |u_2(x,y) - \hat{v}_{2,n,0}(x,y)| \leq \sum_{\xi=0}^{n-1} hk\overline{K} \|e_\xi\|$$
$$+ \overline{K} \int_{x_n}^x \int_0^y |u_1(t,s) - \hat{v}_{1,n,0}(t,s)| + |u_2(t,s) - \hat{v}_{2,n,0}(t,s)|dsdt,$$

where $\overline{K} = \overline{K}_1 + \overline{K}_2$. Then by Lemma 3.3,

$$|u_d(x,y) - \hat{v}_{d,n,0}(x,y)| \leq \sum_{\xi=0}^{n-1} h \underbrace{b\overline{K} \exp\left(\overline{K}ab\right)}_{\lambda_1} \|e_\xi\|, \qquad d = 1, 2.$$

Which implies, by Taylor's theorem, that

$$|e_{d,n,0}(x,y)| \leq |u_d(x,y) - \hat{v}_{d,n,0}(x,y)| + |\hat{v}_{d,n,0}(x,y) - v_{d,n,0}(x,y)|$$
$$\leq \sum_{\xi=0}^{n-1} h\lambda_1 \|e_\xi\| + \sum_{i+j=p} \frac{1}{i!j!} \left\| \frac{\partial^{i+j} \hat{v}_{d,n,0}}{\partial x^i \partial y^j} \right\| h^i k^j,$$

hence, we obtain $|e_{d,n,0}(x,y)| \leq \sum_{\xi=0}^{n-1} h\lambda_1\|e_\xi\| + \frac{\alpha(p)}{p!}(h+k)^p, \qquad d=1,2.$ Then, by Lemma 3.1, we have

$$\|e_n\| \leq \frac{\alpha(p)}{p!}(h+k)^p \exp(a\lambda_1).$$

Thus, we take $C_2 = \frac{\alpha(p)}{p!}\exp(a\lambda_1)$.

Claim 3. Define the error $e_{n,m} = e|_{D_{n,m}}$ by $e_{d,n,m}(x,y) = u_d(x,y) - v_{d,n,m}(x,y)$ for all $n \in \{0,\ldots,N-1\}$, $m \in \{0,\ldots,M-1\}$ and $d=1,2$.
There exists a constant C_3 independent of h and k such that

$$\|e_{n,m}\| \leq C_3(h+k)^p$$

for all $n=0,\ldots,N-1$ and $m=1,\ldots,M-1$. Let $(x,y) \in D_{n,m}$, we have from (6)

$$|u_d(x,y) - \hat{v}_{d,n,m}(x,y)| \leq \sum_{\xi=0}^{n-1}\sum_{\rho=0}^{m-1} hk\overline{K}_d\|e_{\xi,\rho}\| + \sum_{\xi=0}^{n-1} hk\overline{K}_d\|e_{\xi,m}\| + \sum_{\rho=0}^{m-1} hk\overline{K}_d\|e_{n,\rho}\|$$
$$+ \overline{K}_d\int_{x_n}^{x}\int_{y_m}^{y} |u_1(t,s) - \hat{v}_{1,n,m}(t,s)| + |u_2(t,s) - \hat{v}_{2,n,m}(t,s)|dsdt, \qquad d=1,2.$$

By adding the two inequalities, we have

$$|u_1(t,s) - \hat{v}_{1,n,m}(t,s)| + |u_2(t,s) - \hat{v}_{2,n,m}(t,s)| \leq \sum_{\xi=0}^{n-1}\sum_{\rho=0}^{m-1} hk\overline{K}\|e_{\xi,\rho}\| + \sum_{\xi=0}^{n-1} hk\overline{K}\|e_{\xi,m}\|$$
$$+ \sum_{\rho=0}^{m-1} hk\overline{K}\|e_{n,\rho}\| + \overline{K}\int_{x_n}^{x}\int_{y_m}^{y} |u_1(t,s) - \hat{v}_{1,n,m}(t,s)| + |u_2(t,s) - \hat{v}_{2,n,m}(t,s)|dsdt,$$

then by Lemma 3.3,

$$|u_d(x,y) - \hat{v}_{d,n,m}(x,y)| \leq \sum_{\xi=0}^{n-1}\sum_{\rho=0}^{m-1} hk\underbrace{\overline{K}\exp\left(\overline{K}ab\right)}_{\lambda_2}\|e_{\xi,\rho}\|$$
$$+ \sum_{\xi=0}^{n-1} h\underbrace{b\overline{K}\exp\left(\overline{K}ab\right)}_{\lambda_3}\|e_{\xi,m}\| + \sum_{\rho=0}^{m-1} k\underbrace{a\overline{K}\exp\left(\overline{K}ab\right)}_{\lambda_4}\|e_{n,\rho}\|, \qquad d=1,2.$$

Which implies, by Taylor's theorem, that

$$|e_{d,n,m}(x,y)| \leq |u_d(x,y) - \hat{v}_{d,n,m}(x,y)| + |\hat{v}_{d,n,m}(x,y) - v_{d,n,m}(x,y)|$$
$$\leq \sum_{\xi=0}^{n-1}\sum_{\rho=0}^{m-1} hk\lambda_2\|e_{\xi,\rho}\| + \sum_{\xi=0}^{n-1} hk\lambda_3\|e_{\xi,m}\| + \sum_{\rho=0}^{m-1} hk\lambda_4\|e_{n,\rho}\|$$
$$+ \sum_{i+j=p}\frac{1}{i!j!}\left\|\frac{\partial^{i+j}\hat{v}_{d,n,m}}{\partial x^i\partial y^j}\right\| h^i k^j, \qquad d=1,2.$$

Hence, we obtain for $d=1,2$,

$$\|e_{n,m}\| \leq \sum_{\xi=0}^{n-1}\sum_{\rho=0}^{m-1} hk\lambda_2\|e_{\xi,\rho}\| + \sum_{\xi=0}^{n-1} hk\lambda_3\|e_{\xi,m}\| + \sum_{\rho=0}^{m-1} hk\lambda_4\|e_{n,\rho}\| + \frac{\alpha(p)}{p!}(h+k)^p.$$

Then, by Lemma 3.2, we obtain $\|e_{n,m}\| \leq \frac{\alpha(p)}{p!}(h+k)^p \exp(\gamma_2(a+b))$,
where $\gamma_2 = \frac{1}{2}(\lambda_3 + \lambda_4 + \sqrt{(\lambda_3+\lambda_4)^2 + 4\lambda_2})$. Thus, we take $C_3 = \frac{\alpha(p)}{p!}\exp(\gamma_2(a+b))$.
The proof is completed by taking $C = \max\{C_1, C_2, C_3\}$. □

4 Numerical Examples

In this section, two numerical examples are given to show the efficiency of our proposed method for approximating the solution of a system of 2D VIEs.

Example 4.1 Consider the following system of 2 DVIEs:

$$\begin{cases} u_1(x,y) = g_1(x,y) + \int_0^x \int_0^y cos(s)u_1(t,s) + sin(s)u_2(t,s)dsdt, \\ u_2(x,y) = g_2(x,y) + \int_0^x \int_0^y xt^2u_1(t,s) + (x+t)u_2(t,s)dsdt, \end{cases}$$

where $g_1(x,y) = xcos(y) - \frac{1}{2}yx^2$, $g_2(x,y) = xsin(y) - \frac{1}{4}x^5sin(y) + \frac{5}{6}x^3cos(y) - \frac{5}{6}x^3$.
The exact solution of this system is $u_1(x,y) = xcos(y)$ and $u_2(x,y) = xsin(y)$.

The absolute error of the proposed method for $N = M = 10$, $p = 3, 5$ is shown in Table 1.

(x,y)	$p=3$		$p=5$	
	$\|e_1\|$	$\|e_2\|$	$\|e_1\|$	$\|e_2\|$
$(0,0)$	0	0	0	0
$(0.1,0.1)$	$8.32e-07$	$3.88e-09$	$4.30e-10$	$6.00e-12$
$(0.2,0.2)$	$3.34e-06$	$1.19e-07$	$2.00e-09$	$9.63e-09$
$(0.3,0.3)$	$7.61e-06$	$7.06e-07$	$3.60e-08$	$1.08e-07$
$(0.4,0.4)$	$1.37e-05$	$2.42e-06$	$1.91e-07$	$5.67e-07$
$(0.5,0.5)$	$2.19e-05$	$6.29e-06$	$6.70e-07$	$2.01e-06$
$(0.6,0.6)$	$3.23e-05$	$1.37e-05$	$1.84e-06$	$5.68e-06$
$(0.7,0.7)$	$4.54e-05$	$2.68e-05$	$4.35e-06$	$1.36e-05$
$(0.8,0.8)$	$6.17e-05$	$4.38e-05$	$9.15e-06$	$2.94e-05$
$(0.9,0.9)$	$8.19e-05$	$8.24e-05$	$1.77e-05$	$5.83e-05$

Table 1: Absolute errors in Example 4.1 for $N = M = 10$.

Example 4.2 Consider the following system of 2D VIEs:

$$\begin{cases} u_1(x,y) = g_1(x,y) + \int_0^x \int_0^y \frac{x-y+t-s}{4}u_2(t,s)dsdt, \\ u_2(x,y) = g_2(x,y) + \int_0^x \int_0^y \frac{x-y+t-s}{4}u_1(t,s)dsdt, \end{cases}$$

where

$$g_1(x,y) = xe^{1-y} - \frac{e}{24}y^2(3+3x-5y+e^{-x}(-3-6x+5y)),$$

$$g_2(x,y) = ye^{1-x} + \frac{e}{24}x^2(3-5x+3y+e^{-y}(-3+5x-6y)).$$

The exact solution of this system is $u_1(x,y) = xe^{1-y}$ and $u_2(x,y) = ye^{1-x}$.

Comparison of the absolute errors of the hybrid functions method (HFM) [7] and the proposed method (TCM) for $N = M = 10$, $p = 4$ is shown in Table 2.

(x, y)	HFM [7]		TCM	
	$\|e_{1,2,5}\|$	$\|e_{2,2,5}\|$	$\|e_1\|$	$\|e_2\|$
$(0, 0)$	$1.11e-07$	$5.02e+11$	0	0
$(0.1, 0.1)$	$4.90e-08$	$3.25e-08$	$1.00e-10$	$2.00e-10$
$(0.2, 0.2)$	$1.41e-07$	$1.34e-07$	$2.60e-09$	$1.90e-09$
$(0.3, 0.3)$	$2.10e-07$	$2.03e-07$	$1.07e-08$	$8.50e-09$
$(0.4, 0.4)$	$1.53e-07$	$1.37e-07$	$3.12e-08$	$2.71e-08$
$(0.5, 0.5)$	$6.80e-07$	$6.80e-07$	$7.60e-08$	$6.45e-08$
$(0.6, 0.6)$	$1.18e-07$	$1.18e-07$	$1.54e-07$	$1.35e-07$
$(0.7, 0.7)$	$2.84e-07$	$2.84e-07$	$2.83e-07$	$2.51e-07$
$(0.8, 0.8)$	$3.29e-07$	$3.28e-07$	$4.80e-07$	$4.26e-07$
$(0.9, 0.9)$	$1.86e-07$	$1.87e-07$	$7.68e-07$	$6.76e-07$

Table 2: Absolute errors in Example 4.2.

5 Conclusion

In this paper, we developed and applied the Taylor Collocation Method (TCM) to approximate the solution of a system of linear two-dimensional Volterra integral equations (2D-VIEs). Unlike traditional numerical approaches, which often rely on discretization or transformation into algebraic systems, the proposed method directly exploits the Taylor series expansion to construct a highly accurate collocation solution while preserving the integral structure of the equations. This methodological advantage enhances both accuracy and computational efficiency.

The numerical results confirm the effectiveness and reliability of the method, demonstrating high convergence rates and excellent agreement between the theoretical error estimates and practical computations. The approach is particularly well-suited for problems in applied mathematics and systems theory, where integral equations naturally arise in modeling processes with memory effects.

A key contribution of this work is the extension of TCM to systems of 2D-VIEs, which has been less explored in the literature compared to one-dimensional cases. In future work, we aim to generalize this framework to larger systems of n Volterra integral equations in two dimensions and explore its application to integral equations with weakly singular kernels or variable delays.

Acknowledgements

The authors are grateful to the anonymous referees and the editor for their constructive comments.

References

[1] F. Birem, A. Boulmerka, H. Laib and C. Hennous. An algorithm for solving first-kind two-dimensional Volterra integral equations using the collocation method. *Nonlinear Dynamics and Systems Theory* **23** (5) (2023) 475–486.

[2] F. Birem, A. Boulmerka, H. Laib and C. Hennous. Goursat problem in hyperbolic partial differential equations with variable coefficients solved by Taylor collocation method. *Iranian Journal of Numerical Analysis and Optimization* **14** (2) (2024) 613–637.

[3] H. Bouzeraieb, H. Laib and A. Boulmerka. Numerical solution of neutral double delay Volterra integral equations using Taylor collocation method. *Nonlinear Dynamics and Systems Theory* **24** (3) (2024) 236–245.

[4] H. Brunner. Collocation methods for Volterra integral and related functional differential equations. *Cambridge University Press* (15) (2004).

[5] M. Javidi. Modified homotopy perturbation method for solving system of linear Fredholm integral equations. *Mathematical and Computer Modelling* **50** (1-2) (2009) 159–165.

[6] H. Laib, A. Bellour and A. Boulmerka. Taylor collocation method for high-order neutral delay Volterra integro-differential equations. *Journal of Innovation in Applied Mathematics and Computer Science* **2** (1) (2022) 53–77.

[7] K. Maleknejad and M. Shahabi. Numerical solutions of system of two-dimensional Volterra integral equations via operational matrices of hybrid functions. *Journal of Mathematical Modeling* **10** (2) (2022) 349–365.

[8] S. McKee, T. Tang and T. Diogo. An Euler-type method for two-dimensional Volterra integral equations of the first kind. *IMA Journal of Numerical Analysis* **20** (3) (2000) 423–440.

[9] B. G. Pachpatte. Multidimensional integral equations and inequalities. *Springer Science and Business Media* (9) (2011).

[10] Y. Qian, I. Wu and Y. Zhang. A note on the unique solution of the integral equations in the framework of fixed point theorem on partially ordered metric space. *American Journal of Applied Mathematics and Statistics* **4** (5) (2016) 154–160.

[11] P. K. Sahu and S. S. Ray. Numerical solutions for the system of Fredholm integral equations of second kind by a new approach involving semiorthogonal B-Spline wavelet collocation method. *Applied Mathematics and Computation* **234** (2014) 368–379.

[12] P. K. Sahu and S. S. Ray. Hybrid Legendre Block-Pulse functions for the numerical solutions of system of nonlinear Fredholm–Hammerstein integral equations. *Applied Mathematics and Computation* **270** (2015) 871–878.

[13] V. I. Smirnov. *A Course of Higher Mathematics: Complex Variables, Special Functions. translated by D. E. Brown, edited by I. N. Sneddon, Pergamon Press,* 1964.

[14] B. G. Wendroff. *Integral and Finite Difference Inequalities and Applications. North-Holland and American Elsevier,* 2006.

Nonlinear Dynamics and Systems Theory, **26** (1) (2026) 41–55

Fractional Boole Type Inequalities for Differentiable s-Convex Functions

W. Kaidouchi [1*], M. Benssaad [2] and B. Meftah [2]

[1] *Higher Normal School of Technological Education-Skikda, Department of Mathematics and Informatics. Azzaba, Algeria.*
[2] *Department of Mathematics, Faculty of Mathematics, Computer Science and Material Sciences, University 8 Mai 1945, Guelma, Algeria.*

Received: March 6, 2025; Revised: February 10, 2026

Abstract: We introduce a new identity involving five-point Newton-Cotes inequalities called Boole's inequalities. By employing this identity, we establish some Boole-type inequalities for functions whose first derivatives are s-convex via Riemann-Liouville fractional integral operators. The results provide a generalization of classical inequalities by using tools from fractional calculus. Additionally, we present applications that highlight the utility and relevance of the obtained inequalities in various mathematical contexts.

Keywords: *Boole's inequality, s-convex functions, Hölder inequality, Riemann-Liouville fractional integrals.*

Mathematics Subject Classification (2020): 26D10, 26D15, 26A51, 70K45, 70K75.

1 Introduction

Let $I \subset \mathbb{R}$ be an interval. A function $\eth : I \to \mathbb{R}$ is said to be convex if

$$\eth(\varrho x + (1-\varrho)y) \leq \varrho\eth(x) + (1-\varrho)\eth(y)$$

holds for all $x, y \in I$ and $\varrho \in [0,1]$.

The first finding between convex functions and integrals was the Hermite–Hadamard inequality, which can be stated as follows: for every convex function $\eth$ on the interval $[\xi_1, \xi_2]$ with $\xi_1 < \xi_2$, we have

$$\eth\left(\tfrac{\xi_1+\xi_2}{2}\right) \leq \tfrac{1}{\xi_2-\xi_1}\int_{\xi_1}^{\xi_2} \eth(x)\,dx \leq \tfrac{\eth(\xi_1)+\eth(\xi_2)}{2}. \tag{1}$$

* Corresponding author: mailto:kaidouchi.wahida@gmail.com

© 2026 InforMath Publishing Group/1562-8353 (print)/1813-7385 (online)/http://e-ndst.kiev.ua

The above inequality has many advantages and is broadly utilized, especially in numerical integration, operator theory, approximation theory, and engineering problems. Because of its numerous applications, mathematicians have extensively worked on it and obtained numerous results related to (1), see [3, 5, 6, 10, 15, 24, 26].

The idea of convexity has been generalized in different ways. One of these generalizations is presented by Breckner, called the s-convexity and declared as follows.

A nonnegative function $\eth : I \subset [0,\infty) \to \mathbb{R}$ is said to be s-convex in the second sense for some fixed $s \in (0,1]$ if

$$\eth(\varrho x + (1-\varrho)y) \ \leq \varrho^s \eth(x) + (1-\varrho)^s \eth(y)$$

holds for all $x, y \in I$ and $\varrho \in [0,1]$.

Dragomir and Fitzpatrick [8] proved the following variant of inequality (1) which holds for s-convex functions in the second sense. For every positive and s-convex function in the second sense $\eth$ on the interval $[\xi_1, \xi_2]$ with $\xi_1 < \xi_2$, we have

$$2^{s-1}\eth\left(\tfrac{\xi_1+\xi_2}{2}\right) \leq \tfrac{1}{\xi_2-\xi_1}\int_{\xi_1}^{\xi_2} \eth(x)\,dx \leq \tfrac{\eth(\xi_1)+\eth(\xi_2)}{s+1}. \tag{2}$$

Fractional calculus has become an important topic in mathematical analysis nowdays, and has attracted the attention of many researchers due to its wide applications in pure and applied mathematics as well as other sciences. Indeed, it provides an excellent tool for the description of memory and heritable properties of various materials and processes. In the literature, several fractional operators have been introduced [1, 7, 16, 17, 25], however the most used is that attributed to Liouville.

The Riemann-Liouville operator is defined as follows.

Definition 1.1 Let $\eth \in L^1[\xi_1, \xi_2]$. The Riemann-Liouville fractional integrals $I^{\alpha}_{\xi_1^+}\eth$ and $I^{\alpha}_{\xi_2^-}\eth$ of order $\alpha > 0$ with $\xi_1 \geq 0$ are defined by

$$\begin{aligned} I^{\alpha}_{\xi_1^+}\eth(x) &= \tfrac{1}{\Gamma(\alpha)}\int_{\xi_1}^{x} (x-\varrho)^{\alpha-1}\eth(\varrho)d\varrho, \quad x > \xi_1, \\ I^{\alpha}_{\xi_2^-}\eth(x) &= \tfrac{1}{\Gamma(\alpha)}\int_{x}^{\xi_2} (\varrho-x)^{\alpha-1}\eth(\varrho)d\varrho, \quad \xi_2 > x, \end{aligned}$$

respectively, where $\Gamma(\alpha) = \int_0^{\infty} e^{-\varrho}\varrho^{\alpha-1}d\varrho$ is the Gamma function and $I^0_{\xi_1^+}\eth(x) = I^0_{\xi_2^-}\eth(x) = \eth(x)$.

For papers dealing with the applications and other characteristics of convex functions and their variant forms via various types of fractional integral operators, we refer the readers to [2, 4, 5, 9, 12, 13, 14, 18-23, 27] and the references therein.

In this paper, we propose to study one of the five-point Newton-Cotes inequalities given as follows:

$$\left|\tfrac{7\eth(\xi_1)+32\eth\left(\frac{\xi_1+3\xi_2}{4}\right)+12\eth\left(\frac{\xi_1+\xi_2}{2}\right)+32\eth\left(\frac{3\xi_1+\xi_2}{4}\right)+7\eth(\xi_2)}{90} - \tfrac{1}{\xi_2-\xi_1}\int_{\xi_1}^{\xi_2}\eth(u)\,du\right| \leq \tfrac{4(\xi_2-\xi_1)^6}{945}\left\|\eth^{(6)}\right\|,$$

where $\eth$ is a 6-times differentiable mapping and $\left\|\eth^{(6)}\right\| = \sup_{x\in[\xi_1,\xi_2]} \left|\eth^{(6)}(x)\right| < +\infty$ (see [11]). For this, we first prove a new identity involving Riemann-Liouville fractional integrals. By using this identity, we establish some new fractional Boole-type integral inequalities for functions whose first derivatives are s-convex in the second sense. We end this work by some applications to quadrature formulas and inequalities for special means.

2 Main Results

Before giving our main results, let us recall some special functions.

Definition 2.1 For any complex number and non-positive integers x, y such that $Re(x) > 0$ and $Re(y) > 0$, the Beta function is defined by

$$B(x,y) = \int_0^1 \varrho^{x-1}(1-\varrho)^{y-1}\, d\varrho.$$

The definition of the incomplete Beta function is given as follows.

Definition 2.2 For any complex number and non-positive integers x, y such that $Re(x) > 0$ and $Re(y) > 0$, we have

$$B_{\xi_1}(x,y) = \int_0^{\xi_1} \varrho^{x-1}(1-\varrho)^{y-1}\, d\varrho, \quad \xi_1 < 1.$$

Definition 2.3 The hypergeometric function is defined for $Re(c) > Re(\xi_2) > 0$ and $|z| < 1$, as follows:

$${}_2F_1(\xi_1,\xi_2,c,z) = \frac{1}{B(\xi_2, c-\xi_2)} \int_0^1 \varrho^{\xi_2-1}(1-\varrho)^{c-\xi_2-1}(1-z\varrho)^{-\xi_1} d\varrho,$$

where $c > \xi_2 > 0, |z| < 1$ and $B(.,.)$ is the Beta function.

Lemma 2.1 *Let $\eth : I \subset \mathbb{R} \to \mathbb{R}$ be a differentiable function on I°, $\xi_1, \xi_2 \in I^\circ$ with $\xi_1 < \xi_2$, and $\eth' \in L^1[\xi_1, \xi_2]$, then the following equality holds:*

$$\begin{aligned} &\frac{7\eth(\xi_1)+32\eth\left(\frac{\xi_1+3\xi_2}{4}\right)+12\eth\left(\frac{\xi_1+\xi_2}{2}\right)+32\eth\left(\frac{3\xi_1+\xi_2}{4}\right)+7\eth(\xi_2)}{90} - \frac{4^{\alpha-1}\Gamma(\alpha+1)}{(\xi_2-\xi_1)^\alpha}\mathcal{B}\left(\xi_1,\xi_2,I^\alpha\eth\right) \\ = \;& \frac{\xi_2-\xi_1}{16}\left(\int_0^1 \left(\varrho^\alpha - \frac{14}{45}\right)\eth'\left((1-\varrho)\,\xi_1 + \varrho\frac{3\xi_1+\xi_2}{4}\right) d\varrho\right. \end{aligned}$$

$$-\int_0^1 \left((1-\varrho)^\alpha - \tfrac{4}{15}\right) \eth'\left((1-\varrho)\tfrac{3\xi_1+\xi_2}{4} + \varrho\tfrac{\xi_1+\xi_2}{2}\right) d\varrho$$
$$+\int_0^1 \left(\varrho^\alpha - \tfrac{4}{15}\right) \eth'\left((1-\varrho)\tfrac{\xi_1+\xi_2}{2} + \varrho\tfrac{\xi_1+3\xi_2}{4}\right) d\varrho$$
$$-\int_0^1 \left((1-\varrho)^\alpha - \tfrac{14}{45}\right) \eth'\left((1-\varrho)\tfrac{\xi_1+3\xi_2}{4} + \varrho\xi_2\right) d\varrho\Bigg),$$

where

$$\mathcal{B}\left(\xi_1,\xi_2,I^\alpha\eth\right) =$$
$$= I^\alpha_{\left(\frac{3\xi_1+\xi_2}{4}\right)^-}\eth(\xi_1) + I^\alpha_{\left(\frac{3\xi_1+\xi_2}{4}\right)^+}\eth(\tfrac{\xi_1+\xi_2}{2}) + I^\alpha_{\left(\frac{\xi_1+3\xi_2}{4}\right)^-}\eth(\tfrac{\xi_1+\xi_2}{2}) + I^\alpha_{\left(\frac{\xi_1+3\xi_2}{4}\right)^+}\eth(\xi_2). \quad (3)$$

Proof. Let

$$I = I_1 - I_2 + I_3 - I_4, \quad (4)$$

where

$$I_1 = \int_0^1 \left(\varrho^\alpha - \tfrac{14}{45}\right) \eth'\left((1-\varrho)\xi_1 + \varrho\tfrac{3\xi_1+\xi_2}{4}\right) d\varrho,$$
$$I_2 = \int_0^1 \left((1-\varrho)^\alpha - \tfrac{4}{15}\right) \eth'\left((1-\varrho)\tfrac{3\xi_1+\xi_2}{4} + \varrho\tfrac{\xi_1+\xi_2}{2}\right) d\varrho,$$
$$I_3 = \int_0^1 \left(\varrho^\alpha - \tfrac{4}{15}\right) \eth'\left((1-\varrho)\tfrac{\xi_1+\xi_2}{2} + \varrho\tfrac{\xi_1+3\xi_2}{4}\right) d\varrho$$

and

$$I_4 = \int_0^1 \left((1-\varrho)^\alpha - \tfrac{14}{45}\right) \eth'\left((1-\varrho)\tfrac{\xi_1+3\xi_2}{4} + \varrho\xi_2\right) d\varrho.$$

Integrating by parts I_1, we get

$$I_1 = \tfrac{4}{\xi_2-\xi_1}\left(\varrho^\alpha - \tfrac{14}{45}\right)\eth\left((1-\varrho)\xi_1 + \varrho\tfrac{3\xi_1+\xi_2}{4}\right)\Big|_{\varrho=0}^{\varrho=1} - \tfrac{4\alpha}{\xi_2-\xi_1}\int_0^1 \varrho^{\alpha-1}\eth\left((1-\varrho)\xi_1 + \varrho\tfrac{3\xi_1+\xi_2}{4}\right) d\varrho$$
$$= \tfrac{124}{45(\xi_2-\xi_1)}\eth\left(\tfrac{3\xi_1+\xi_2}{4}\right) + \tfrac{56}{45(\xi_2-\xi_1)}\eth(\xi_1) - \tfrac{4\alpha}{\xi_2-\xi_1}\int_0^1 \varrho^{\alpha-1}\eth\left((1-\varrho)\xi_1 + \varrho\tfrac{3\xi_1+\xi_2}{4}\right) d\varrho$$
$$= \tfrac{124}{45(\xi_2-\xi_1)}\eth\left(\tfrac{3\xi_1+\xi_2}{4}\right) + \tfrac{56}{45(\xi_2-\xi_1)}\eth(\xi_1) - \tfrac{4^{\alpha+1}\alpha}{(\xi_2-\xi_1)^{\alpha+1}}\int_{\xi_1}^{\frac{3\xi_1+\xi_2}{4}} (u-\xi_1)^{\alpha-1}\eth(u)\, du$$
$$= \tfrac{124}{45(\xi_2-\xi_1)}\eth\left(\tfrac{3\xi_1+\xi_2}{4}\right) + \tfrac{56}{45(\xi_2-\xi_1)}\eth(\xi_1) - \tfrac{4^{\alpha+1}\Gamma(\alpha+1)}{(\xi_2-\xi_1)^{\alpha+1}} I^\alpha_{\left(\frac{3\xi_1+\xi_2}{4}\right)^-}\eth(\xi_1). \quad (5)$$

Similarly, I_2, I_3 and I_4 can be found as

$$\begin{aligned} I_2 &= -\tfrac{16}{15(\xi_2-\xi_1)}\eth\left(\tfrac{\xi_1+\xi_2}{2}\right)-\tfrac{44}{15(\xi_2-\xi_1)}\eth\left(\tfrac{3\xi_1+\xi_2}{4}\right)+\tfrac{4^{\alpha+1}\Gamma(\alpha+1)}{(\xi_2-\xi_1)^{\alpha+1}}I^{\alpha}_{\left(\frac{3\xi_1+\xi_2}{4}\right)^{+}}\eth(\tfrac{\xi_1+\xi_2}{2}), \quad (6)\\ I_3 &= \tfrac{44}{15(\xi_2-\xi_1)}\eth\left(\tfrac{\xi_1+3\xi_2}{4}\right)+\tfrac{16}{15(\xi_2-\xi_1)}\eth\left(\tfrac{\xi_1+\xi_2}{2}\right)-\tfrac{4^{\alpha+1}\Gamma(\alpha+1)}{(\xi_2-\xi_1)^{\alpha+1}}I^{\alpha}_{\left(\frac{\xi_1+3\xi_2}{4}\right)^{-}}\eth(\tfrac{\xi_1+\xi_2}{2}), \quad (7)\\ I_4 &= -\tfrac{56}{45(\xi_2-\xi_1)}\eth(\xi_2)-\tfrac{124}{45(\xi_2-\xi_1)}\eth\left(\tfrac{\xi_1+3\xi_2}{4}\right)+\tfrac{4^{\alpha+1}\Gamma(\alpha+1)}{(\xi_2-\xi_1)^{\alpha+1}}I^{\alpha}_{\left(\frac{\xi_1+3\xi_2}{4}\right)^{+}}\eth(\xi_2). \quad (8) \end{aligned}$$

Substituting (5)-(8) into (4), and then multiplying the resulting equality by $\frac{\xi_2-\xi_1}{16}$, we get the desired result.

Theorem 2.1 *Let $\eth:[\xi_1,\xi_2]\to\mathbb{R}$ be a differentiable function on (ξ_1,ξ_2) such that $\eth'\in L^1[\xi_1,\xi_2]$ with $0\le\xi_1<\xi_2$. If $|\eth'|$ is s-convex in the second sense for some fixed $s\in(0,1]$, then we have*

$$\begin{aligned} &\left|\tfrac{7\eth(\xi_1)+32\eth\left(\frac{\xi_1+3\xi_2}{4}\right)+12\eth\left(\frac{\xi_1+\xi_2}{2}\right)+32\eth\left(\frac{3\xi_1+\xi_2}{4}\right)+7\eth(\xi_2)}{90}-\tfrac{4^{\alpha-1}\Gamma(\alpha+1)}{(\xi_2-\xi_1)^{\alpha}}\mathcal{B}\left(\xi_1,\xi_2,I^{\alpha}\eth\right)\right|\\ \le\ &\tfrac{\xi_2-\xi_1}{16}\left(\left(\tfrac{14}{45(s+1)}\left(1-2\left(1-\left(\tfrac{14}{45}\right)^{\frac{1}{\alpha}}\right)^{s+1}\right)-\chi\left(\alpha,s,\tfrac{14}{45}\right)\right)\left(|\eth'(\xi_1)|+|\eth'(\xi_2)|\right)\right.\\ &+\tfrac{2}{(s+1)(\alpha+s+1)}\left(\tfrac{32(s+1)-13\alpha}{45}+\tfrac{\alpha(14)^{1+\frac{s+1}{\alpha}}+\alpha(12)^{1+\frac{s+1}{\alpha}}}{(45)^{1+\frac{s+1}{\alpha}}}\right)\times\\ &\times\left(\left|\eth'\left(\tfrac{3\xi_1+\xi_2}{4}\right)\right|+\left|\eth'\left(\tfrac{\xi_1+3\xi_2}{4}\right)\right|\right)\\ &\left.+2\left(\tfrac{4}{15(s+1)}\left(1-2\left(1-\left(\tfrac{4}{15}\right)^{\frac{1}{\alpha}}\right)^{s+1}\right)-\chi\left(\alpha,s,\tfrac{4}{15}\right)\right)\left|\eth'\left(\tfrac{\xi_1+\xi_2}{2}\right)\right|\right), \end{aligned}$$

where $\alpha>0,\mathcal{B}\left(\xi_1,\xi_2,I^{\alpha}\eth\right)$ is defined by (3) and

$$\chi(\alpha,s,x)=B_{x^{\frac{1}{\alpha}}}(\alpha+1,s+1)-B_{1-x^{\frac{1}{\alpha}}}(s+1,\alpha+1). \quad (9)$$

Proof. From Lemma 2.1, the modulus and s-convexity of $|\eth'|$, we have

$$\begin{aligned} &\left|\tfrac{7\eth(\xi_1)+32\eth\left(\frac{\xi_1+3\xi_2}{4}\right)+12\eth\left(\frac{\xi_1+\xi_2}{2}\right)+32\eth\left(\frac{3\xi_1+\xi_2}{4}\right)+7\eth(\xi_2)}{90}-\tfrac{4^{\alpha-1}\Gamma(\alpha+1)}{(\xi_2-\xi_1)^{\alpha}}\mathcal{B}\left(\xi_1,\xi_2,I^{\alpha}\eth\right)\right|\\ \le\ &\tfrac{\xi_2-\xi_1}{16}\left(\int_0^1\left|\varrho^{\alpha}-\tfrac{14}{45}\right|\left|\eth'\left((1-\varrho)\xi_1+\varrho\tfrac{3\xi_1+\xi_2}{4}\right)\right|d\varrho\right.\\ &\left.+\int_0^1\left|(1-\varrho)^{\alpha}-\tfrac{4}{15}\right|\left|\eth'\left((1-\varrho)\tfrac{3\xi_1+\xi_2}{4}+\varrho\tfrac{\xi_1+\xi_2}{2}\right)\right|d\varrho\right. \end{aligned}$$

$$
\begin{aligned}
&+\int_0^1 \left|\varrho^\alpha-\tfrac{4}{15}\right|\left|\partial'\left((1-\varrho)\,\tfrac{\xi_1+\xi_2}{2}+\varrho\tfrac{\xi_1+3\xi_2}{4}\right)\right|d\varrho\\
&+\int_0^1 \left|(1-\varrho)^\alpha-\tfrac{14}{45}\right|\left|\partial'\left((1-\varrho)\,\tfrac{\xi_1+3\xi_2}{4}+\varrho\xi_2\right)\right|d\varrho\Bigg)\\
\leq\ & \tfrac{\xi_2-\xi_1}{16}\left(\left(\tfrac{14}{45(s+1)}\left(1-2\left(1-\left(\tfrac{14}{45}\right)^{\frac{1}{\alpha}}\right)^{s+1}\right)-\chi\left(\alpha,s,\tfrac{14}{45}\right)\right)\left(|\partial'(\xi_1)|+|\partial'(\xi_2)|\right)\right.\\
&+\tfrac{2}{(s+1)(\alpha+s+1)}\left(\tfrac{32(s+1)-13\alpha}{45}+\tfrac{\alpha(14)^{1+\frac{s+1}{\alpha}}+\alpha(12)^{1+\frac{s+1}{\alpha}}}{(45)^{1+\frac{s+1}{\alpha}}}\right)\times\\
&\times\left(\left|\partial'\left(\tfrac{3\xi_1+\xi_2}{4}\right)\right|+\left|\partial'\left(\tfrac{\xi_1+3\xi_2}{4}\right)\right|\right)\\
&\left.+2\left(\tfrac{4}{15(s+1)}\left(1-2\left(1-\left(\tfrac{4}{15}\right)^{\frac{1}{\alpha}}\right)^{s+1}\right)-\chi\left(\alpha,s,\tfrac{4}{15}\right)\right)\left|\partial'\left(\tfrac{\xi_1+\xi_2}{2}\right)\right|\right),
\end{aligned}
$$

where we have used

$$\int_0^1 \left|\varrho^\alpha-\tfrac{14}{45}\right|(1-\varrho)^s\,d\varrho = \tfrac{14}{45(s+1)}\left(1-2\left(1-\left(\tfrac{14}{45}\right)^{\frac{1}{\alpha}}\right)^{s+1}\right)-\chi\left(\alpha,s,\tfrac{14}{45}\right), \quad (10)$$

$$\int_0^1 \left|\varrho^\alpha-\tfrac{14}{45}\right|\varrho^s d\varrho = \tfrac{31(s+1)-14\alpha}{45(s+1)(\alpha+s+1)}+\tfrac{2\alpha}{(s+1)(\alpha+s+1)}\left(\tfrac{14}{45}\right)^{1+\frac{s+1}{\alpha}}, \quad (11)$$

$$\int_0^1 \left|(1-\varrho)^\alpha-\tfrac{4}{15}\right|(1-\varrho)^s\,d\varrho = \tfrac{11(s+1)-4\alpha}{15(s+1)(\alpha+s+1)}+\tfrac{2\alpha}{(s+1)(\alpha+s+1)}\left(\tfrac{4}{15}\right)^{1+\frac{s+1}{\alpha}}, \quad (12)$$

$$\int_0^1 \left|(1-\varrho)^\alpha-\tfrac{4}{15}\right|\varrho^s d\varrho = \tfrac{4}{15(s+1)}\left(1-2\left(1-\left(\tfrac{4}{15}\right)^{\frac{1}{\alpha}}\right)^{s+1}\right)-\chi\left(\alpha,s,\tfrac{4}{15}\right). \quad (13)$$

The proof is finished.

Remark 2.1 By simple calculation, we easily obtain

$$\chi(1,s,x)=\tfrac{1}{(s+1)(s+2)}+\tfrac{2}{s+2}(1-x)^{s+2}-\tfrac{2}{s+1}(1-x)^{s+1},$$

$$\chi(\alpha,1,x)=\tfrac{2}{\alpha+1}x^{1+\frac{1}{\alpha}}-\tfrac{2}{\alpha+2}x^{1+\frac{2}{\alpha}}-\tfrac{1}{(\alpha+1)(\alpha+2)}, \quad \chi(1,1,x)=\tfrac{6x^2-4x^3-1}{6}.$$

Corollary 2.1 *In Theorem 2.1, if we take $\alpha=1$, then we obtain*

$$
\begin{aligned}
&\left|\tfrac{7\partial(\xi_1)+32\partial\left(\frac{\xi_1+3\xi_2}{4}\right)+12\partial\left(\frac{\xi_1+\xi_2}{2}\right)+32\partial\left(\frac{3\xi_1+\xi_2}{4}\right)+7\partial(\xi_2)}{90}-\tfrac{1}{\xi_2-\xi_1}\int_{\xi_1}^{\xi_2}\partial(w)\,dw\right|\\
\leq\ & \tfrac{\xi_2-\xi_1}{16}\left(\left(\tfrac{14s-17}{45(s+1)(s+2)}+\tfrac{2}{(s+1)(s+2)}\left(\tfrac{31}{45}\right)^{s+2}\right)\left(|\partial'(\xi_1)|+|\partial'(\xi_2)|\right)\right.\\
&+\tfrac{2}{(s+1)(s+2)}\left(\tfrac{32s+19}{45}+\tfrac{(14)^{s+2}+(12)^{s+2}}{(45)^{s+2}}\right)\left(\left|\partial'\left(\tfrac{3\xi_1+\xi_2}{4}\right)\right|+\left|\partial'\left(\tfrac{\xi_1+3\xi_2}{4}\right)\right|\right)\\
&\left.+2\left(\tfrac{4s-7}{15(s+1)(s+2)}+\tfrac{2}{(s+1)(s+2)}\left(\tfrac{11}{15}\right)^{s+2}\right)\left|\partial'\left(\tfrac{\xi_1+\xi_2}{2}\right)\right|\right).
\end{aligned}
$$

Corollary 2.2 *In Theorem 2.1, if we take $s=1$, then we obtain*

$$\begin{aligned}
&\left|\frac{7\eth(\xi_1)+32\eth\left(\frac{\xi_1+3\xi_2}{4}\right)+12\eth\left(\frac{\xi_1+\xi_2}{2}\right)+32\eth\left(\frac{3\xi_1+\xi_2}{4}\right)+7\eth(\xi_2)}{90}-\frac{4^{\alpha-1}\Gamma(\alpha+1)}{(\xi_2-\xi_1)^{\alpha}}\mathcal{B}\left(\xi_1,\xi_2,I^{\alpha}\eth\right)\right| \\
\leq\ & \frac{\xi_2-\xi_1}{16}\left(\left(\frac{45-7(\alpha+1)(\alpha+2)}{45(\alpha+1)(\alpha+2)}+\frac{2\alpha}{\alpha+1}\left(\frac{14}{45}\right)^{1+\frac{1}{\alpha}}-\frac{\alpha}{\alpha+2}\left(\frac{14}{45}\right)^{1+\frac{2}{\alpha}}\right)\left(\left|\eth'(\xi_1)\right|+\left|\eth'(\xi_2)\right|\right)\right. \\
&+\frac{\alpha}{45(\alpha+2)}\left(\frac{64-13\alpha}{\alpha}+\frac{(14)^{1+\frac{2}{\alpha}}+(12)^{1+\frac{2}{\alpha}}}{(45)^{\frac{2}{\alpha}}}\right)\left(\left|\eth'\left(\frac{3\xi_1+\xi_2}{4}\right)\right|+\left|\eth'\left(\frac{\xi_1+3\xi_2}{4}\right)\right|\right) \\
&\left.+2\left(\frac{15-2(\alpha+1)(\alpha+2)}{15(\alpha+1)(\alpha+2)}+\frac{2\alpha}{\alpha+1}\left(\frac{4}{15}\right)^{1+\frac{1}{\alpha}}-\frac{\alpha}{\alpha+2}\left(\frac{4}{15}\right)^{1+\frac{2}{\alpha}}\right)\left|\eth'\left(\frac{\xi_1+\xi_2}{2}\right)\right|\right).
\end{aligned}$$

Corollary 2.3 *In Theorem 2.1, if we take $\alpha=s=1$, then we obtain*

$$\begin{aligned}
&\left|\frac{7\eth(\xi_1)+32\eth\left(\frac{\xi_1+3\xi_2}{4}\right)+12\eth\left(\frac{\xi_1+\xi_2}{2}\right)+32\eth\left(\frac{3\xi_1+\xi_2}{4}\right)+7\eth(\xi_2)}{90}-\frac{1}{\xi_2-\xi_1}\int_{\xi_1}^{\xi_2}\eth(w)\,dw\right| \\
\leq\ & \frac{239(\xi_2-\xi_1)}{3240}\times \\
&\left(\frac{53507\left|\eth'(\xi_1)\right|+215494\left|\eth'\left(\frac{3\xi_1+\xi_2}{4}\right)\right|+107298\left|\eth'\left(\frac{\xi_1+\xi_2}{2}\right)\right|+215494\left|\eth'\left(\frac{3\xi_1+\xi_2}{4}\right)\right|+53507\left|\eth'(\xi_2)\right|}{645300}\right).
\end{aligned}$$

Theorem 2.2 *Let $\eth:[\xi_1,\xi_2]\to\mathbb{R}$ be a differentiable function on (ξ_1,ξ_2) such that $\eth'\in L^1[\xi_1,\xi_2]$ with $0\leq\xi_1<\xi_2$. If $|\eth'|^q$ is s-convex in the second sense for some fixed $s\in(0,1]$ and $q>1$ with $\frac{1}{q}+\frac{1}{p}=1$, then we have*

$$\begin{aligned}
&\left|\frac{7\eth(\xi_1)+32\eth\left(\frac{\xi_1+3\xi_2}{4}\right)+12\eth\left(\frac{\xi_1+\xi_2}{2}\right)+32\eth\left(\frac{3\xi_1+\xi_2}{4}\right)+7\eth(\xi_2)}{90}-\frac{4^{\alpha-1}\Gamma(\alpha+1)}{(\xi_2-\xi_1)^{\alpha}}\mathcal{B}\left(\xi_1,\xi_2,I^{\alpha}\eth\right)\right| \\
\leq\ & \frac{\xi_2-\xi_1}{16}\left(\left(\left(\frac{14}{45}\right)^{p+\frac{1}{\alpha}}\frac{1}{\alpha}B\left(\frac{1}{\alpha},p+1\right)+\left(\frac{31}{45}\right)^{p+\frac{1}{\alpha}}\frac{{}_2F_1\left(1-\frac{1}{\alpha},1,p+2;\frac{31}{45}\right)}{\alpha(p+1)}\right)^{\frac{1}{p}}\right. \\
&\times\left(\left(\frac{\left|\eth'(\xi_1)\right|^q+\left|\eth'\left(\frac{3\xi_1+\xi_2}{4}\right)\right|^q}{s+1}\right)^{\frac{1}{q}}+\left(\frac{\left|\eth'\left(\frac{\xi_1+3\xi_2}{4}\right)\right|^q+\left|\eth'(\xi_2)\right|^q}{s+1}\right)^{\frac{1}{q}}\right) \\
&+\left(\left(\frac{4}{15}\right)^{p+\frac{1}{\alpha}}\frac{1}{\alpha}B\left(\frac{1}{\alpha},p+1\right)+\left(\frac{11}{15}\right)^{p+\frac{1}{\alpha}}\frac{{}_2F_1\left(1-\frac{1}{\alpha},1,p+2;\frac{11}{15}\right)}{\alpha(p+1)}\right)^{\frac{1}{p}} \\
&\left.\times\left(\left(\frac{\left|\eth'\left(\frac{3\xi_1+\xi_2}{4}\right)\right|^q+\left|\eth'\left(\frac{\xi_1+\xi_2}{2}\right)\right|^q}{s+1}\right)^{\frac{1}{q}}+\left(\frac{\left|\eth'\left(\frac{\xi_1+\xi_2}{2}\right)\right|^q+\left|\eth'\left(\frac{\xi_1+3\xi_2}{4}\right)\right|^q}{s+1}\right)^{\frac{1}{q}}\right)\right),
\end{aligned}$$

where $\mathcal{B}\left(\xi_1,\xi_2,I^{\alpha}\eth\right)$ is defined by (3) and B and ${}_2F_1$ are the Beta and hypergeometric functions, respectively.

Proof. From Lemma 2.1, the modulus, Hölder's inequality and s-convexity of

$|\partial'|^q$, we have

$$
\begin{aligned}
&\left|\frac{7\partial(\xi_1)+32\partial\left(\frac{\xi_1+3\xi_2}{4}\right)+12\partial\left(\frac{\xi_1+\xi_2}{2}\right)+32\partial\left(\frac{3\xi_1+\xi_2}{4}\right)+7\partial(\xi_2)}{90}-\frac{4^{\alpha-1}\Gamma(\alpha+1)}{(\xi_2-\xi_1)^{\alpha}}\mathcal{B}\left(\xi_1,\xi_2,I^{\alpha}\partial\right)\right| \\
\leq\ & \frac{\xi_2-\xi_1}{16}\left(\left(\int_0^1\left|\varrho^{\alpha}-\tfrac{14}{45}\right|^p d\varrho\right)^{\frac{1}{p}}\left(\int_0^1\left|\partial'\left((1-\varrho)\,\xi_1+\varrho\tfrac{3\xi_1+\xi_2}{4}\right)\right|^q d\varrho\right)^{\frac{1}{q}}\right. \\
&+\left(\int_0^1\left|(1-\varrho)^{\alpha}-\tfrac{4}{15}\right|^p d\varrho\right)^{\frac{1}{p}}\left(\int_0^1\left|\partial'\left((1-\varrho)\,\tfrac{3\xi_1+\xi_2}{4}+\varrho\tfrac{\xi_1+\xi_2}{2}\right)\right|^q d\varrho\right)^{\frac{1}{q}} \\
&+\left(\int_0^1\left|\varrho^{\alpha}-\tfrac{4}{15}\right|^p d\varrho\right)^{\frac{1}{p}}\left(\int_0^1\left|\partial'\left((1-\varrho)\,\tfrac{\xi_1+\xi_2}{2}+\varrho\tfrac{\xi_1+3\xi_2}{4}\right)\right|^q d\varrho\right)^{\frac{1}{q}} \\
&\left.+\left(\int_0^1\left|(1-\varrho)^{\alpha}-\tfrac{14}{45}\right|^p d\varrho\right)^{\frac{1}{p}}\left(\int_0^1\left|\partial'\left((1-\varrho)\,\tfrac{\xi_1+3\xi_2}{4}+\varrho\xi_2\right)\right|^q d\varrho\right)^{\frac{1}{q}}\right) \\
=\ & \frac{\xi_2-\xi_1}{16}\left(\left(\left(\tfrac{14}{45}\right)^{p+\frac{1}{\alpha}}\tfrac{1}{\alpha}B\left(\tfrac{1}{\alpha},p+1\right)+\left(\tfrac{31}{45}\right)^{p+\frac{1}{\alpha}}\tfrac{{}_2F_1\left(1-\frac{1}{\alpha},1,p+2;\frac{31}{45}\right)}{\alpha(p+1)}\right)^{\frac{1}{p}}\right. \\
&\times\left(\left(\frac{\left|\partial'(\xi_1)\right|^q+\left|\partial'\left(\frac{3\xi_1+\xi_2}{4}\right)\right|^q}{s+1}\right)^{\frac{1}{q}}+\left(\frac{\left|\partial'\left(\frac{\xi_1+3\xi_2}{4}\right)\right|^q+\left|\partial'(\xi_2)\right|^q}{s+1}\right)^{\frac{1}{q}}\right) \\
&+\left(\left(\tfrac{4}{15}\right)^{p+\frac{1}{\alpha}}\tfrac{1}{\alpha}B\left(\tfrac{1}{\alpha},p+1\right)+\left(\tfrac{11}{15}\right)^{p+\frac{1}{\alpha}}\tfrac{{}_2F_1\left(1-\frac{1}{\alpha},1,p+2;\frac{11}{15}\right)}{\alpha(p+1)}\right)^{\frac{1}{p}} \\
&\left.\times\left(\left(\frac{\left|\partial'\left(\frac{3\xi_1+\xi_2}{4}\right)\right|^q+\left|\partial'\left(\frac{\xi_1+\xi_2}{2}\right)\right|^q}{s+1}\right)^{\frac{1}{q}}+\left(\frac{\left|\partial'\left(\frac{\xi_1+\xi_2}{2}\right)\right|^q+\left|\partial'\left(\frac{\xi_1+3\xi_2}{4}\right)\right|^q}{s+1}\right)^{\frac{1}{q}}\right)\right),
\end{aligned}
$$

where we have used the fact that

$$
\begin{aligned}
\int_0^1\left|\varrho^{\alpha}-\tfrac{14}{45}\right|^p d\varrho &= \int_0^{\left(\frac{14}{45}\right)^{\frac{1}{\alpha}}}\left(\tfrac{14}{45}-\varrho^{\alpha}\right)^p d\varrho+\int_{\left(\frac{14}{45}\right)^{\frac{1}{\alpha}}}^1\left(\varrho^{\alpha}-\tfrac{14}{45}\right)^p d\varrho \\
&= \left(\tfrac{14}{45}\right)^{p+\frac{1}{\alpha}}\tfrac{1}{\alpha}B\left(\tfrac{1}{\alpha},p+1\right)+\left(\tfrac{31}{45}\right)^{p+\frac{1}{\alpha}}\tfrac{{}_2F_1\left(1-\frac{1}{\alpha},1,p+2;\frac{31}{45}\right)}{\alpha(p+1)}
\end{aligned}
$$

and

$$
\int_0^1\left|\varrho^{\alpha}-\tfrac{4}{15}\right|^p d\varrho=\left(\tfrac{4}{15}\right)^{p+\frac{1}{\alpha}}\tfrac{1}{\alpha}B\left(\tfrac{1}{\alpha},p+1\right)+\left(\tfrac{11}{15}\right)^{p+\frac{1}{\alpha}}\tfrac{{}_2F_1\left(1-\frac{1}{\alpha},1,p+2;\frac{11}{15}\right)}{\alpha(p+1)}.
$$

The proof is finished.

Corollary 2.4 *In Theorem 2.2, if we take $\alpha = 1$, we obtain*

$$\begin{aligned}
&\left|\frac{7\eth(\xi_1)+32\eth\left(\frac{\xi_1+3\xi_2}{4}\right)+12\eth\left(\frac{\xi_1+\xi_2}{2}\right)+32\eth\left(\frac{3\xi_1+\xi_2}{4}\right)+7\eth(\xi_2)}{90}-\frac{1}{\xi_2-\xi_1}\int_{\xi_1}^{\xi_2}\eth(w)\,dw\right| \\
\leq\ & \frac{\xi_2-\xi_1}{16}\left(\frac{1}{p+1}\right)^{\frac{1}{p}}\left(\left(\frac{14^{p+1}+31^{p+1}}{45^{p+1}}\right)^{\frac{1}{p}}\left(\left(\frac{\left|\eth'(\xi_1)\right|^q+\left|\eth'\left(\frac{3\xi_1+\xi_2}{4}\right)\right|^q}{s+1}\right)^{\frac{1}{q}}\right.\right. \\
&+\left.\left(\frac{\left|\eth'\left(\frac{\xi_1+3\xi_2}{4}\right)\right|^q+\left|\eth'(\xi_2)\right|^q}{s+1}\right)^{\frac{1}{q}}\right)+\left(\frac{4^{p+1}+11^{p+1}}{15^{p+1}}\right)^{\frac{1}{p}} \\
&\times\left.\left(\left(\frac{\left|\eth'\left(\frac{3\xi_1+\xi_2}{4}\right)\right|^q+\left|\eth'\left(\frac{\xi_1+\xi_2}{2}\right)\right|^q}{s+1}\right)^{\frac{1}{q}}+\left(\frac{\left|\eth'\left(\frac{\xi_1+\xi_2}{2}\right)\right|^q+\left|\eth'\left(\frac{\xi_1+3\xi_2}{4}\right)\right|^q}{s+1}\right)^{\frac{1}{q}}\right)\right).
\end{aligned}$$

Corollary 2.5 *In Theorem 2.2, if we take $s = 1$, we obtain*

$$\begin{aligned}
&\left|\frac{7\eth(\xi_1)+32\eth\left(\frac{\xi_1+3\xi_2}{4}\right)+12\eth\left(\frac{\xi_1+\xi_2}{2}\right)+32\eth\left(\frac{3\xi_1+\xi_2}{4}\right)+7\eth(\xi_2)}{90}-\frac{4^{\alpha-1}\Gamma(\alpha+1)}{(\xi_2-\xi_1)^{\alpha}}\mathcal{B}\left(\xi_1,\xi_2,I^{\alpha}\eth\right)\right| \\
\leq\ & \frac{\xi_2-\xi_1}{16}\left(\left(\left(\frac{14}{45}\right)^{p+\frac{1}{\alpha}}\frac{1}{\alpha}B\left(\frac{1}{\alpha},p+1\right)+\left(\frac{31}{45}\right)^{p+\frac{1}{\alpha}}\frac{{}_2F_1\left(1-\frac{1}{\alpha},1,p+2;\frac{31}{45}\right)}{\alpha(p+1)}\right)^{\frac{1}{p}}\right. \\
&\times\left(\left(\frac{\left|\eth'(\xi_1)\right|^q+\left|\eth'\left(\frac{3\xi_1+\xi_2}{4}\right)\right|^q}{2}\right)^{\frac{1}{q}}+\left(\frac{\left|\eth'\left(\frac{\xi_1+3\xi_2}{4}\right)\right|^q+\left|\eth'(\xi_2)\right|^q}{2}\right)^{\frac{1}{q}}\right) \\
&+\left(\left(\frac{4}{15}\right)^{p+\frac{1}{\alpha}}\frac{1}{\alpha}B\left(\frac{1}{\alpha},p+1\right)+\left(\frac{11}{15}\right)^{p+\frac{1}{\alpha}}\frac{{}_2F_1\left(1-\frac{1}{\alpha},1,p+2;\frac{11}{15}\right)}{\alpha(p+1)}\right)^{\frac{1}{p}} \\
&\times\left.\left(\left(\frac{\left|\eth'\left(\frac{3\xi_1+\xi_2}{4}\right)\right|^q+\left|\eth'\left(\frac{\xi_1+\xi_2}{2}\right)\right|^q}{2}\right)^{\frac{1}{q}}+\left(\frac{\left|\eth'\left(\frac{\xi_1+\xi_2}{2}\right)\right|^q+\left|\eth'\left(\frac{\xi_1+3\xi_2}{4}\right)\right|^q}{2}\right)^{\frac{1}{q}}\right)\right).
\end{aligned}$$

Corollary 2.6 *In Theorem 2.2, if we take $\alpha = s = 1$, we obtain*

$$\begin{aligned}
&\left|\frac{7\eth(\xi_1)+32\eth\left(\frac{\xi_1+3\xi_2}{4}\right)+12\eth\left(\frac{\xi_1+\xi_2}{2}\right)+32\eth\left(\frac{3\xi_1+\xi_2}{4}\right)+7\eth(\xi_2)}{90}-\frac{1}{\xi_2-\xi_1}\int_{\xi_1}^{\xi_2}\eth(w)\,dw\right| \\
\leq\ & \frac{\xi_2-\xi_1}{16}\left(\frac{1}{p+1}\right)^{\frac{1}{p}}\left(\left(\frac{14^{p+1}+31^{p+1}}{45^{p+1}}\right)^{\frac{1}{p}}\left(\left(\frac{\left|\eth'(\xi_1)\right|^q+\left|\eth'\left(\frac{3\xi_1+\xi_2}{4}\right)\right|^q}{2}\right)^{\frac{1}{q}}\right.\right. \\
&+\left.\left(\frac{\left|\eth'\left(\frac{\xi_1+3\xi_2}{4}\right)\right|^q+\left|\eth'(\xi_2)\right|^q}{2}\right)^{\frac{1}{q}}\right)+\left(\frac{4^{p+1}+11^{p+1}}{15^{p+1}}\right)^{\frac{1}{p}} \\
&\times\left.\left(\left(\frac{\left|\eth'\left(\frac{3\xi_1+\xi_2}{4}\right)\right|^q+\left|\eth'\left(\frac{\xi_1+\xi_2}{2}\right)\right|^q}{2}\right)^{\frac{1}{q}}+\left(\frac{\left|\eth'\left(\frac{\xi_1+\xi_2}{2}\right)\right|^q+\left|\eth'\left(\frac{\xi_1+3\xi_2}{4}\right)\right|^q}{2}\right)^{\frac{1}{q}}\right)\right).
\end{aligned}$$

Theorem 2.3 *Let $\eth : [\xi_1, \xi_2] \to \mathbb{R}$ be a differentiable function on (ξ_1, ξ_2) such that $\eth' \in L^1[\xi_1, \xi_2]$ with $0 \leq \xi_1 < \xi_2$. If $|\eth'|^q$ is s-convex in the second sense for some fixed*

$s \in (0,1]$ and $q \geq 1$, then we have

$$\begin{aligned}
&\left|\frac{7\partial(\xi_1)+32\partial\left(\frac{\xi_1+3\xi_2}{4}\right)+12\partial\left(\frac{\xi_1+\xi_2}{2}\right)+32\partial\left(\frac{3\xi_1+\xi_2}{4}\right)+7\partial(\xi_2)}{90} - \frac{4^{\alpha-1}\Gamma(\alpha+1)}{(\xi_2-\xi_1)^{\alpha}}\mathcal{B}\left(\xi_1,\xi_2,I^{\alpha}\partial\right)\right| \\
\leq\ & \frac{\xi_2-\xi_1}{16}\left(\left(\mathcal{V}\left(\alpha,0,\frac{14}{45}\right)\right)^{1-\frac{1}{q}}\left(\left(\mathcal{K}\left(\alpha,s,\frac{14}{45}\right)\left|\partial'\left(\xi_1\right)\right|^q+\mathcal{V}\left(\alpha,s,\frac{14}{45}\right)\left|\partial'\left(\frac{3\xi_1+\xi_2}{4}\right)\right|^q\right)^{\frac{1}{q}}\right.\right. \\
&\left.\left.+\left(\mathcal{K}\left(\alpha,s,\frac{4}{15}\right)\left|\partial'\left(\frac{\xi_1+\xi_2}{2}\right)\right|^q+\mathcal{V}\left(\alpha,s,\frac{4}{15}\right)\left|\partial'\left(\frac{\xi_1+3\xi_2}{4}\right)\right|^q\right)^{\frac{1}{q}}\right) \\
&+\left(\mathcal{V}\left(\alpha,0,\frac{4}{15}\right)\right)^{1-\frac{1}{q}}\left(\left(\mathcal{V}\left(\alpha,s,\frac{4}{15}\right)\left|\partial'\left(\frac{3\xi_1+\xi_2}{4}\right)\right|^q+\mathcal{K}\left(\alpha,s,\frac{4}{15}\right)\left|\partial'\left(\frac{\xi_1+\xi_2}{2}\right)\right|^q\right)^{\frac{1}{q}}\right. \\
&\left.+\left(\mathcal{V}\left(\alpha,s,\frac{14}{45}\right)\left|\partial'\left(\frac{\xi_1+3\xi_2}{4}\right)\right|^q+\mathcal{K}\left(\alpha,s,\frac{14}{45}\right)\left|\partial'\left(\xi_2\right)\right|^q\right)^{\frac{1}{q}}\right),
\end{aligned}$$

where $\mathcal{B}\left(\xi_1,\xi_2,I^{\alpha}\partial\right)$ is defined by (3),

$$\mathcal{K}\left(\alpha,s,x\right)=\frac{x}{s+1}\left(1-2\left(1-x^{\frac{1}{\alpha}}\right)^{s+1}\right)-\chi\left(\alpha,s,x\right) \tag{14}$$

and

$$\mathcal{V}\left(\alpha,s,x\right)=\frac{(1-x)(s+1)-x\alpha}{(s+1)(\alpha+s+1)}+\frac{2\alpha}{(s+1)(\alpha+s+1)}x^{1+\frac{s+1}{\alpha}}. \tag{15}$$

Proof. From Lemma 2.1, the modulus, power mean inequality and s-convexity of $|\partial'|$, we have

$$\begin{aligned}
&\left|\frac{7\partial(\xi_1)+32\partial\left(\frac{\xi_1+3\xi_2}{4}\right)+12\partial\left(\frac{\xi_1+\xi_2}{2}\right)+32\partial\left(\frac{3\xi_1+\xi_2}{4}\right)+7\partial(\xi_2)}{90} - \frac{4^{\alpha-1}\Gamma(\alpha+1)}{(\xi_2-\xi_1)^{\alpha}}\mathcal{B}\left(\xi_1,\xi_2,I^{\alpha}\partial\right)\right| \\
\leq\ & \frac{\xi_2-\xi_1}{16}\left(\left(\int_0^1\left|\varrho^{\alpha}-\frac{14}{45}\right|d\varrho\right)^{1-\frac{1}{q}}\left(\int_0^1\left|\varrho^{\alpha}-\frac{14}{45}\right|\left|\partial'\left(\left(1-\varrho\right)\xi_1+\varrho\frac{3\xi_1+\xi_2}{4}\right)\right|^q d\varrho\right)^{\frac{1}{q}}\right. \\
&+\left(\int_0^1\left|(1-\varrho)^{\alpha}-\frac{4}{15}\right|d\varrho\right)^{1-\frac{1}{q}} \\
&\left.\times\left(\int_0^1\left|(1-\varrho)^{\alpha}-\frac{4}{15}\right|\left|\partial'\left(\left(1-\varrho\right)\frac{3\xi_1+\xi_2}{4}+\varrho\frac{\xi_1+\xi_2}{2}\right)\right|^q d\varrho\right)^{\frac{1}{q}}\right)
\end{aligned}$$

$$
\begin{aligned}
&+\left(\int_0^1 \left|\varrho^{\alpha}-\tfrac{4}{15}\right| d\varrho\right)^{1-\frac{1}{q}} \left(\int_0^1 \left|\varrho^{\alpha}-\tfrac{4}{15}\right| \left|\partial'\left((1-\varrho)\,\tfrac{\xi_1+\xi_2}{2}+\varrho\tfrac{\xi_1+3\xi_2}{4}\right)\right|^q d\varrho\right)^{\frac{1}{q}}\\
&+\left(\int_0^1 \left|(1-\varrho)^{\alpha}-\tfrac{14}{45}\right| d\varrho\right)^{1-\frac{1}{q}}\\
&\times\left(\int_0^1 \left|(1-\varrho)^{\alpha}-\tfrac{14}{45}\right| \left|\partial'\left((1-\varrho)\,\tfrac{\xi_1+3\xi_2}{4}+\varrho\xi_2\right)\right|^q d\varrho\right)^{\frac{1}{q}}\Bigg)\\
=\;& \tfrac{\xi_2-\xi_1}{16}\Bigg(\left(\mathcal{V}\left(\alpha,0,\tfrac{14}{45}\right)\right)^{1-\frac{1}{q}}\Bigg(\left(\mathcal{K}\left(\alpha,s,\tfrac{14}{45}\right)\left|\partial'\left(\xi_1\right)\right|^q+\mathcal{V}\left(\alpha,s,\tfrac{14}{45}\right)\left|\partial'\left(\tfrac{3\xi_1+\xi_2}{4}\right)\right|^q\right)^{\frac{1}{q}}\\
&+\left(\mathcal{K}\left(\alpha,s,\tfrac{4}{15}\right)\left|\partial'\left(\tfrac{\xi_1+\xi_2}{2}\right)\right|^q+\mathcal{V}\left(\alpha,s,\tfrac{4}{15}\right)\left|\partial'\left(\tfrac{\xi_1+3\xi_2}{4}\right)\right|^q\right)^{\frac{1}{q}}\Bigg)\\
&+\left(\mathcal{V}\left(\alpha,0,\tfrac{4}{15}\right)\right)^{1-\frac{1}{q}}\Bigg(\left(\mathcal{V}\left(\alpha,s,\tfrac{4}{15}\right)\left|\partial'\left(\tfrac{3\xi_1+\xi_2}{4}\right)\right|^q+\mathcal{K}\left(\alpha,s,\tfrac{4}{15}\right)\left|\partial'\left(\tfrac{\xi_1+\xi_2}{2}\right)\right|^q\right)^{\frac{1}{q}}\\
&+\left(\mathcal{V}\left(\alpha,s,\tfrac{14}{45}\right)\left|\partial'\left(\tfrac{\xi_1+3\xi_2}{4}\right)\right|^q+\mathcal{K}\left(\alpha,s,\tfrac{14}{45}\right)\left|\partial'\left(\xi_2\right)\right|^q\right)^{\frac{1}{q}}\Bigg),
\end{aligned}
$$

where $\mathcal{K}$ and $\mathcal{V}$ are defined by (14) and (15), respectively. The proof is completed.

Corollary 2.7 *In Theorem 2.3, if we take $\alpha=1$, we obtain*

$$
\left|\frac{7\partial(\xi_1)+32\partial\left(\frac{\xi_1+3\xi_2}{4}\right)+12\partial\left(\frac{\xi_1+\xi_2}{2}\right)+32\partial\left(\frac{3\xi_1+\xi_2}{4}\right)+7\partial(\xi_2)}{90}-\frac{1}{\xi_2-\xi_1}\int_{\xi_1}^{\xi_2}\partial\left(w\right)dw\right|
$$

$$
\begin{aligned}
\leq\;& \tfrac{\xi_2-\xi_1}{16}\Bigg(\left(\tfrac{1157}{4050}\right)^{1-\frac{1}{q}}\Bigg(\left(\mathcal{K}\left(1,s,\tfrac{14}{45}\right)\left|\partial'\left(\xi_1\right)\right|^q+\mathcal{V}\left(1,s,\tfrac{14}{45}\right)\left|\partial'\left(\tfrac{3\xi_1+\xi_2}{4}\right)\right|^q\right)^{\frac{1}{q}}\\
&+\left(\mathcal{K}\left(1,s,\tfrac{4}{15}\right)\left|\partial'\left(\tfrac{\xi_1+\xi_2}{2}\right)\right|^q+\mathcal{V}\left(1,s,\tfrac{4}{15}\right)\left|\partial'\left(\tfrac{\xi_1+3\xi_2}{4}\right)\right|^q\right)^{\frac{1}{q}}\Bigg)\\
&+\left(\tfrac{137}{450}\right)^{1-\frac{1}{q}}\Bigg(\left(\mathcal{V}\left(1,s,\tfrac{4}{15}\right)\left|\partial'\left(\tfrac{3\xi_1+\xi_2}{4}\right)\right|^q+\mathcal{K}\left(1,s,\tfrac{4}{15}\right)\left|\partial'\left(\tfrac{\xi_1+\xi_2}{2}\right)\right|^q\right)^{\frac{1}{q}}\\
&+\left(\mathcal{V}\left(1,s,\tfrac{14}{45}\right)\left|\partial'\left(\tfrac{\xi_1+3\xi_2}{4}\right)\right|^q+\mathcal{K}\left(1,s,\tfrac{14}{45}\right)\left|\partial'\left(\xi_2\right)\right|^q\right)^{\frac{1}{q}}\Bigg),
\end{aligned}
$$

where

$$
\begin{aligned}
\mathcal{K}\left(1,s,\tfrac{14}{45}\right)&=\tfrac{14s-17}{45(s+1)(s+2)}+\tfrac{2}{(s+1)(s+2)}\left(\tfrac{31}{45}\right)^{s+2},\\
\mathcal{V}\left(1,s,\tfrac{14}{45}\right)&=\tfrac{31s+17}{45(s+1)(s+2)}+\tfrac{2}{(s+1)(s+2)}\left(\tfrac{14}{45}\right)^{s+2},\\
\mathcal{K}\left(1,s,\tfrac{4}{15}\right)&=\tfrac{4s-7}{15(s+1)(s+2)}+\tfrac{2}{(s+1)(s+2)}\left(\tfrac{11}{15}\right)^{s+2},\\
\mathcal{V}\left(1,s,\tfrac{4}{15}\right)&=\tfrac{11s+7}{15(s+1)(s+2)}+\tfrac{2}{(s+1)(s+2)}\left(\tfrac{4}{15}\right)^{s+2}.
\end{aligned}
$$

Corollary 2.8 *In Theorem 2.3, if we take $s=1$, we obtain*

$$\begin{aligned}
&\left|\frac{7\eth(\xi_1)+32\eth\left(\frac{\xi_1+3\xi_2}{4}\right)+12\eth\left(\frac{\xi_1+\xi_2}{2}\right)+32\eth\left(\frac{3\xi_1+\xi_2}{4}\right)+7\eth(\xi_2)}{90}-\frac{4^{\alpha-1}\Gamma(\alpha+1)}{(\xi_2-\xi_1)^{\alpha}}\mathcal{B}\left(\xi_1,\xi_2,I^{\alpha}\eth\right)\right| \\
\leq\ & \frac{\xi_2-\xi_1}{16}\left(\left(\frac{31-14\alpha}{45(\alpha+1)}+\frac{2\alpha}{\alpha+1}\left(\frac{14}{45}\right)^{1+\frac{1}{\alpha}}\right)^{1-\frac{1}{q}}\right. \\
&\times\left(\left(\mathcal{K}\left(\alpha,1,\tfrac{14}{45}\right)\left|\eth'\left(\xi_1\right)\right|^{q}+\mathcal{V}\left(\alpha,1,\tfrac{14}{45}\right)\left|\eth'\left(\frac{3\xi_1+\xi_2}{4}\right)\right|^{q}\right)^{\frac{1}{q}}\right. \\
&\left.+\left(\mathcal{K}\left(\alpha,1,\tfrac{4}{15}\right)\left|\eth'\left(\frac{\xi_1+\xi_2}{2}\right)\right|^{q}+\mathcal{V}\left(\alpha,1,\tfrac{4}{15}\right)\left|\eth'\left(\frac{\xi_1+3\xi_2}{4}\right)\right|^{q}\right)^{\frac{1}{q}}\right) \\
&+\left(\frac{11-4\alpha}{15(\alpha+1)}+\frac{2\alpha}{\alpha+1}\left(\frac{4}{15}\right)^{1+\frac{1}{\alpha}}\right)^{1-\frac{1}{q}} \\
&\times\left(\left(\mathcal{V}\left(\alpha,1,\tfrac{4}{15}\right)\left|\eth'\left(\frac{3\xi_1+\xi_2}{4}\right)\right|^{q}+\mathcal{K}\left(\alpha,1,\tfrac{4}{15}\right)\left|\eth'\left(\frac{\xi_1+\xi_2}{2}\right)\right|^{q}\right)^{\frac{1}{q}}\right. \\
&\left.\left.+\left(\mathcal{V}\left(\alpha,1,\tfrac{14}{45}\right)\left|\eth'\left(\frac{\xi_1+3\xi_2}{4}\right)\right|^{q}+\mathcal{K}\left(\alpha,1,\tfrac{14}{45}\right)\left|\eth'\left(\xi_2\right)\right|^{q}\right)^{\frac{1}{q}}\right),
\end{aligned}$$

where

$$\mathcal{K}\left(\alpha,1,\tfrac{14}{45}\right)=\frac{45-7(\alpha+1)(\alpha+2)}{45(\alpha+1)(\alpha+2)}+\frac{28\alpha}{45(\alpha+1)}\left(\frac{14}{45}\right)^{\frac{1}{\alpha}}-\frac{14\alpha}{45(\alpha+2)}\left(\frac{14}{45}\right)^{\frac{2}{\alpha}},$$

$$\mathcal{V}\left(\alpha,1,\tfrac{14}{45}\right)=\frac{31-7\alpha}{45(\alpha+2)}+\frac{14\alpha}{54(\alpha+2)}\left(\frac{14}{45}\right)^{\frac{2}{\alpha}},$$

$$\mathcal{K}\left(\alpha,1,\tfrac{4}{15}\right)=\frac{15-2(\alpha+1)(\alpha+2)}{15(\alpha+1)(\alpha+2)}+\frac{8\alpha}{15(\alpha+1)}\left(\frac{4}{15}\right)^{\frac{1}{\alpha}}-\frac{4\alpha}{15(\alpha+2)}\left(\frac{4}{15}\right)^{\frac{2}{\alpha}},$$

$$\mathcal{V}\left(\alpha,1,\tfrac{4}{15}\right)=\frac{11-2\alpha}{15(\alpha+2)}+\frac{4\alpha}{15(\alpha+2)}\left(\frac{4}{15}\right)^{\frac{2}{\alpha}}.$$

Corollary 2.9 *In Theorem 2.3, if we take $\alpha=s=1$, we obtain*

$$\begin{aligned}
&\left|\frac{7\eth(\xi_1)+32\eth\left(\frac{\xi_1+3\xi_2}{4}\right)+12\eth\left(\frac{\xi_1+\xi_2}{2}\right)+32\eth\left(\frac{3\xi_1+\xi_2}{4}\right)+7\eth(\xi_2)}{90}-\frac{1}{\xi_2-\xi_1}\int_{\xi_1}^{\xi_2}\eth\left(w\right)dw\right| \\
\leq\ & \frac{\xi_2-\xi_1}{16}\left(\left(\frac{1157}{4050}\right)^{1-\frac{1}{q}}\left(\left(\frac{53507}{546750}\left|\eth'\left(\xi_1\right)\right|^{q}+\frac{102688}{546750}\left|\eth'\left(\frac{3\xi_1+\xi_2}{4}\right)\right|^{q}\right)^{\frac{1}{q}}\right.\right. \\
&\left.+\left(\frac{1987}{20250}\left|\eth'\left(\frac{\xi_1+\xi_2}{2}\right)\right|^{q}+\frac{4178}{20250}\left|\eth'\left(\frac{\xi_1+3\xi_2}{4}\right)\right|^{q}\right)^{\frac{1}{q}}\right) \\
&+\left(\frac{137}{450}\right)^{1-\frac{1}{q}}\left(\left(\frac{4178}{20250}\left|\eth'\left(\frac{3\xi_1+\xi_2}{4}\right)\right|^{q}+\frac{1987}{20250}\left|\eth'\left(\frac{\xi_1+\xi_2}{2}\right)\right|^{q}\right)^{\frac{1}{q}}\right. \\
&\left.\left.+\left(\frac{102688}{546750}\left|\eth'\left(\frac{\xi_1+3\xi_2}{4}\right)\right|^{q}+\frac{53507}{546750}\left|\eth'\left(\xi_2\right)\right|^{q}\right)^{\frac{1}{q}}\right),
\end{aligned}$$

3 Applications

Let Υ be the partition of the points $\xi_1 = x_0 < x_1 < ... < x_n = \xi_2$ of the interval $[\xi_1, \xi_2]$, and consider the quadrature formula

$$\int_{\xi_1}^{\xi_2} \eth(u)\, du = \lambda(\eth, \Upsilon) + R(\eth, \Upsilon),$$

where

$$\begin{aligned}\lambda(\eth, \Upsilon) &= \sum_{i=0}^{n-1} \tfrac{x_{i+1}-x_i}{90}\left(7\eth(x_i) + 32\eth\left(\tfrac{3x_i+x_{i+1}}{4}\right) + 12\eth\left(\tfrac{x_i+x_{i+1}}{2}\right)\right.\\ &\quad \left. + 32\eth\left(\tfrac{x_i+3x_{i+1}}{4}\right) + 7\eth(x_{i+1})\right)\end{aligned}$$

and $R(\eth, \Upsilon)$ denotes the associated approximation error.

Proposition 3.1 *Let $n \in \mathbb{N}$ and $\eth : [\xi_1, \xi_2] \to \mathbb{R}$ be a differentiable function on (ξ_1, ξ_2) with $0 \le \xi_1 < \xi_2$ and $\eth' \in L^1[\xi_1, \xi_2]$. If $|\eth'|$ is an s-convex function in the second sense for some fixed $s \in (0, 1]$, we have*

$$\begin{aligned}|R(\eth, \Upsilon)| &\le \sum_{i=0}^{n-1} \tfrac{(x_{i+1}-x_i)^2}{16}\left(\left(\tfrac{14s-17}{45(s+1)(s+2)} + \tfrac{2}{(s+1)(s+2)}\left(\tfrac{31}{45}\right)^{s+2}\right)(|\eth'(x_i)| + |\eth'(x_{i+1})|)\right.\\ &\quad + \tfrac{2}{(s+1)(s+2)}\left(\tfrac{32s+19}{45} + \tfrac{(14)^{s+2}+(12)^{s+2}}{(45)^{s+2}}\right)\left(\left|\eth'\left(\tfrac{3x_i+x_{i+1}}{4}\right)\right| + \left|\eth'\left(\tfrac{x_i+3x_{i+1}}{4}\right)\right|\right)\\ &\quad \left. + 2\left(\tfrac{4s-7}{15(s+1)(s+2)} + \tfrac{2}{(s+1)(s+2)}\left(\tfrac{11}{15}\right)^{s+2}\right)\left|\eth'\left(\tfrac{x_i+x_{i+1}}{2}\right)\right|\right).\end{aligned}$$

Proof. Applying Corollary 2.1, on the subintervals $[x_i, x_{i+1}]$ $(i = 0, 1, ..., n-1)$ of the partition Υ, we get

$$\begin{aligned}&\left|\tfrac{7\eth(x_i)+32\eth\left(\frac{x_i+3x_{i+1}}{4}\right)+12\eth\left(\frac{x_i+x_{i+1}}{2}\right)+32\eth\left(\frac{3x_i+x_{i+1}}{4}\right)+7\eth(x_{i+1})}{90} - \tfrac{1}{x_{i+1}-x_i}\int_{x_i}^{x_{i+1}} \eth(w)\, dw\right|\\ \le\ & \tfrac{x_{i+1}-x_i}{16}\left(\left(\tfrac{14s-17}{45(s+1)(s+2)} + \tfrac{2}{(s+1)(s+2)}\left(\tfrac{31}{45}\right)^{s+2}\right)(|\eth'(x_i)| + |\eth'(x_{i+1})|)\right.\\ &+ \tfrac{2}{(s+1)(s+2)}\left(\tfrac{32s+19}{45} + \tfrac{(14)^{s+2}+(12)^{s+2}}{(45)^{s+2}}\right)\left(\left|\eth'\left(\tfrac{3x_i+x_{i+1}}{4}\right)\right| + \left|\eth'\left(\tfrac{x_i+3x_{i+1}}{4}\right)\right|\right)\\ &\left. + 2\left(\tfrac{4s-7}{15(s+1)(s+2)} + \tfrac{2}{(s+1)(s+2)}\left(\tfrac{11}{15}\right)^{s+2}\right)\left|\eth'\left(\tfrac{x_i+x_{i+1}}{2}\right)\right|\right). \qquad (16)\end{aligned}$$

Multiplying both sides of (16) by $(x_{i+1} - x_i)$, and then summing the obtained inequalities for all $i = 0, 1, ..., n-1$, and using the triangular inequality, we get the desired result.

Application to special means.

For arbitrary real numbers ξ_1, ξ_2, we have:

The Arithmetic mean: $A(\xi_1, \xi_2) = \frac{\xi_1+\xi_2}{2}$.

The Geometric mean: $G(\xi_1, \xi_2) = \sqrt{\xi_1\xi_2}$, $\xi_1, \xi_2 > 0$.

The p-Logarithmic mean: $L_p(\xi_1, \xi_2) = \left(\frac{\xi_2^{p+1}-\xi_1^{p+1}}{(p+1)(\xi_2-\xi_1)}\right)^{\frac{1}{p}}$, $\xi_1, \xi_2 > 0, \xi_1 \ne \xi_2$ and $p \in \mathbb{R}\setminus\{-1, 0\}$.

Proposition 3.2 *Let $\xi_1, \xi_2 \in \mathbb{R}$ with $0 < \xi_1 < \xi_2$, then we have*

$$\begin{aligned}
&\left|7A\left(\xi_1^{\frac{1}{2}}, \xi_2^{\frac{1}{2}}\right) + 32A^2\left(\left(\tfrac{\xi_1+3\xi_2}{4}\right)^{\frac{1}{2}}, \left(\tfrac{3\xi_1+\xi_2}{4}\right)^{\frac{1}{2}}\right) + 6A^{\frac{1}{2}}(\xi_1,\xi_2) - 45L_2^2(\xi_1,\xi_2)\right| \\
\leq\ & \tfrac{3\sqrt{62}(\xi_2-\xi_1)}{16}\left(\left(\tfrac{241}{279}\right)^{\frac{1}{2}}\left(\left(\xi_1^2 + \left(\tfrac{3\xi_1+\xi_2}{4}\right)^2\right)^{\frac{1}{2}} + \left(\left(\tfrac{\xi_1+3\xi_2}{4}\right)^2 + \xi_2^2\right)^{\frac{1}{2}}\right)\right. \\
&\left. + \left(\left(\left(\tfrac{3\xi_1+\xi_2}{4}\right)^2 + \left(\tfrac{\xi_1+\xi_2}{2}\right)^2\right)^{\frac{1}{2}} + \left(\left(\tfrac{\xi_1+\xi_2}{2}\right)^2 + \left(\tfrac{\xi_1+3\xi_2}{4}\right)^2\right)^{\frac{1}{2}}\right)\right).
\end{aligned}$$

Proof. The assertion follows from Theorem 2.3 applied to the function $\eth(x) = x^2$ with $p = q = 2$.

4 Conclusion

This study is part of the approach of applying analysis tools to differential and integral equations as well as other branches. So, we first established a new identity involving five points, based on this identity and playing on the s-convexity of the first derivative, we obtained new inequalities of Boole type. Finally, we gave some applications to quadrature formula and inequalities for special means.

References

[1] T. Abdeljawad. On conformable fractional calculus. *J. Comput. Appl. Math.* **279** (2015) 57–66.

[2] P. Agarwal, M. Jleli and M. Tomar. Certain Hermite-Hadamard type inequalities via generalized k-fractional integrals. *J. Inequal. Appl.* **55** (2017) 10 pp.

[3] M. B. Almatrafi, W. Saleh, A. Lakhdari, F. Jarad and B. Meftah. On the multiparameterized fractional multiplicative integral inequalities. *J. Inequal. Appl.* **(52)** (2024) 27 pp.

[4] M. U. Awan, S. Talib, Y.-M. Chu, M. A. Noor and K. I. Noor. Some new refinements of Hermite-Hadamard-type inequalities involving ψ_k-Riemann-Liouville fractional integrals and applications. *Math. Probl. Eng. Art.* (2020) 10 pp.

[5] M. Benssaad, B. Meftah, S. Ghomrani, W. Kaidouchi. Fractional Hermite-Hadamard type inequalities for functions whose mixed derivatives are co-ordinated $(log, (s, m))$-convex. *Int. J. Nonlinear Anal. Appl.* **13** (2) (2022) 159–171.

[6] B. Bin-Mohsin, A. Lakhdari, N. E. I. Karabadji, M. U. Awan, A. B. Makhlouf, B., Meftah and S. S. Dragomir. An Extension of Left Radau Type Inequalities to Fractal Spaces and Applications. *Axioms.* **13** (9) (2024) 653.

[7] S. Dhar and J. T. Neugebauer. Lyapunov-Type Inequalities for a Fractional Boundary Value Problem with a Fractional Boundary Condition. *Nonlinear Dynamics and Systems Theory.* **22** (2) (2022) 133–143.

[8] S. S. Dragomir and S. Fitzpatrick. The Hadamard inequalities for s-convex functions in the second sense. *Demonstratio Math.* **32** (4) (1999) 687–696.

[9] T. Du, C. Luo and Z. Cao. On the Bullen-type inequalities via generalized fractional integrals and their applications. *Fractals* **29** (07) (2021) 2150188.

[10] T. Du and X. Yuan. On the parameterized fractal integral inequalities and related applications. *Chaos Solitons Fractals* **170** (2023) Paper No. 113375 22 pp.

[11] I. Franjić, J. Pečarić and I. Perić. General Euler-Boole's and dual Euler-Boole's formulae. *Math. Inequal. Appl.* **8** (2) (2005) 287–303.

[12] S. Ghomrani, B. Meftah, W. Kaidouchi, M. Benssaad. Fractional Hermite-Hadamard type integral inequalities for functions whose modulus of the mixed derivatives are co-ordinated $(\log, (\alpha, m))$-preinvex. *Afr. Mat.* **32** (5-6) (2021) 925–940.

[13] S. Hamida and B. Meftah. Fractional Bullen type inequalities for differentiable preinvex functions. *ROMAI J.* **16** (2) (2020) 63–74.

[14] W. Kaidouchi, B.Meftah, M. Benssaad and S. Ghomrani. Fractional Hermite-Hadamard type integral inequalities for functions whose modulus of the mixed derivatives are co-ordinated extended (s_1, m_1)-(s_2, m_2)-preinvex. *Real Anal. Exchange.* **44** (2) (2019) 305-332.

[15] A. Kashuri, B. Meftah and P.O. Mohammed. Some weighted Simpson type inequalities for differentiable s-convex functions and their applications. *J. Frac. Calc. and Nonlinear Sys.* **1** (1) (2020) 75-94.

[16] U. N. Katugampola. A new approach to generalized fractional derivatives. *Bull. Math. Anal. Appl.* **6** (4) (2014) 1–15.

[17] R. Khalil, M. Al Horani, A. Yousef, M. Sababheh. A new definition of fractional derivative. *J. Comput. Appl. Math.* **264** (2014) 65–70.

[18] A. Lakhdari, B. Bin-Mohsin, F. Jarad, H. Xu and B. Meftah. A parametrized approach to generalized fractional integral inequalities: Hermite-Hadamard and Maclaurin variants. *Journal of King Saud University-Science* **(36)** (11) (2024) 103523.

[19] A. Lakhdari, H. Budak, M. U. Awan and B. Meftah. Extension of Milne-type inequalities to Katugampola fractional integrals. *Bound. Value Probl.* **100** (2024) 16 pp.

[20] Q. R. Liu, M. U. Awan, B. Bin-Mohsin, M. Z. Javed, L. Ciurdariu and B. Meftah. Bridging Pre-Invex Mappings and Fractional Integrals: A Pathway to Iterative Schemes via Error Boundaries of Maclaurin's Rule. *Fractal and Fractional* **8** (12) (2024) 734.

[21] B. Meftah, M. Benssaad,W. Kaidouchi and S. Ghomrani. Conformable fractional Hermite-Hadamard type inequalities for product of two harmonic s-convex functions. *Proc. Amer. Math. Soc.* **149** (4) (2021) 1495–1506.

[22] J. E. V. Nápoles and B. Bayraktar. On the generalized inequalities of the Hermite-Hadamard type. *Filomat* **35** (14) (2021) 4917–4924.

[23] J. E. V. Nápoles and F. Rabossi. A note on some fractional integral inequalities via generalized fractional integral. *An. Ştiinţ. Univ. Al. I. Cuza Iaşi. Mat. (N.S.)* **68** (1) (2022) 79–89.

[24] Soufiane Benyoussef, Oumkeltoum Benhamouda, Mohamed Dalah and Khaled Zennir. A New Numerical Scheme for Solving Time-Fractional Variable-Order Partial Differential Equations. *Nonlinear Dynamics and Systems Theory* **24** (4) (2024) 340–353.

[25] H. Xu, A. Lakhdari, F. Jarad, T. Abdeljawad and B. Meftah. On multiparametrized integral inequalities via generalized α-convexity on fractal set. *Math. Methods Appl. Sci.* **48** (1) (2025) 980–1002.

[26] W. S. Zhu, B. Meftah, H. Xu, F. Jarad and A. Lakhdari. On parameterized inequalities for fractional multiplicative integrals. *Demonstr. Math.* **57** (1) (2024) Paper No. 20230155, 17 pp.

Nonlinear Dynamics and Systems Theory, **26** (1) (2026) 56–68

Fractional-Order Shapovalov Mid-Size Firm Model: Dynamical Analysis, Chaos Control and Synchronization

H. Kamli*, S. Rouar and O. Zehrour

Laboratoty LSDC, Department of Mathematics and Informatics, University of Oum El Bouaghi, Oum El Bouaghi, Algeria.

Received: June 10, 2025; Revised: February 8, 2026

Abstract: This paper presents a novel fractional-order formulation of the Shapovalov mid-size firm model incorporating Caputo derivatives, offering a more flexible framework for capturing memory effects in economic dynamics. The fundamental dynamical properties of the system are analyzed. Stabilization of the model is achieved through the design of both linear and nonlinear feedback control strategies. In addition, the complete synchronization problem is investigated using a simple linear control law. Numerical simulations confirm the effectiveness and feasibility of the proposed methods. Beyond theoretical insights, the approach enhances forecasting reliability and enables precise tuning of the economic mechanism, thereby improving the overall efficiency of decision-making processes in complex economic systems.

Keywords: *fractional-order derivative; Shapovalov model; Lyapunov exponents; feedback control; active control; complete synchronization.*

Mathematics Subject Classification (2020): 34C28, 37D45, 37M05, 70k20, 93-10.

* Corresponding author: mailto:kamlihanan04@gmail.com

© 2026 InforMath Publishing Group/1562-8353 (print)/1813-7385 (online)/http://e-ndst.kiev.ua 56

1 Introduction

Chaos theory is a fundamental branch of mathematics with diverse applications across numerous fields, including meteorology, biology, medicine, engineering, social sciences, and economics [7–9]. It has become an essential tool for studying complex systems characterized by inherent uncertainty and unpredictability.

Nonlinear dynamics investigates systems where outputs are not directly proportional to inputs, leading to phenomena such as chaos, emergence, and bifurcation. Economic models are often intricate, involving interacting economic agents whose nonlinear behaviors can result in chaotic and unstable dynamics. Consequently, economic forecasting based on these models is challenging, underscoring the critical role of chaos theory in addressing the complexities inherent in nonlinear economic systems.

Fractional-order calculus extends differentiation and integration to non-integer orders. This branch of mathematics has garnered increasing interest due to its ability to describe memory effects and hereditary properties in many real-world processes, making it a valuable tool for modeling and decision-making in physics, engineering, biology, medicine, and financial economics [10, 13, 14]. Fractional-order systems offer a more accurate representation of complex behaviors, particularly in systems exhibiting long-term dependencies.

Chaotic behavior in economic models complicates the prediction of market trends, investment risks, and policy outcomes, posing significant challenges for economists and decision-makers. Consequently, developing methods to stabilize chaotic economic systems has become a vital research focus, aiming to enhance the reliability of economic forecasts and support the design of effective control strategies [1, 3].

Numerous studies have investigated chaotic economic models, including the open economy new Keynesian model [4], the Gali and Monacelli model [5], and the Shapovalov mid-size firm model [3].

The Shapovalov model is an economic framework developed to analyze the dynamic behavior of medium-sized firms. It is formulated as a system of differential equations that describe the dynamic interactions among three key production factors: loan amount, fixed capital, and number of employees.

This model has attracted increasing academic attention, with several studies investigating its dynamic properties—such as stability, chaos, and multistability—using analytical tools including Lyapunov methods and attractor theory [2].

The Shapovalov model provides a valuable foundation for studying the nonlinear dynamics of economic systems and contributes to enhancing predictive accuracy in volatile and uncertain economic environments. Furthermore, it serves as an effective instrument for guiding strategic decision-making and informing economic policies tailored to medium-sized enterprises.

This paper aims to study the stabilization and synchronization problems of the fractional version of the Shapovalov system through the implementation of designed feedback control strategies and the application of a linear control law.

The rest of the paper is organized as follows. Section 2 provides the definition of the Caputo fractional-order derivative and theorems concerning the stability of Caputo fractional-order nonlinear dynamical systems. Section 3 presents the fractional-order Shapovalov system, a dynamical system characterized by Caputo fractional derivatives, which captures complex nonlinear behaviors. In Section 4, the stabilization problems of the proposed system are examined through the implementation of designed feedback

control strategies. Section 5 analyzes the complete synchronization of the fractional-order Shapovalov system through the application of a simple linear control law. Finally, Section 6 summarizes the findings, outlines potential directions for future research, and highlights the importance of this study.

2 Preliminaries

This section presents the definition of the Caputo fractional derivative and some stability theorems pertaining to fractional-order nonlinear dynamical systems. For more details, the reader is referred to [11].

Definition 2.1 *The α-th order Caputo fractional derivative of the function $f(t)$ with respect to t and the terminal point 0 is defined as follows:*

$$ {}^{C}D_{t}^{\alpha} f = \frac{d^{\alpha} f(t)}{dt^{\alpha}} = \frac{1}{\Gamma(m-\alpha)} \int_{0}^{t} \frac{f^{(m)}(\tau)}{(t-\tau)^{\alpha+1-m}} d\tau, $$

where m is an integer such that $m-1 \leq \alpha \leq m$, and Γ is the well-known Gamma function.

We define the Caputo fractional-order nonlinear dynamical system as follows:

$$ {}^{C}D_{t}^{\alpha} x_i = f_i(x_1, x_2, ..., x_n), \ \left(i = \overline{1,n}, \ 0 < \alpha < 1\right). \tag{1} $$

The equilibrium points of system (1) can be determined by solving the equations

$$ f_i(x_1, x_2, ..., x_n) = 0, \ \left(i = \overline{1,n}, \ 0 < \alpha < 1\right). $$

To analyze the stability of system (1), the following theorem is essential.

Theorem 2.1 *[6] The system (1) is asymptotically stable if all the eigenvalues λ_i , $i = \overline{1,n}$, of the Jacobian matrix J evaluated at the equilibrium point of system (1) satisfy the condition*

$$ |\arg(\lambda_i)| > \alpha \frac{\pi}{2}, \left(i = \overline{1,n}, \ 0 < \alpha < 1\right), $$

where the Jacobian matrix is defined as

$$ J = \frac{\partial f}{\partial x}, \ f = (f_1, f_2, ..., f_n), \ x = (x_1, x_2, ..., x_n)^{T}. $$

Theorem 2.2 *[6] Let $x(t) \in \mathbb{R}^n$ be a vector of continuous and differentiable function, then the relationship*

$$ \frac{1}{2} {}^{C}D_{t}^{\alpha} x^{T}(t) x(t) \leq x^{T}(t) {}^{C}D_{t}^{\alpha} x(t) $$

holds.

Theorem 2.3 *[6] The equilibrium point of system (1) is stable if for each x, $x(t)^{T} f(x(t)) \leq 0$, and it is asymptotically stable if $\forall x \neq 0$, $x(t)^{T} f(x(t)) < 0$.*

3 Fractional-Order Shapovalov Model

To facilitate a deeper understanding and enable more accurate predictions of economic management systems, Shapovalov [12] proposed a differential equation model describing the behavior of a medium-sized firm, formulated as follows:

$$\begin{cases} \dot{x} = -\sigma x + \delta y, \\ \dot{y} = \mu x + \mu y - \beta x z, \\ \dot{z} = -\gamma z + \alpha x y, \end{cases} \tag{2}$$

where $\alpha, \beta, \gamma, \delta, \mu, \sigma$ are positive parameters, and the variables x, y, z represent the growth of three key production factors: the loan amount x , the fixed capital y , and the number of employees z.

Through the coordinate transformation $(x, y, z) \to \left(\frac{\mu}{\sqrt{\alpha\beta}}x, \frac{\mu\sigma}{\delta\sqrt{\alpha\beta}}y, \frac{\mu\sigma}{\delta\beta}z\right)$ and the time rescaling $t \to \frac{t}{\mu}$, system (2) can be simplified into a Lorenz-like system

$$\begin{cases} \dot{x} = -cx + cy, \\ \dot{y} = rx + y - xz, \\ \dot{z} = -bz + xy. \end{cases} \tag{3}$$

The system described, where $c = \frac{\sigma}{\mu}, r = \frac{\delta}{\sigma}$ *and* $b = \frac{\gamma}{\mu}$, differs slightly from the classical Lorenz system due to the coefficient of y in the second equation. In this case, the coefficient is 1, whereas in the Lorenz system, it is -1. Despite this difference, chaos can still arise in system (3) just as it does in the Lorenz system.

Solving the following equilibrium equations:

$$\begin{cases} -cx + cy = 0 \\ rx + y - xz = 0 \\ -bz + xy = 0 \end{cases}$$

with $c = 18.3, r = 51, b = 5.7$, we can easily have three equilibrium points
$E_1 = (0, 0, 0)$, $E_2 = (17.216, 17.216, 52.0)$, $E_3 = (-17.216, -17.216, 52.0)$.

The chaotic attractors are shown in Figure 1.

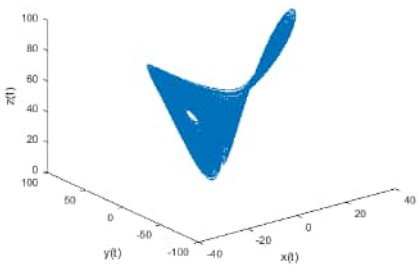

Figure 1: The chaotic attractor of system(3) with c=18.3,r=51,b=5.7.

This paper proposes to study the fractional system

$$\begin{cases} {}^{C}D_t^{\alpha}x = -cx + cy, \\ {}^{C}D_t^{\alpha}y = rx + y - xz, \\ {}^{C}D_t^{\alpha}z = -bz + xy. \end{cases} \tag{4}$$

${}^{C}D_t^{\alpha}$ denotes the derivatives of order α ; $(0 < \alpha < 1;\ i = \overline{1,n})$ in the sense of Caputo, with $c = 18.3, r = 51, b = 5.7$.

4 Dynamical Analysis of Fractional-Order Shapovalov Model

Suppose system (4) has an equilibrium point $E^* = (x^*, y^*, z^*)$, then the Jacobian matrix J at the equilibrium point is

$$J(E^*) = \begin{pmatrix} -c & c & 0 \\ r - \overset{*}{z} & 1 & -\overset{*}{x} \\ \overset{*}{y} & \overset{*}{x} & -b \end{pmatrix}.$$

The characteristic equation $|\lambda I - J|$ at the equilibrium point E^*, for $c = 18.3, r = 51$, $b = 5.7$, is

$$f(\lambda) = |\lambda I - J| = \begin{vmatrix} \lambda + 18.3 & -18.3 & 0 \\ -51 + z^* & \lambda - 1 & x^* \\ -y^* & -x^* & \lambda + 5.7 \end{vmatrix} = 0. \tag{5}$$

It is clear that the system (4) has the same equilibria

$$E_1 = (0,0,0),\ E_2 = (17.216, 17.216, 52.0),\ E_3 = (-17.216, -17.216, 52.0).$$

Lemma 4.1 *The equilibrium point $E_1 = (0,0,0)$ is unstable for $0 < \alpha < 1$.*

Proof. By substituting the value of E_1 into the characteristic equation (5), we obtain the following expression:

$$f(\lambda) = \lambda^3 + 23.0\lambda^2 - 852.99\lambda - 5424.1 = 0.$$

Thus the roots of Equation (5) are $\lambda_1 = 23.388$, $\lambda_2 = -5.7000$, $\lambda_3 = -40.688$. Because λ_1 is a positive real number and

$$\min_{1 \le i \le 3} |\arg(\lambda_i)| = |\arg(\lambda_1)| = 0 < \alpha\frac{\pi}{2} \qquad (0 < \alpha < 1),$$

by Theorem 2.1, the equilibrium point E_1 is a saddle point and it is unstable for $0 < \alpha < 1$.

Lemma 4.2 *Equilibrium points E_2, E_3 are asymptotically stable for $\alpha < 0.97$.*

Proof. By applying the same method as in the previous proof, we find

$$|\arg(\lambda_{2,3})| = 87.65 \quad \text{for all} \quad \alpha \in (0,1).$$

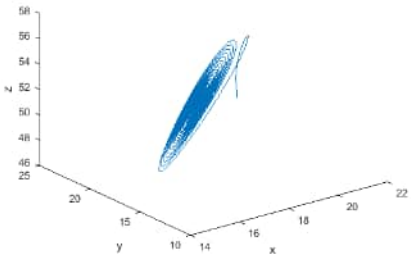

(*a*) x, y, z phase plane at $\alpha = 0.965$

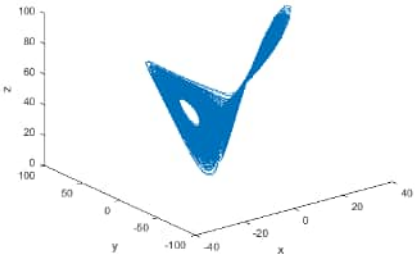

(*b*) x, y, z phase plane at $\alpha = 0.975$

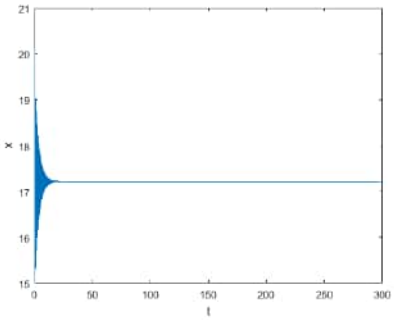

(*c*) Time evolution of x for $\alpha = 0.965$

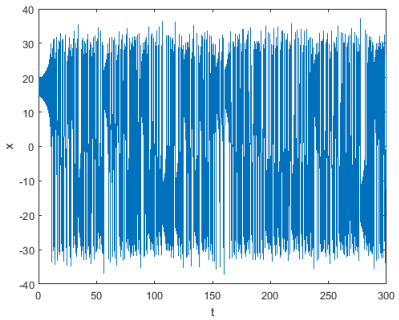

(*d*) Time evolution of x for $\alpha = 0.975$

Figure 2: The attractors and time evolution of x of the fractional-order system for $\alpha = 0.965$ and $\alpha = 0.975$.

By Theorem 2.1, equilibrium points E_2, E_3 are asymptotically stable when

$$\alpha < \frac{2}{\pi} |\arg(\lambda_{2,3})| \simeq 0.97.$$

For the selected parameters $c = 18.3$, $r = 51$, and $b = 5.7$, Figures 2(a)–(d) illustrate the attractors and the time evolution of x for the fractional-order system (4) at two different derivative orders, $a = 0.965$ and $a = 0.975$, with initial conditions $(x(0), y(0), z(0)) = (20, 20, 50)$. Figures 2(a) and 2(c) show that the system converges to a fixed point, whereas Figures 2(b) and 2(d) reveal the presence of chaotic attractors. These observations indicate that the fractional-order system (4) can exhibit chaotic behavior when the derivative order exceeds 0.97.

5 Feedback Control

5.1 Linear feedback control

In this section, we examine the chaotic control of system (4) through linear control techniques. This strategy facilitates the attainment of local stability at any unstable equilibrium point within system (4). The representation of the linear controlled fractional-order

system is as follows:

$$\begin{cases} {}^{C}D_t^{\alpha}x = -cx + cy - k_1\left(x - x^*\right), \\ {}^{C}D_t^{\alpha}y = rx + y - xz - k_2\left(y - y^*\right), \\ {}^{C}D_t^{\alpha}z = -bz + xy - k_3\left(z - z^*\right), \end{cases} \tag{6}$$

where k_1, k_2, k_3 are three linear control parameters, the fractional order $\alpha = 0.98$, and the equilibrium point of the system is (x^*, y^*, z^*).

The Jacobian matrix of the system (6) at the equilibrium point (x^*, y^*, z^*) is given as

$$J\left(E^*\right) = \begin{pmatrix} -c - k_1 & c & 0 \\ r - \overset{*}{z} & 1 - k_2 & -\overset{*}{x} \\ \overset{*}{y} & \overset{*}{x} & -b - k_3 \end{pmatrix}.$$

The corresponding characteristic equation for $c = 18.3, r = 51, b = 5.7$, reads

$$f\left(\lambda\right) = \left|\lambda I - J\right| = \begin{vmatrix} \lambda + 18.3 + k_1 & -18.3 & 0 \\ -51 + \overset{*}{z} & \lambda - 1 + k_2 & \overset{*}{x} \\ -\overset{*}{y} & -\overset{*}{x} & \lambda + 5.7 + k_3 \end{vmatrix}. \tag{7}$$

Remark 5.1 In order to stabilize the system (4), the control parameters k_1, k_2, k_3 are chosen such that all eigenvalues λ_i of Equation (7) satisfy

$$\left|\arg\left(\lambda_i\right)\right| > \alpha\frac{\pi}{2}, \left(i = \overline{1,3},\ 0 < \alpha < 1\right).$$

Lemma 5.1 *The system* (6) *is locally asymptotically stable at the equilibrium point* $E_1 = (0, 0, 0)$ *with the control parameters* $k_1 = 25, k_2 = 25, k_3 = 25$.

Proof. Substituting the given values of E_1, k_1, k_2 and k_3 into the characteristic equation (7), we obtain

$$f\left(\lambda\right) = \left|\lambda I - J\right| = \begin{vmatrix} \lambda + 18.3 + 25 & -18.3 & 0 \\ -51 & \lambda - 1 + 25 & 0 \\ 0 & 0 & \lambda + 5.7 + 25 \end{vmatrix}.$$

The characteristic roots of this equation are approximately

$$\lambda_1 = -1.612\,2\ , \lambda_2 = -30.700\ ,\ \lambda_3 = -65.688.$$

By Theorem 2.1, $\left|\arg\left(\lambda_i\right)\right| = \pi > \alpha\frac{\pi}{2}, \left(i = \overline{1,3},\ 0 < \alpha < 1\right)$. Hence, the controlled fractional-order system (6) is locally asymptotically stable at E_1.

Lemma 5.2 *The system* (6) *is locally asymptotically stable at the equilibrium points* $E_2 = (17.216, 17.216, 52.0)$ *and* $E_3 = (-17.216, -17.216, 52.0)$ *with the control parameters* $k_1 = 1, k_2 = 40, k_3 = 70$.

Proof. Substituting the given values of E_2, k_1, k_2 and k_3 into the characteristic equation (7), we obtain

$$f\left(\lambda\right) = \left|\lambda I - J\right| = \begin{vmatrix} \lambda + 18.3 + 1 & -18.3 & 0 \\ -51 + 52.0 & \lambda - 1 + 40 & 17.216 \\ -17.216 & -17.216 & \lambda + 5.7 + 70 \end{vmatrix}.$$

The roots of this equation are approximately

$$\lambda_1 = -26.035\ ,\lambda_2 = -38.353\ ,\ \lambda_3 = -69.612.$$

By Theorem 2.1, $|\arg(\lambda_i)| = \pi\ > \alpha\frac{\pi}{2}, \left(i = \overline{1,3},\ 0 < \alpha < 1\right)$. Hence, the controlled fractional-order system (6) is locally asymptotically stable at E_2. Similarly, for $k_1 = 1, k_2 = 40, k_3 = 70$, system (6) is also locally asymptotically stable at the equilibrium point E_3.

The three linear feedback controllers are capable of effectively stabilizing the fractional-order Shapovalov system (4) at different equilibrium points.

As depicted in Figure 3 (a)-(c), the controllers are activated at $t = 20s$ with a derivative order $\alpha = 0.98$. When $t < 20s$, system (4) exhibits chaotic behavior. After the controllers are activated, the state vectors x, y, and z gradually converge to different equilibrium points, namely E_1, E_2, and E_3, respectively.

5.2 Nonlinear feedback control

The nonlinear controlled fractional-order system is defined as

$$\begin{cases} {}^{C}D_t^{\alpha}x = -cx + cy + u_1, \\ {}^{C}D_t^{\alpha}y = rx + y - xz + u_2, \\ {}^{C}D_t^{\alpha}z = -bz + xy + u_3, \end{cases} \tag{8}$$

where u_1, u_2 and u_3 are nonlinear controllers that will be designed later.

Lemma 5.3 *System* (4) *can achieve global asymptotic stability under the nonlinear controllers*

$$u_1 = -k_1x - 0.1x^3,\ u_2 = -k_2(y + x) - 0.05y^3 \text{ and } u_3 = -k_3z - 0.02z^3 \tag{9}$$

if and only if the conditions $k_1 > -c,\ k_2 > c + r$ *and* $k_3 > -b$ *hold.*

Proof. Choose a positive definite Lyapunov function

$$V = \frac{1}{2}\left(x^2 + y^2 + z^2\right). \tag{10}$$

Using expressions (8) and (9), the fractional derivative of the Lyapunov function (10) is obtained by

$${}^{C}D_t^{\alpha}V \le x\ {}^{C}D_t^{\alpha}x + y{}^{C}D_t^{\alpha}y + z\ {}^{C}D_t^{\alpha}z$$

$$= x(-cx + cy + u_1) + y(rx + y - xz + u_2) + z(-bz + xy)$$

$$= x\left(-cx + cy - k_1x - 0.1x^3\right) + y\left(rx + y - xz - k_2(y + x) - 0.05y^3\right)$$

$$+z\left(-bz + xy - k_3z - 0.02z^3\right)$$

$$= -cx^2 + cxy - k_1x^2 - 0.1x^4 + rxy + y^2 - xyz - k_2y^2 - k_5xy - 0.05y^4 - bz^2 + xyz - k_3z^2 - 0.02z^4$$

$$= -(c + k_1)x^2 - (k_2 - 1)y^2 - (k_3 + b)z^2 - (k_2 - c - r)xy - 0.1x^4 - 0.05y^4 - 0.02z^4.$$

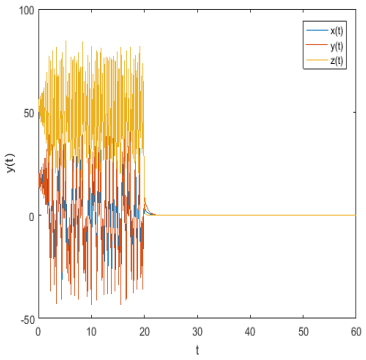

(a) Stabilization of the equilibrium point E_1

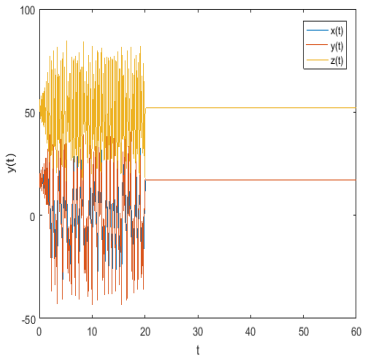

(b) Stabilization of the equilibrium point E_2

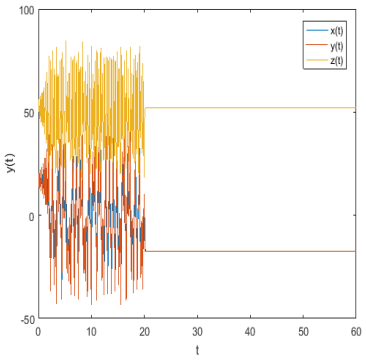

(c) Stabilization of the equilibrium point E_3

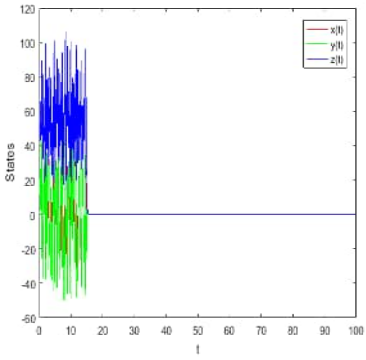

(d) Global stabilization

Figure 3: Chaotic control of the fractional-order Shapovalov system.

If $k_1 > -c$, $k_2 > c + r$, and $k_3 > -b$ hold, then the fractional derivative of the Lyapunov function is strictly negative. According to Theorem 2.3, the controlled system (8) is globally asymptotically stable.

As illustrated in Figure 3(d), with the parameters $c = 18.3$, $r = 51$, $b = 5.7$ and $\alpha = 0.98$, and when selecting $k_1 = 69.4$, $k_2 = 69.4$, and $k_3 = 2$, the system transitions from chaotic behavior to a state of global asymptotic stability when the controllers are activated at $t = 15\,\mathrm{s}$.

6 Synchronization of the Fractional-Order System

In this section, we investigate the complete synchronization of the fractional-order Shapovalov system by employing a simple linear control law. To this end, we consider the following master–slave systems:

Master system:

$$\begin{cases} {}^{C}D_t^{\alpha} x_1 = -c x_1 + c y_1, \\ {}^{C}D_t^{\alpha} y_1 = r x_1 + y_1 - x_1 z_1, \\ {}^{C}D_t^{\alpha} z_1 = -b z_1 + x_1 y_1. \end{cases} \tag{11}$$

Slave system:

$$\begin{cases} {}^{C}D_t^{\alpha} x_2 = -cx_2 + cy_2 + U_1, \\ {}^{C}D_t^{\alpha} y_2 = rx_2 + y_2 - x_2 z_2 + U_2, \\ {}^{C}D_t^{\alpha} z_2 = -bz_2 + x_2 y_2 + U_3, \end{cases} \tag{12}$$

where $X(t) = [x_1(t),\ y_1(t),\ z_1(t)]^T \in \mathbb{R}^3$ and $Y(t) = [x_2(t),\ y_2(t),\ z_2(t)]^T \in \mathbb{R}^3$ are the state vectors of the master and slave systems, respectively. The vector $[x_1(0),\ y_1(0),\ z_1(0)]^T$ denotes the unknown initial state of the master system, while $[x_2(0),\ y_2(0),\ z_2(0)]^T$ is the given initial state of the slave system.

To achieve complete synchronization, we design a simple control law

$$U(t) = [U_1(t),\ U_2(t),\ U_3(t)]^T \in \mathbb{R}^3,$$

which ensures that the states of the drive dynamical system (11) synchronize with those of the response dynamical system (12). Define the synchronization error vector as

$$e(t) = [e_1(t),\ e_2(t),\ e_3(t)]^T = Y(t) - X(t),$$

where $e_1(t) = x_2(t) - x_1(t)$, $e_2(t) = y_2(t) - y_1(t)$, and $e_3(t) = z_2(t) - z_1(t)$.

Definition 6.1 Systems (11) and (12) mentioned above are said to achieve complete synchronization if

$$\lim_{t \to +\infty} \|Y(t) - X(t)\| = 0.$$

Subsequently, we can deduce the following result concerning the complete synchronization between systems (11) and (12).

Theorem 6.1 *For the control law given by*

$$U_1(t) = -k_1 e_1, \quad U_2(t) = -k_2 e_2 + z_1 e_1, \quad U_3(t) = -k_3 e_3 - y_1 e_1, \tag{13}$$

the master system (11) and the slave system (12) achieve complete synchronization.

Proof. From systems (11) and (12), we infer that the error system is given by

$$\begin{cases} D_t^{\alpha} e_1 = -ce_1 + ce_2 + U_1, \\ D_t^{\alpha} e_2 = re_1 + e_2 - e_1 e_3 - x_1 e_3 - e_1 z_1 + U_2, \\ D_t^{\alpha} e_3 = -be_3 + e_1 e_2 + x_1 e_2 + e_1 y_1 + U_3. \end{cases} \tag{14}$$

Let the Lyapunov candidate function be

$$V(t) = \frac{1}{2}\left(e_1^2(t) + e_2^2(t) + e_3^2(t)\right).$$

The Caputo fractional derivative of $V(t)$ along the trajectories of system (14) satisfies

$${}^{C}D_t^{\alpha} V(t) \leq e_1 \cdot {}^{C}D_t^{\alpha} e_1 + e_2 \cdot {}^{C}D_t^{\alpha} e_2 + e_3 \cdot {}^{C}D_t^{\alpha} e_3.$$

Substitute the expressions from the error dynamics and the control law (13)

$$\begin{aligned} {}^{C}D_t^{\alpha} V(t) = {} & e_1(-ce_1 + ce_2 - k_1 e_1) \\ & + e_2\left(re_1 + e_2 - e_1 e_3 - x_1 e_3 - e_1 z_1 - k_2 e_2 + z_1 e_1\right) \\ & + e_3\left(-be_3 + e_1 e_2 + x_1 e_2 + e_1 y_1 - k_3 e_3 - y_1 e_1\right). \end{aligned}$$

Simplifying, we obtain

$$\begin{aligned} {}^{C}D_t^{\alpha}V(t) = &-(k_1+c)e_1^2-(k_2-1)e_2^2-(k_3+b)e_3^2 \\ &+(c+r)e_1e_2-z_1e_1e_2+z_1e_1e_2+y_1e_1e_3-y_1e_1e_3. \end{aligned}$$

Hence, cross terms cancel out, and we are left with

$${}^{C}D_t^{\alpha}V(t) \leq -(k_1+c)e_1^2-(k_2-1)e_2^2-(k_3+b)e_3^2+\frac{1}{2}(c+r)(e_1^2+e_2^2).$$

Rewriting this

$$\begin{aligned} {}^{C}D_t^{\alpha}V(t) &= -\left(k_1+c-\frac{1}{2}(c+r)\right)e_1^2-\left(k_2-1-\frac{1}{2}(c+r)\right)e_2^2-(k_3+b)e_3^2 \\ &= -\left(k_1+\frac{1}{2}c-\frac{1}{2}r\right)e_1^2-\left(k_2-\frac{1}{2}(c+r)-1\right)e_2^2-(k_3+b)e_3^2. \end{aligned}$$

The derivative ${}^{C}D_t^{\alpha}V(t) < 0$ holds if the following conditions are satisfied:

$$k_1 > -\frac{1}{2}c+\frac{1}{2}r, \quad k_2 > \frac{1}{2}(c+r)+1, \quad k_3 > -b.$$

For example, when the parameters are given as $c = 18.3$, $r = 51$, $b = 5.7$, and when selecting $k_1 = 17$, $k_2 = 36$, $k_3 = 10$, the derivative of the Lyapunov function becomes negative definite.

Therefore, according to Theorem 2.3, the origin of the error system (14) is asymptotically stable, and the synchronization errors $e_1(t)$, $e_2(t)$, and $e_3(t)$ converge to zero. This confirms that the master and slave systems achieve complete synchronization.

To assess the effectiveness of complete synchronization through numerical simulation, we consider the control law given in equation (13), with control gains selected as $k_1 = 17$, $k_2 = 36$, and $k_3 = 10$. The fractional derivative order is set to $\alpha = 0.99$.

The initial state vector of the master system (11) is chosen as $[x_1(0),\ y_1(0),\ z_1(0)] = [1,\ 1,\ 1]$, while the initial state of the slave system (12) is set to $[x_2(0),\ y_2(0),\ z_2(0)] = [2,\ 2,\ 2]$.

According to the definition of the synchronization error, the initial condition of the error system (14) is therefore $[e_1(0),\ e_2(0),\ e_3(0)] = [1,\ 1,\ 1]$.

Figure 4(a) illustrates the time evolution of the synchronization errors $e_1(t)$, $e_2(t)$, $e_3(t)$, which all converge to zero, indicating successful synchronization. Figure 4(b) depicts the trajectories of systems (11) and (12) in the 3D phase space, showing their convergence. Figure 4(c) presents the time responses of the state variables $x(t)$, $y(t)$, $z(t)$ for both systems, highlighting the agreement between their dynamics over time.

7 Conclusion

This study explores the chaotic behavior of the fractional-order Shapovalov model, an economic system developed to analyze the dynamic behavior of medium-sized enterprises. The incorporation of fractional calculus offers a powerful framework for modeling real-world economic phenomena more accurately, as it captures memory effects and hereditary characteristics often overlooked by classical integer-order models.

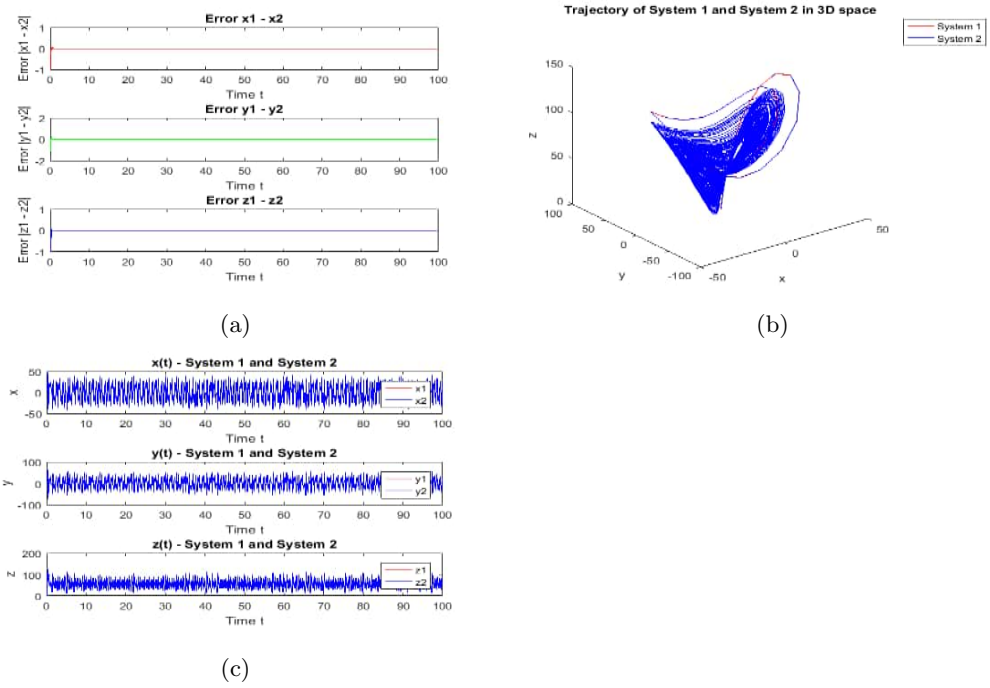

Figure 4: The complete synchronization between systems (11) and (12).

In this context, the suppression of chaos is addressed through the design of both linear and nonlinear feedback controllers. Additionally, the problem of complete synchronization is analyzed using the Lyapunov stability approach. Numerical simulations further validate the effectiveness of the proposed methods in stabilizing the chaotic dynamics of the system.

Stabilizing such economic models contributes meaningfully to the field by providing strategies for managing chaotic behavior and enhancing the reliability of economic forecasting and policy-making. Studying the dynamics of the Shapovalov model, along with the application of control and synchronization techniques, can support the forecasting processes in medium-sized enterprises. Moreover, it can assist in guiding these enterprises toward achieving their strategic goals by modifying and regulating their dynamic behavior.

Acknowledgement

The first author would like to express her sincere gratitude to her parents, husband, and family members, particularly her sister, for their unwavering support and encouragement throughout her studies.

References

[1] T. A. Alexeeva, N. V. Kuznetsov, T. N. Mokaev and I. Zelinka. Chaotic dynamics in an overlapping generations model: Forecasting and regularization. *Chaos, Solitons and Fractals* **196** (2025) 116371. https://doi.org/10.1016/j.chaos.2025.116371.

[2] T.A. Alexeeva, N.V. Kuznetsov and T.N. Mokaev. Study of irregular dynamics in an economic model: attractor localization and Lyapunov exponents. *Chaos Solitons and Fractals* **152** (9) (2021). https://doi.org/ 10.1016/j.chaos.2021.111365.

[3] T.A. Alexeeva, W.A. Barnett, N.V. Kuznetsov and T.N. Mokaev. Time-delay control for stabilization of the Shapovalov mid-size firm model. *IFAC-PapersOnLine* **53** (2) (2020) 16971–16976. https://doi.org/ 10.1016/j.ifacol.2020.12.1245.

[4] W.A. Barnett and U. Eryilmaz. An analytical and numerical search for bifurcations in open economy New Keynesian models. *Macroeconomic Dynamics* **20** (2) (2016) 482–503. https://doi.org/10.1017/S1365100514000224.

[5] J. Gali and T. Monacelli. Monetary policy and exchange rate volatility in a small open economy. *Review of Economic Studies* **72** (3) (2005) 707–734. https://doi.org/10.1111/j.1467-937X.2005.00349.x.

[6] J. He and F. Chen. Dynamical analysis of a new fractional-order Rabinovich system and its fractional matrix projective synchronization. *Chinese Journal of physics* **56** (5) (2018) 2627–2637. https://doi.org/10.1016/j.cjph.2018.09.014.

[7] K. Kalaichelvi, R. Rameshbabu, V. Dharshini Priya, P. Gokula Rithanya, G.K. Bhavadharani and K.S. Gayathiri, A novel chaotic jerk system with multistability and its circuit implementation. *Nonlinear Dynamics and Systems Theory* **25** (2) (2025) 161–170.

[8] A.R. Mamat, M.A. Mohamed, S. Vaidyanathan, A. Sambas, L. Patria, R. Ramesh, Electronic circuit and complete synchronization via active backstepping control for a new chaotic 3-D Jerk System. *Nonlinear Dynamics and Systems Theory* **25** (2) (2025) 206–216.

[9] A. Mashuri, N.H. Adenan, N.S. Abd Karim, T.S.Wei and Z. Zeng. Application of Chaos Theory in Different Fields -A Literature Review. *Journal of Science and Mathematics Letters* **12** (1) (2024) 92–101. https://doi.org/10.37134/jsml.vol12.1.11.2024.

[10] T. R. Nandi, A. K. Saha and S. Roy. Analysis of a fractional order epidemiological model for tuberculosis transmission with vaccination and reinfection. *Sci. Rep.* **14** (1) (2024) p. 28290. https://doi.org/10.1038/s41598-024-73392-x.

[11] I. Podlubny, Fractional Differential Equations. Academic Press, San Diego, 1999.

[12] V.I. Shapovalov, V.F. Kablov, V.A. Bashmakov and V.E. Avvakumov. Synergetic stability model for an average firm. In: Synergetics and Problems in Control Theory. Fizmatlit: Moscow, Russia, 2004.

[13] V.P. Singh and S. Singh. Fractional Calculus and Its Applications. A Comprehensive Review. *International Journal on Science and Technology* **16** (1) (2025) 1–7. https://doi.org/10.71097/IJSAT.v16.i1.2012.

[14] V. E. Tarasov. On History of Mathematical Economics: Application of Fractional Calculus. Mathematics **7** (6) (2019) p. 509. https://doi.org/10.3390/math7060509.

Nonlinear Dynamics and Systems Theory, **26** (1) (2026) 69–78

Optimal Thermal Diffusivity via Deep Learning for Heat Equation Image Denoising

H. Kharro [1*], S. M. Douiri [1] and M. Moumni [2]

[1] *IMIA Laboratory, A2MSDS Team, Department of Mathematics, Faculty of Sciences and Technics, Moulay Ismaïl University of Meknes, P.O. Box 509 Boutalamine, Errachidia 52000, Morocco.*

[2] *MAMCS Team, Department of Mathematics, Faculty of Sciences and Technics, Moulay Ismaïl University of Meknes, P.O. Box 509 Boutalamine, Errachidia 52000, Morocco.*

Received: December 16, 2024; Revised: January 27, 2026

Abstract: Modern cameras inevitably introduce noise into images, which impacts their visual quality. As a result, various noise reduction strategies are necessary. Researchers have proposed numerous techniques for reducing noise, including approaches based on the linear and nonlinear partial differential equations. The choice of parameter values in partial differential equations plays a significant role in image denoising. Accurate tuning of these parameters can balance noise reduction and detail preservation, leading to higher quality denoised image. On the other hand, misadjusted parameters can result in either excessive smoothing or insufficient noise removal. Given these reasons, in this paper, we will concentrate on denoising the image using the heat equation and aim to identify the optimal thermal diffusivity value by solving a nonlinear inverse problem, which will allow us to achieve the best possible image denoising results. Finally, for the numerical experiments, we will employ deep learning and the Physics-Informed Neural Networks method to find this optimal value.

Keywords: *image denoising; heat equation; heat inverse problem; deep learning; physics-informed neural networks.*

Mathematics Subject Classification (2020): 68U10, 35K05, 34A34, 34A55, 65D15, 68T07.

* Corresponding author: mailto:hafida.kharro10@gmail.com

© 2026 InforMath Publishing Group/1562-8353 (print)/1813-7385 (online)/http://e-ndst.kiev.ua

1 Introduction

One of the main challenges in computer vision and image processing is image denoising, which aims to estimate the original image by reducing noise from the contaminated version. Intrinsic and extrinsic conditions, such as sensor and environmental factors, can lead to image noise, which is often unavoidable in practical situations. Image denoising is quite important in many different applications, including image registration, image restoration, image classification and image segmentation, where reclaiming the original image content is essential for achieving high performance in these fields. Although several algorithms have been put forth for denoising images, the challenge of suppressing image noise persists, especially when images are captured under suboptimal conditions with high noise levels.

Generally, there are two typical methods for reducing image noise. One approach involves acquiring the data multiple times and averaging it, but this results in an extended acquisition time. Another method is to use post-processing techniques to reduce noise in the image. Numerous techniques have been proposed in the literature for image denoising [1]; these include the classic spatial and temporal filters, the nonlocal means algorithm, methods using anisotropic diffusion filters, bilateral and trilateral filters, the transformations of the curvelet and the contourlet, the wavelet transform, deep learning based methods, the maximum likelihood approach, and models based on partial differential equations (PDEs) [2, 3].

Recently, there has been a surge of interest in segmentation schemes based on PDEs, due to their many advantages, such as the reduction in computational complexity and their simplicity, since the problem reduces to the form of a PDE solution, which could be solved by iterative methods like the Finite Difference Method [4, 5]. One of the most widely used PDEs is the heat diffusion equation, which is defined as

$$\begin{cases} v_t(x,y,t) - \rho\Delta v(x,y,t) = 0 & \text{in } \mathcal{D}\times J, \\ v(x,y,0) = v_0 & \text{on } \mathcal{D}, \\ v(x,y,t) = 0 & \text{on } \partial\mathcal{D}\times J, \end{cases} \tag{1}$$

where $\mathcal{D} \subset \mathbb{R}^2$ is a bounded domain, $J = [0,T]$ is the interval of time with $T > 0$ and ρ represents the thermal diffusivity. The solution of this equation (1) can be represented as a convolution with a Gaussian function $G_\sigma(x,y)$ [6], specifically

$$v(x,y,t) = G_\sigma * v_0(x,y).$$

Instead of using the original image's classical convolution with G_σ, it is possible to solve the linear heat equation using the original image as the initial condition.

One of the biggest challenges when trying to denoise an image is the optimal choice of ρ value. As shown in Figure 1, each choice of ρ results in different denoising, and it is clear that the image is denoised better by $\rho = 0.8$ than by $\rho = 0.2$ since the PSNR value in the first case is equal to 25.50 and in the second case to 21.51, The question remains whether we can find the value that provides the best denoising. Indeed, searching for these optimal values often leads to inverse problems [7], which can be quite challenging in mathematics, and requires careful consideration and analysis to find the best solution. One of the techniques used in solving an inverse problem is the Physics-Informed Neural Networks (PINNs) method [8]. Recently, PINNs have appeared as a simple alternative method to solve many problems in engineering and computational science. Specifically, they

do not need meshes and may effectively resolve forward problems and ill-posed inverse problems [9, 10], which are typically challenging or unfeasible to resolve by employing conventional numerical techniques.

The primary advantage of the PINNs method is its capability to smoothly integrate all provided information, including initial/boundary conditions, experimental data, and governing equations, into the loss function. This effectively converts the original problem into an equivalent optimization problem. In the specific case of denoising using the heat equation, PINNs can learn the optimal value of ρ by minimizing the difference between the original and predicted denoised images. This approach can significantly reduce the computational cost and time required for denoising. The primary aim of this paper is to

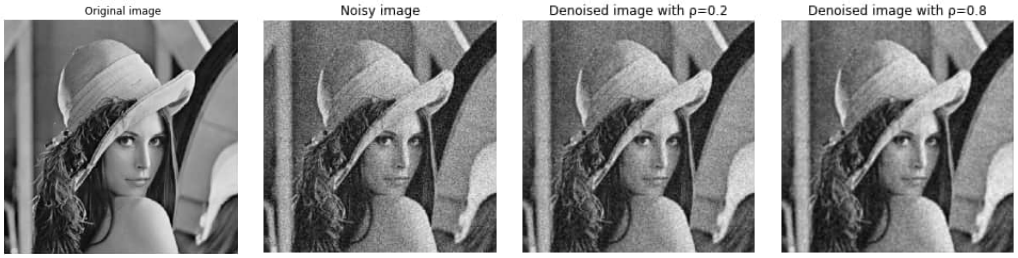

Figure 1: Image denoising using heat equation with various ρ values.

determine the optimal ρ to achieve the best image denoising using the PINNs method.

This paper is structured into several sections, which are outlined below. In Section 2, we demonstrate the existence of ρ. In Section 3, we use deep learning and the PINNs method to solve the heat inverse problem and find the optimal ρ. In Section 4, we perform a series of numerical experiments. The paper concludes with a summarization of key insights and findings.

2 Heat Inverse Problem

In this part, we are interested in the theoretical existence of ρ. The primary elements introduced in this section are Lemma 2.1 [11] and Theorem 2.1 [12,13]. Then we consider the problem (1) and we frequently receive the terminal condition observation given by

$$v(x,T) = r(x) \qquad \forall x \in \mathcal{D},$$

where $\mathcal{D}$ represents a bounded domain in $\mathbb{R}^d (d \geq 1)$ with a boundary Π that is piecewise smooth.

To establish the existence of ρ, we will require the following space:

$$GL(\mathcal{D}) = \{\rho \in L^1(\mathcal{D}); ||\rho||_{GL(\mathcal{D})} < \infty\},$$

where

$$||\rho||_{GL(\mathcal{D})} = ||\rho||_{L^1(\mathcal{D})} + \int_{\mathcal{D}} |D\rho|,$$

and

$$\int_{\mathcal{D}} |D\rho| = sup\Big\{ \int_{\mathcal{D}} \rho \, \mathrm{div} g dx;\ g \in (C_0^1(\mathcal{D}))^d\,; |g(x)| \leq 1 \quad \text{in } \mathcal{D}\Big\}.$$

We define the parameter identification problem as the subsequent constrained minimization process

$$\min_{\rho\in Q} J(\rho) = \frac{1}{2}\int_{\mathcal{D}} \rho|\nabla(w(\rho;T)-r)|^2 dx + \gamma P(\rho), \tag{2}$$

where $w = w(\rho;t) \in H_0^1(\mathcal{D})$ satisfying

$$w(x,0) = v_0(x), \tag{3}$$

and for a.e $t \in (0,T)$,

$$\int_{\mathcal{D}} w_t \phi dx + \int_{\mathcal{D}} \rho\nabla w\nabla\phi dx = 0 \qquad \forall\phi \in H_1^0(\mathcal{D}). \tag{4}$$

We denote the solution to the variational problem (3) and (4) as $w(\rho;t)$ or $w(\rho)$. In (2), the function $r \in H_0^1(\mathcal{D})$ represents the measured data, and $P(\rho)$ serves as a regularization term with a weighting coefficient $\gamma > 0$. Specifically,

$$P(\rho) = \int_{\mathcal{D}} |D\rho|$$

defines the semi-norm in the GL-space or in $H^1(\mathcal{D})$. The Q is a subset of $H^1(\mathcal{D})$ or $GL(\mathcal{D})$ and is defined by

$$Q = \big\{\rho \in L^1(\mathcal{D});\ |||\rho||| < \infty \text{ and } \beta_1 \le \rho \le \beta_2 \text{ a.e in } \mathcal{D}\big\},$$

where $|||\rho||| = ||\rho||_{H^1(\mathcal{D})}$ or $|||\rho||| = ||\rho||_{GL(\mathcal{D})}$, β_1 and β_2 are two positive constants.

It is essential to recognize that evaluating the cost functional $J(\rho)$ necessitates having the terminal state value of the solution $w(\rho;t)$ for the system described by (3) and (4) at $t = T$. This implies the regularity $w \in C(0,T;H_0^1(\mathcal{D}))$.

For the purposes of this analysis, we will consider the following assumption about the initial data for the problem (1):

$$v_0 \in H^1(\mathcal{D}). \tag{5}$$

Assuming (5), classical parabolic theory assures that for every $\rho \in Q$, there exists a unique solution $w(\rho;t)$ to the parabolic problem, which corresponds to the variational problem defined in (3) and (4). This solution exhibits the following regularity properties:

$$w(\rho) \in L^2(0,T;H_0^1(\mathcal{D})), \quad w(\rho) \in H^1(0,T;L^2(\mathcal{D})), \quad w(\rho) \in C(0,T;L^2(\mathcal{D})).$$

Instead of using the system described in (2)-(4), we will adopt a simpler formulation as follows:

$$\min_{\rho\in Q} J(\rho) = \frac{1}{2}\int_{T-\sigma}^{T}\int_{\mathcal{D}} \rho|\nabla(w(\rho;t)-r)|^2 dxdt + \gamma P(\rho), \tag{6}$$

where σ is a small constant number and $w = w(\rho;t) \in H_0^1(\mathcal{D})$ satisfying

$$w(x,0) = v_0(x) \quad \text{in } \mathcal{D}, \tag{7}$$

$$\int_{\mathcal{D}} w_t\phi dx + \int_{\mathcal{D}} \rho\nabla w\nabla\phi = 0 \qquad \forall\phi \in H_0^1(\mathcal{D}), \tag{8}$$

for a.e, $t \in (0,T)$.

We will now show that the problem (6)-(8) has a minimizer by employing the following lemma.

Lemma 2.1 *[11] Let $\{\rho_m\}$ be a sequence in Q that converges to $\rho \in L^1(\mathcal{D})$ as $m \to \infty$, then we have*

$$\lim_{m\to\infty} \int_{T-\sigma}^{T} \int_{\mathcal{D}} \rho_m |\nabla(w(\rho_m) - r)|^2 dxdt = \int_{T-\sigma}^{T} \int_{\mathcal{D}} \rho |\nabla(w(\rho) - r)|^2 dxdt.$$

Using Lemma 2.1, we obtain the following result.

Theorem 2.1 *[12, 13] For the optimization problem* (6)-(8)*, there is at least one minimizer.*

3 Using Deep Learning for Solving the Heat Inverse Problem and Finding ρ Optimal

We use heat equation (1) to denoise the image, knowing that the solution to the equation is the denoised image. The noisy image is denoted as v_0, the original image as v_T, and the Laplacian Δv is defined as the convolution product between the noisy image and the kernel I, which is defined as

$$I = \begin{bmatrix} 0 & 1 & 0 \\ 1 & -4 & 1 \\ 0 & 1 & 0 \end{bmatrix}.$$

The choice of ρ is very important, so we will look for an optimal ρ which is a solution to the heat inverse problem (1), and to solve it we use PINNs. To define the algorithm for PINNs, we can refer to [14].

Algorithm 3.1 *PINNs for Solving the Inverse Problem*

1. *Create a neural network (NN) with parameter ρ, initialized randomly.*
2. *Identify the training datasets.*
3. *Define the loss function as the weighted sum of the L^2 norms of: the initial condition residual, the PDE residual, and the final-time solution residual.*
4. *Train the NN to optimize the parameter ρ by minimizing the loss function.*

First, a NN denoted by $\hat{v}(X;\theta;\rho)$ with $X = (x, y, t)$ is constructed as a surrogate of the solution of the problem (1) $v(x, y, t)$, and it takes the coordinates (x, y, t) as the inputs, and outputs a vector that has the same dimension as v. Here, the NN parameters that will be tuned at the training stage are denoted by θ, namely, θ contains all of the biases b and weights w, and ρ is a specific parameter representing thermal diffusivity. One benefit of employing PINNs, where neural networks are utilized as approximators for v, is that it enables us to compute the derivatives of $\hat{v}$ with respect to its input X. This is achieved through the chain rule for differentiating function compositions, supported by automatic differentiation tools [14] that are commonly integrated into machine learning packages such as PyTorch and TensorFlow. In the following step, it is necessary to ensure that the neural network $\hat{v}$ conforms to the physical constraints dictated by the PDE and the boundary/initial conditions. Practically, this is accomplished by constraining $\hat{v}$ at a series of scattered points, which serve as the training data $\tau = \{X_1, X_2, \ldots, X_\tau\}$ with a size of $|\tau|$.

To evaluate the disparity between the constraints and the neural network $\hat{v}$, we define the loss function as

$$\chi(\theta;\rho) = ||v_t - q\Delta v||_{L^2} + ||v - v_0||_{L^2} + ||v - v_T||_{L^2}.$$

In the last step, we employ gradient-based optimization methods, including Adam, to minimize the loss function and find the optimal parameters θ (θ^*) and ρ (ρ^*). Refer to Figure 2 for a visual representation of a neural network.

Consider the noisy image as a given gray-scale intensity map $v_0 : \mathcal{D} \to [0, 255]$ for the image domain $\mathcal{D} \in \mathbb{R}^2$. The solution of the problem (1) denotes the restored image, and v_T is the original image. We can find ρ^* by following Algorithm 3.2.

Algorithm 3.2 *Finding ρ^* using deep learning*

1. *Read the image from a file using an image processing library (e.g., OpenCV, PIL, or skimage).*
2. *Add noise to the image.*
3. *Discretize a two-dimensional spatial domain (x, y) and a temporal domain (t) using* ***linspace*** *from the NumPy library.*
4. *Generate a meshgrid of coordinates X and Y from given 1D arrays x and y, and define initial time (t_0) and final time (t_f).*
5. *Define X_{star}, X_{starf}, and X_{star0} using* ***hstack()****.*
6. *Define the function* ***heat_loss****, which takes three parameters:* $\boldsymbol{v}$*, ρ, and X_{star}, and returns the squared sum of $v_t - \rho\nabla v$.*
7. *Define the function* ***heat_loss0****, which takes three parameters:* $\boldsymbol{v}$*, ρ, and X_{star0}, and returns the squared sum of the difference between the noisy image and the neural network's output.*
8. *Define the function* ***heat_lossT****, which takes three parameters:* $\boldsymbol{v}$*, ρ, and X_{starf}, and returns the squared sum of the difference between the original image and the neural network's output.*
9. *Define a total loss function as the sum of* ***heat_loss****,* ***heat_loss0****, and* ***heat_lossT****.*
10. *Construct a neural network (NN) with parameter ρ.*
11. *Train the model and optimize the loss function using the Adam optimizer.*

4 Numerical Results

In this part, we perform our experiments using the well-known images Lena.png, Barbara.png and Mandrill.png noised with Gaussian additive noise ($\sigma = 50$). All tests were performed with PYTHON.
We use Algorithm 3.2 for three images Lena.png, Barbara.png, and Mandrill.png. The hyperparameters used are listed in Table 1. After determining ρ^*, the obtained values are presented in Table 2.

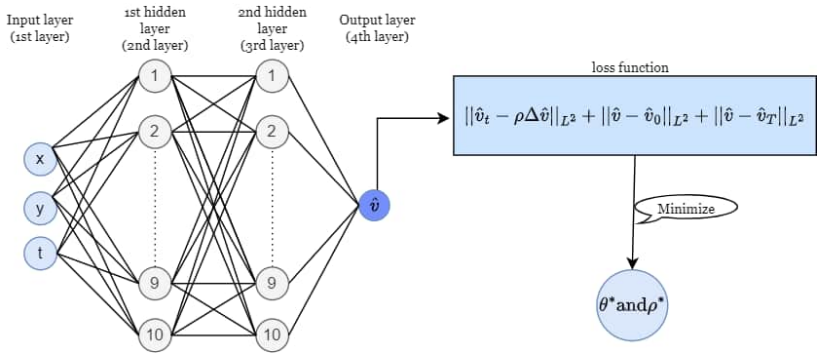

Figure 2: PINNs schematic for solving the heat inverse problem.

Activation function	Optimizer	Learning rate
tanh	Adam	0.0001

Table 1: Hyperparameters used for all experiments.

Image	Lena.png	Barbara.png	Mandrill.png
ρ^*	0.9634	0.9360	0.9752

Table 2: Optimal ρ values (ρ^*) for various images.

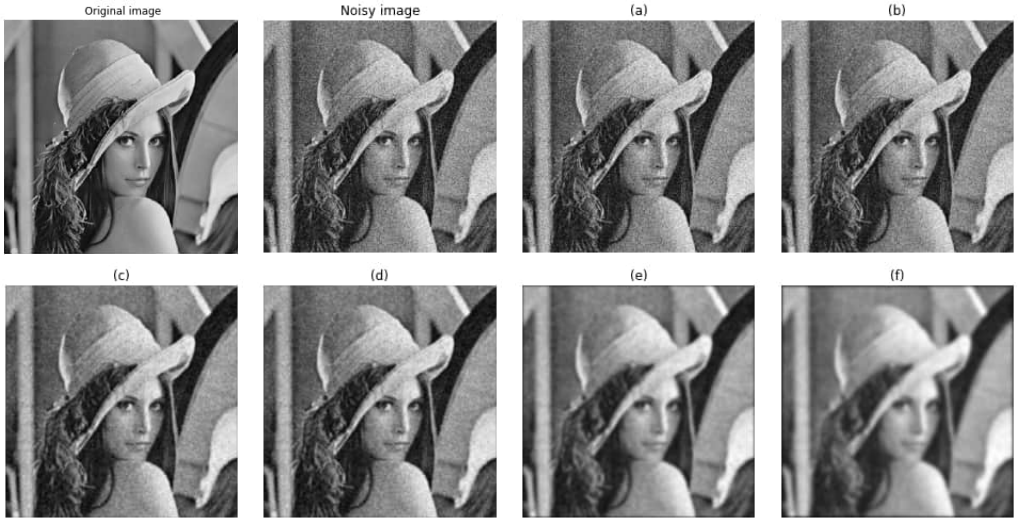

Figure 3: Denoising results for Lena.png image with various ρ values: (a) $\rho = 0.01$, (b) $\rho = 0.1$, (c) $\rho = 0.9634$, (d) $\rho = 1$, (e) $\rho = 4$, (f) $\rho = 8$.

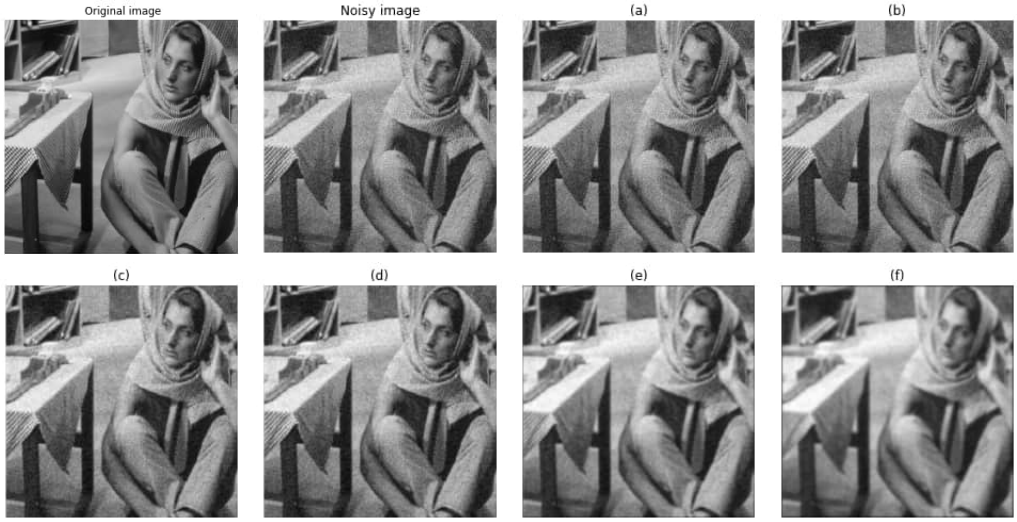

Figure 4: Denoising results for Barbara.png image with various ρ values: (a) $\rho = 0.01$, (b) $\rho = 0.1$, (c) $\rho = 0.9360$, (d) $\rho = 1$, (e) $\rho = 4$, (f) $\rho = 8$.

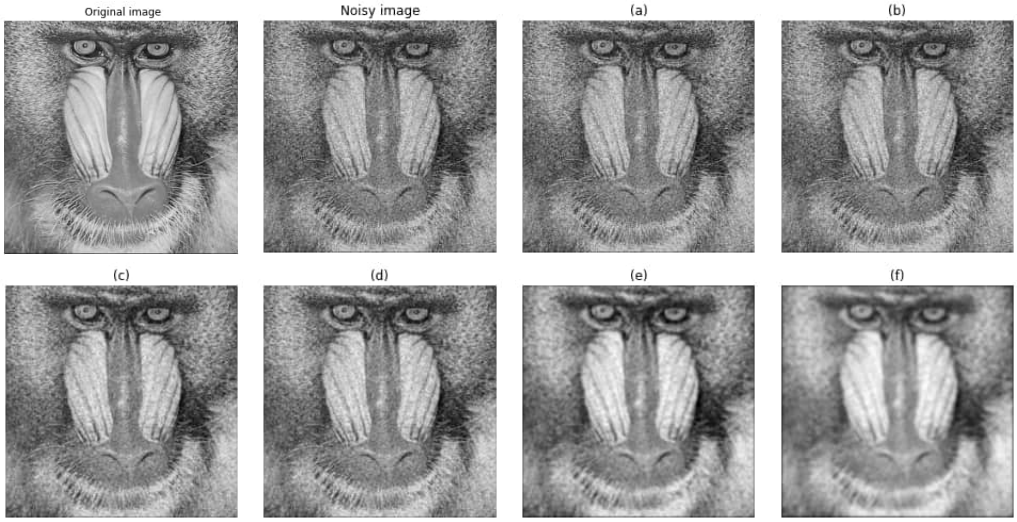

Figure 5: Denoising results for Mandrill.png image with various ρ values: (a) $\rho = 0.01$, (b) $\rho = 0.1$, (c) $\rho = 0.9752$, (d) $\rho = 1$, (e) $\rho = 4$, (f) $\rho = 8$.

Then restore the image using the heat equation with Δt equal to 0.001. The denoising results are illustrated in Figures 3, 4 and 5.

To evaluate image quality and perform comparisons, we will utilize the widely-used metric, peak-signal-to-noise ratio (PSNR) [15], which is defined as

$$PSNR = 10 \log_{10} \left(\frac{MN \times 255^2}{\sum_{i,j} (l_{ij} - m_{ij})^2} \right),$$

where $M \times N$ represents the image dimensions, and m_{ij} and l_{ij} are the values of the pixels of the restored and original images, respectively.

Tables 3, 4, 5 illustrate the PSNR values for each ρ value for the three images, and we observe that the highest PSNR value is the value corresponding to ρ^*.

ρ	0.01	0.1	0.7	0.8	**0.9634**	1	2	4	8
PSNR	15.26	18.80	25.40	25.48	**25.5079**	25.4934	24.71	23.21	21.52

Table 3: PSNR (dB) of different ρ values for Lena.png image.

ρ	0.01	0.1	0.7	0.8	**0.9360**	1	2	4	8
PSNR	10.07	18.58	25.59	25.70	**25.7434**	25.7341	25.01	24.28	23.45

Table 4: PSNR (dB) of different ρ values for Barbara.png image.

ρ	0.01	0.1	0.7	0.8	**0.9752**	1	2	4	8
PSNR	14.73	16.50	21.31	21.42	**21.4819**	21.4813	21.08	20.48	19.84

Table 5: PSNR (dB) of different ρ values for Mandrill.png image.

5 Conclusion

In this study, we investigated the use of the heat equation for image denoising and demonstrated the existence of the optimal value of the thermal diffusivity ρ by solving a nonlinear inverse problem. We also introduced a novel algorithm that combines deep learning and Physics-Informed Neural Networks to determine the optimal ρ for each image. To demonstrate the effectiveness of our proposed method, we conducted a numerical simulation and compared the denoising results for three images using the optimal $\rho^\star$ and various other ρ values. Then, in Tables 3, 4 and 5, we present the PSNR values for each ρ value, highlighting that the highest PSNR value occurs at the optimal $\rho^\star$. The results of our study show that the optimal choice of thermal diffusivity $\rho^\star$ plays a crucial role in achieving the best image denoising performance. The combination of deep learning techniques and Physics-Informed Neural Networks proves to be an effective and innovative approach to determining this optimal value. Our numerical experiments demonstrate that this method outperforms traditional techniques and offers a promising solution for image denoising in various practical applications. For future research, we would like to work with other types of noise, and we will focus on other models based on PDEs.

References

[1] A. Buades and B. Coll and J. M. Morel. A review of image denoising algorithms, with a new one. *Multiscale modeling and simulation* **4** (2) (2005) 490–530.

[2] B. Kawar and M. Elad and S. Ermon and J. Song. Denoising diffusion restoration models. *Advances in Neural Information Processing Systems* **35** (2022) 23593–23606.

[3] S. M. Douiri and H. Farjil and M. Moumni. Improved Perona-Malik Model with a Leray-Lions Operator for Image Denoising. *Bol. Soc. Paran. Mat* **43** (2025) 1–14.

[4] A. Z. Arifin and M. I. Joesidawati and T. Herlambang and S. Mizan and A. A. Suryanto. Simulation of Tsunami Wave Propagation Using the Finite Difference Method for Disaster Early Warning System. *Nonlinear Dynamics and Systems Theory* **25** (1) (2025).

[5] M. Khumalo and A. Dlamini. The Finite Element Method for Nonlinear Nonstandard Volterra Integral Equations. *Nonlinear Dynamics and Systems Theory* **20** (2) (2020) 191–202.

[6] Q. D. Ho and H. T. Huynh. An Image Denoising Model Based on Nonlinear Partial Diferential Equation Using Deep Learning. *Future Data and Security Engineering. Big Data, Security and Privacy, Smart City and Industry 4.0 Applications, Springer Nature* **1688** (2022) 407–418.

[7] A. Benguesmia and I. M. Batiha and T. E. Oussaeif and A. Ouannas and W. G. Alshanti. Inverse problem of a semilinear parabolic equation with an integral overdetermination condition. *Nonlinear Dynamics and Systems Theory* **23** (2) (2023) 249–260.

[8] M. Raissi and P. Perdikaris and G. E. Karniadakis. Physics-informed neural networks: a deep learning framework for solving forward and inverse problems involving nonlinear partial differential equations. *Journal of Computational Physics* **378** (2019) 686–707.

[9] A. D. Jagtap and E. Kharazmi and G. E. Karniadakis. Conservative physics-informed neural networks on discrete domains for conservation laws: Applications to forward and inverse problems. *Computer Methods in Applied Mechanics and Engineering* **365** (2020) 113028.

[10] M. Moumni and M. Tilioua. A neural network approximation for a model of micromagnetism. *Nonlinear Dynamics and Systems Theory* **22** (4) (2022) 432–446.

[11] Y. L. Keung and J. Zou. Numerical identifications of parameters in parabolic systems. *Inverse Problems* **14** (1) (1998) 83.

[12] Y. L. Keung and J. Zou. Identifying Parameters in Parabolic Systems by Finite Element Methods. *Technical Report 97–10 126*, Department of Mathematics, The Chinese University of Hong Kong, (1997).

[13] K. Kunisch and W. Ring. Regularization of nonlinear illposed problems with closed operators. *Numerical functional analysis and optimization* **14** (3–4) (1993) 389–404.

[14] L. Lu and X. Meng and Z. Mao and G. E. Karniadakis. DeepXDE: A Deep Learning Library for Solving Differential Equations. *SIAM review* **63** (1) (2021) 208–228.

[15] S. I. Hong and K. R. Dong and Y. H. Ryu. SNR and PSNR measurements and analysis of median filtering for the removal of impulse noise from CR imaging. *International Journal of Contents* **5** (4) (2009) 7–12.

Nonlinear Dynamics and Systems Theory, **26** (1) (2026) 79–88

A Reliable Service Provider System-Mathematical Model and Dynamical Behavior

P. R. S. Rao [1], K. V. Ratnam [2*] and G. Shirisha [3]

[1] *Govt.Polytechnic, Kalidindi - 521344, Krishna District, A.P., India.*
[2] *Department of Mathematics, Birla Institute of Technology and Science-Pilani, Hyderabad Campus, Hyderabad-500078, India.*
[3] *Department of Mathematics, Stanley College of Engineering and Technology for Women, Abids, Hyderabad-500001, Telangana, India.*

Received: November 3,, 2021; Revised: January 13, 2026

Abstract: In this paper, a two-layered service provider system is considered in which one layer directly interacts with a client system and each member of the first layer is supported by a sub-group of members in the second layer, in completing a task put forth by the client. The mathematical model presented is a modification of an existing model studied by the authors. Since different groups are working on the task, a consensus is to be achieved by the system. In terms of mathematics, sufficient conditions are established on the system parameters so that the solutions remain asymptotically close to each other, and upon restricting the inputs, the solutions become bounded. This means that all the solutions approach a bounded solution of the system, implying that a consensus is formed. Once it is established that all members of the system are working together, it is necessary to meet the requirements of the client. Mathematically, it is achieved in terms of asymptotic stability of the desired solution through the Lyapunov functional method. For this, a set of sufficient conditions is obtained for the parameters and the functional relations of the system. Numerical examples are provided to verify the results and are supported by simulations. On the whole, our study provides a reliable service provider system that understands the requirements of the client, makes the assessment of its own capacities, gets back to the client for proper inputs and finally, delivers the output desired by the client.

Keywords: *focal and non-focal parts; client and server; time delays; variable inputs; desired solution.*

Mathematics Subject Classification (2020): 34A12, 34K20, 92B20, 93D20.

* Corresponding author: mailto:vrkota@hyderabad.bits-pilani.ac.in

© 2026 InforMath Publishing Group/1562-8353 (print)/1813-7385 (online)/http://e-ndst.kiev.ua

1 Introduction

The world is longing for services - either to provide or to receive. Thus, the service sector is exhibiting growth enormously. Customer satisfaction is the utmost concern for any service provider system for its survival, and it is its most important performance indicator [9, 14]. Service providers can be broadly classified into two categories, namely, (i) product-specific, where the service provider fixes to certain products and offers only relevant services and (ii) client-specific, where the service provider caters to any needs of the client. For example, services to automobiles, electronic goods, etc., may be regarded as product-specific, while services of architects, lawyers, software developers, etc., are client-specific. In this paper, we are going to consider a client-specific service provider system. Usually, such systems maintain different layers. They may have one main layer (consisting of CEOs, Managers, Marketing team, etc., for example) that directly interacts with the client, understands the requirements and defines the problem. The other layers (may consist of the Technical team, Finance team, etc., for example) are equipped with various skills to work on issues of the client as posed by the first layer and report back to the first layer. The system arrives at a final solution due to a combined effort of the two layers. At the same time, clients can be of two types: those who continuously interact and participate in the development of their product along with the server, and those who simply provide necessary inputs, specify what is required and wait for a solution from the server, as this could save their time and resources. We prefer, in this study, clients of the second category.

The service provider system we are going to consider in this work consists of two layers, which may be called the 'outer layer' and the 'inner layer' of the system. The outer layer (may also be called 'focal layer') directly receives inputs from external sources (client), processes the information among its constituents, passes on instructions to inner layer units, and waits for their responses. The inner layer (may be called 'non-focal layer') forms a closed subsystem of the entire system in the sense that it receives and reacts to instructions from the outer layer only. Accordingly, they carry out activities internally. The overall performance of the system is judged by the outcome given by the outer layer in coordination with its inner counterparts. Our aim here is to propose and understand the behavior of such a dynamical system in mathematical terms. Usually, client-server models are understood as queuing models in which customers wait in queue lines for being served. Various performance measures and methods to evaluate them are also available in the literature of queuing theory [1, 2, 6, 8]. The model we are presenting is not a queuing model with a client waiting in a queue, but a system that requires coordination and cooperation among constituent groups for success or survival [2, 3]. The only question considered here is whether the requirements of the client are eventually met by the server system or not. How the parameters and functional relations in the system are to be chosen or restricted to make the system to perform for the satisfaction of the client's needs. This in itself tests the suitability of the model presented.

In general, the performance of a dynamical mathematical model is measured in terms of a qualitative study of its solutions, namely, the existence and uniqueness of solutions (i.e., the availability of non-conflicting solutions), the existence of equilibria (i.e., solutions of known or fixed behavior), boundedness (i.e., controllable solutions) and finally, the stability of an equilibrium solution (i.e., the behavior of other solutions when staying near a known, fixed solution showing that the entire system is controllable and therefore predictable) [12, 13]. Besides this, an important contention of this study is to answer the question: When all the qualities are present in the system, under what extra conditions

the system will approach a pre-specified solution required by the client? Our aim in this paper is to provide reasonable answers to the above questions in terms of mathematical results. The model we are considering here is motivated by the study in [12], wherein the authors considered a two-layered network to understand the dynamics in a cooperative supportive neural network. We modify the model to suit our needs here and finally see that the results presented here are applicable to more general situations and include some of the earlier works on similar models in [12]. Furthermore, making use of the techniques from [13], we wish to obtain concrete results to reach the solution/output desired by the client.

The paper is organized as follows. In Section 2, the model is described in detail, and the basic properties of the dynamical system are discussed. In Section 3, the qualitative properties of solutions, namely, their boundedness and asymptotic closeness, are discussed. In Section 4, sufficient conditions on system parameters are established to ensure client satisfaction under suitable inputs from the client. Theoretical numerical examples with simulations are provided to illustrate the effectiveness of the results. A discussion is presented in Section 5, followed by concluding remarks with some open problems in Section 6.

2 The Model and Basic Properties

The following picture (Figure 1) is a formal representation of our assumptions. We

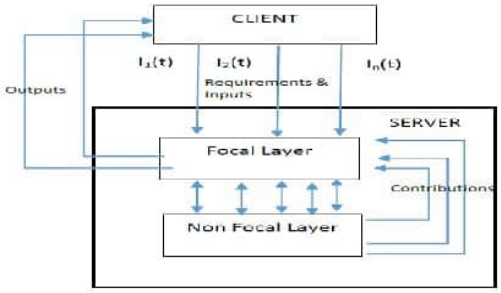

Figure 1: A schematic diagram of the proposed client-service provider system.

provide our mathematical model describing the dynamics of the server system. We consider the following system of equations:

$$\begin{aligned} x_i^{'} &= -a_i x_i + \sum_{j=1}^{n} b_{ij} f_j(x_j(t-\tau_j)) + \sum_{k=1}^{r_i} c_{ii_k} g_{i_k}(x_i, y_{i_k}) + I_i(t), \\ y_{i_k}^{'} &= -c_{i_k} y_{i_k} + \sum_{l=1}^{r_i} d_{i_l} h_{i_l}(y_{i_l}) + J_{i_k}(x_i(t-\delta_i)), \end{aligned} \tag{1}$$

$i = 1, 2, ..., n, k = 1, 2, ..., r_i, 1 \leq r_i \leq n.$

In (1), $x_i(t)$ denotes the state of a typical focal member at any time t and $y_{i_k}(t)$ denotes the state of a typical non-focal member at time t and k is the number of y_{i_k}'s attached to each specific x_i. Here $' = \frac{d}{dt}$ denotes the time derivative of the variables.

The positive constants a_i, c_{i_k} respectively denote the rates at which the members x_i, y_{i_k} come back to resting states in the absence of any activity. They are usually called

resting potentials or passive decay rates in the literature. The functional relations f_j, $j = 1, 2, ..., n$, denote the interactions among the focal members. The constant b_{ij} denotes the connection strength between the i^{th} and j^{th} focal members and is the rate at which focal parts communicate with each other. g_{i_k} shows how focal and non-focal members communicate with each other. This function plays a vital role in the dynamics of x_i's, the response of x_i's to the client, and is the only channel through which y_{i_k}'s contribute to focal parts. c_{ii_k} is the constant rate at which the x_i's receive information from y_{i_k}. $I_i(t)$ is the input at any time t from the client system to an x_i. The parameter d_{i_l} is the constant rate at which a typical member y_{i_l} of the non-focal subgroup corresponds with its co-member y_{i_k}. The function h_{i_l} is the functional response of y_{i_l} towards y_{i_k}. $J_{i_k}(x_i)$ is the functional input or instruction to y_{i_k} from x_i. Further, τ_i and δ_i respectively denote the time delays in the processing of information in the focal part and transmission of information from focal to non-focal parts.

We assume that the nonlinear response functions f_j, g_{i_k} and h_{i_l} satisfy the following local Lipschitz conditions, which are commonly used in the literature to establish the existence of solutions to any dynamical system:

$$\begin{aligned}
&|f_j(x_j) - f_j(\overline{x}_j)| \le p_j|x_j - \overline{x}_j|,\\
&\|g_{i_k}(x_i, y_{i_k}) - g_{i_k}(\overline{x}_i, \overline{y}_{i_k})\| \le M_{1i_k}|y_{i_k} - \overline{y}_{i_k}| + M_{2i_k}|x_i - \overline{x}_i|,\\
&|h_{i_k}(y_{i_k}) - h_{i_k}(\overline{y}_{i_k})| \le q_{i_k}|y_{i_k} - \overline{y}_{i_k}|,\ |J_{i_k}(x_i) - J_{i_k}(\overline{x}_i)| \le N_{i_k}|x_i - \overline{x}_i|. \qquad (2)
\end{aligned}$$

Here, $p_j, M_{1i_k}, M_{2i_k}, q_{i_k}$ and N_{i_k} are the corresponding Lipschitz constants. For the examples of functions commonly used in the literature, one can refer to [12, 13].

Since the inputs from the client should not disturb the aim of the task by deviating too much from what is initially presented to the server, we may assume that

(A). The input functions I_i for $i = 1, 2, ..., n$ are bounded continuous functions of time-variable $t \in [0, \infty]$.

Under the conditions (2) on the response functions J_{i_k} and assumption (A) on the inputs, we may easily establish that the system possesses unique solutions that are continuable in their maximal intervals of existence with suitably chosen initial conditions (see, e.g., [11]). Hence, we assume that these conditions hold throughout the text and proceed with the analysis of the behavior of solutions of the system (1).

3 Behavior of Solutions

Since different members are working on the task/project to meet the requirements of the client, a variety of solutions are expected corresponding to appropriate initial conditions. But there should be an affinity among all such solutions in the sense that they are close enough, all meeting the requirements of the client. In other words, all solutions of the system should be close enough eventually. Further, no solution should be beyond the purview of the system requirements. That is, any solution should be manageable. Mathematically, this requires all solutions to be bounded. This makes the system controllable. We shall see how we need to restrict the system parameter spaces and functional relations suitably to achieve this. First, we begin with the asymptotic nearness of solutions to see how close they are to each other, and no single solution is out of range.

Definition. Two solutions $u(t)$ and $v(t)$ of the system $z'(t) = F(t, z(t))$ are said to be asymptotically near or close to each other if $\lim_{t\to\infty} |u(t) - v(t)| = 0$.

Theorem 3.1 *For any pair of solutions (x_i, y_{i_k}) and $(\overline{x}_i, \overline{y}_{i_k})$ of (1), we have*

$\lim_{t\to\infty}|(x_i, y_{i_k}) - (\overline{x}_i, \overline{y}_{i_k})| = 0$, *provided the response functions satisfy (2) and the parameters satisfy* $\overline{A} = min\{A, B\} > 0$, *where for* $i = 1, 2, ..., n$ *and* $k = 1, 2, ..., r_i$,

$$A = min\Big\{a_i - \sum_{j=1}^{n}|b_{ji}|p_i - \sum_{k=1}^{r_i}\Big(|c_{ii_k}|M_{2i_k} + N_{i_k}\Big)\Big\},$$

$$B = min\Big\{c_{i_k} - \sum_{l=1}^{r_i}|d_{i_l}|q_{i_l} - |c_{ii_k}|M_{1i_k}\Big\}. \tag{3}$$

Proof. We consider the functional $V(t) = \sum_{i=1}^{n}\Bigg[|x_i - \overline{x}_i| + \sum_{j=1}^{n}|b_{ij}|\int_{t-\tau_j}^{t}|f_j(x_j(z)) - f_j(\overline{x}_j(z))|dz + \sum_{k=1}^{r_i}\Big[|y_{i_k} - \overline{y}_{i_k}| + \int_{t-\delta_i}^{t}|J_{i_k}(x_i(z)) - J_{i_k}(\overline{x}_i(z))|dz\Big]\Bigg]$ and use Lyapunov stability to prove the result.

Remark 3.1 It is clear from Theorem 3.1 that all the solutions of system (1) are together, that is, do not behave differently and do not deviate much from each other under the conditions specified. We shall now obtain conditions for the solutions of the system to be bounded. Then, under the conditions of Theorem 3.1, all the solutions stay near a bounded solution. Thus, we may predict the behavior of the system and try to control it.

Theorem 3.2 *Assume that the parameters satisfy the condition (3) and let the response functions satisfy, besides (2), the conditions* $f_j(0) = 0$, $g_{i_k}(0, 0) = 0$, $h_{i_l}(0) = 0$ *and* $J_{i_k}(0) = 0$ *for* $i = j = 1, 2, ..., n$, $k = l = 1, 2, ..., r_i$, *where* $1 \le r_i \le n$. *Further, if the inputs satisfy* $\int_0^\infty \sum_{i=1}^{n}|I_i(s)|ds < \infty$, *then all the solutions of (1) are bounded.*

Proof. To prove the statement, we employ the functional $V(t) = \sum_{i=1}^{n}\Bigg[|x_i(t)| + \sum_{j=1}^{n}|b_{ij}|\int_{t-\tau_j}^{t}|f_j(x_j(z))|dz + \sum_{k=1}^{r_i}\Big[|y_{i_k}(t)| + \int_{t-\delta_i}^{t}|J_{i_k}(x_i(z))|dz\Big]\Bigg]$.

Now we shall establish the conditions under which the solutions of (1) approach each other exponentially. We may expect further restrictions on parameters for such faster convergence. We use the following lemma for our next result.

Lemma 3.1 *([13]) If* $\varphi : [t_0, \infty)$ *is continuous such that* $\varphi'(t) \le -p\varphi(t) + q\sup_{t-t_0\le s\le t}\{\varphi(s)\}$ *for* $t \ge t_0$ *and if* $p > q > 0$, *then there exist positive constants* l, r *such that* $\varphi(t) \le le^{-rt}$ *for* $t \ge t_0$.

Theorem 3.3 *For any set of input functions, any pairs of solutions* (x_i, y_{i_k}) *and* $(\overline{x}_i, \overline{y}_{i_k})$ *of (1) are asymptotically exponentially close, provided the parameters satisfy the condition* $\alpha > \beta$, *where*

$$\alpha \equiv \min_{1\le i\le n, 1\le k\le r_i}\Big\{a_i - \sum_{k=1}^{r_i}\Big(|c_{ii_k}|M_{2i_k}\Big), c_{i_k} - \sum_{k=1}^{r_i}|d_{i_k}|q_{i_k} - |c_{ii_k}|M_{1i_k}\Big\},$$

$$\beta \equiv \sum_{i=1}^{n}\Big[\sum_{j=1}^{n}|b_{ji}|p_i + \sum_{k=1}^{r_i}N_{i_k}\Big]. \tag{4}$$

Proof. Using Lemma 3.1 and by considering the functional $V(t) = \sum_{i=1}^{n} \left[|x_i - \overline{x}_i| + \sum_{k=1}^{r_i} |y_{i_k} - \overline{y}_{i_k}| \right]$, we prove the result.

Remark 3.2 One may notice that the conditions on parameters in (4) are weaker than those in (3). That is, parameters have to take more strain for the solutions to be exponentially close. When we need a faster convergence depending on the client demands, then by straining the parameters more as in Theorem 3.3, any two solutions of the system come close to each other exponentially.

4 Performance of the System

The client system, being the end-user, should know what it needs to provide the server system to get what it requires. This is essential because there should be a correlation between the input provided by the client and the output produced by the server system. First, the client needs to spell out what is required. The focal parts of the server then study the request, understand it, provide the non-focal system with the necessary inputs, obtain its contribution and finally, see how the requirements of the client are to be met. In other words, the client requirements are to be discussed by constituent units and the system is to be checked for its abilities and limitations. It is where the interactions among units (functional relations) and their connection strengths (represented by parameters) play a vital role in deciding whether the client requirements are within the reach of the server system. Once it is identified that the solution is within the scope of the server system, it may ask for the information needed from the client to put forth the desired solution.

This may be consolidated as follows. The client puts forth its required solution. The server system tests itself whether such a solution is possible through its dynamics, functional relations and parametric spaces. The server identifies the suitable information needed from the client. Once the inputs provided by the client are within the range prescribed, the server provides the required solution.
Before going further, we rewrite the system (1) as

$$\begin{aligned} x^{'}(t) &= -ax(t) + bf(x(t-\tau)) + c_1 g(x(t), y(t)) + I(t), \\ y^{'}(t) &= -cy(t) + dh(y(t)) + J(x(t-\delta)). \end{aligned} \tag{5}$$

The present method is motivated by [13]. The technique is different from the usual feedback control techniques [5, 7] used in the literature. As described above, we assume that (i) The solution required by the client is α; (ii) An input of $J(\alpha)$ is provided by focal part x to non-focal part y; (iii) Corresponding to this input, β is the contribution of y with some strain on parameters and functions; (iv) The server then estimates the inputs $I(t)$ required from the client; (v) Once the requisite inputs are provided, the focal part x produces the output α with some strain on parameters and functional relations. Mathematically, the solutions represented by (x, y) of (5) should reach a pre-specified output (α, β). This means an output of α is expected by the client from the focal part x of the system corresponding to an input of $I(t)$, with β denoting the expected contribution of the non-focal part y.

Theorem 4.1 *Assume that the parameters of (5) satisfy the conditions*

$$0 < min\{a - bp - c_1 l - N, c - dq - c_1 m\} < \infty. \tag{6}$$

Assume also that the response functions and J satisfy conditions (2). Then for any arbitrarily chosen output (α, β) *satisfying*

$$J(\alpha) = c\beta - dh(\beta), \tag{7}$$

all solutions $(x,\ y)$ *of system (5) converge to* (α, β)*, provided the input to the focal part satisfies the condition*

$$\int_0^\infty \Big[|I(s) - a\alpha + bf(\alpha) + c_1 g(\alpha, \beta)|\Big] ds < \infty. \tag{8}$$

Proof. We employ the functional $V(t) = |x(t) - \alpha| + |y(t) - \beta| + b\int_{t-\tau}^{t} |f(x(s)) - f(\alpha)|ds + \int_{t-\delta}^{t} |J(x(s)) - J(\alpha)|ds$ and prove the result.

Remark 4.1 In Theorem 4.1, there are three requirements on the functions and parameters of the system. By the condition $J(\alpha) = c\beta - dh(\beta)$ (i.e., equation (7)), we mean that the contribution of y, that is, β, should satisfy the input requirement from x. This may provide a number of solutions $(\alpha,\ \beta)$ for the system over a space of parameters for each choice of J, as may be seen in examples provided below. For a unique solution, we may prefer further conditions such as the monotonicity of h, the interaction function among non-focal members. The condition (8) in Theorem 4.1 indicates that all inputs should eventually stay around the output-based server system requirements (i.e., near $a\alpha - bf(\alpha) - c_1 g(\alpha, \beta)$). This clearly states that the client cannot demand a suitable solution without providing proper inputs. Also, note that the restriction on I depends only on the contributions α and β of x and y, respectively, but not on J, the way how x instructs y. Finally, the sufficient conditions (6) on parameters specify how the server system restricts itself to arrive at the desired solution of the client.

We shall now illustrate Theorem 4.1 through a numerical but theoretical example. We fix up the parameters $(\alpha,\ \beta)$ satisfying $J(\alpha) - c\beta + dh(\beta) = 0$. Using MATLAB, the convergence of solutions of the system to the desired state is confirmed through simulations that are already established by Theorem 4.1. In the example provided here, the Lipschitz constants of (2) are given by $p = l = N = q = m = 1$.

Example 4.1 Consider the system

$$\begin{aligned} x^{'} &= -11x(t) + 3tanh(x(t-\tau)) + 2(x(t) + y(t)) + I(t), \\ y^{'} &= -9y(t) + 4tanh(y(t)) + J(x(t-\delta)). \end{aligned}$$

Corresponding to an expected output of $(\alpha,\ \beta)$, here the external input is chosen as $I(t) = (11\alpha - 3tanh(\alpha) - 2(\alpha + \beta))(1 + te^{-t})$ to satisfy condition (8) of Theorem 4.1.

(i) We let $J(x) = tanhx$. Then the desired output (α, β) is restricted to the region $D = \Big\{(\alpha, \beta)/9\beta - 4tanh(\beta) - tanh(\alpha) = 0, \Big\}$, from (7). We let $\alpha = 23 + 7i$. Then for this value of α, we have $\beta = 0.198$, satisfying the above equation. Clearly, all the conditions of Theorem 4.1 are satisfied, and hence, $(x, y) \to (\alpha,\ \beta) = (23 + 7i, 0.198)$ for large t by

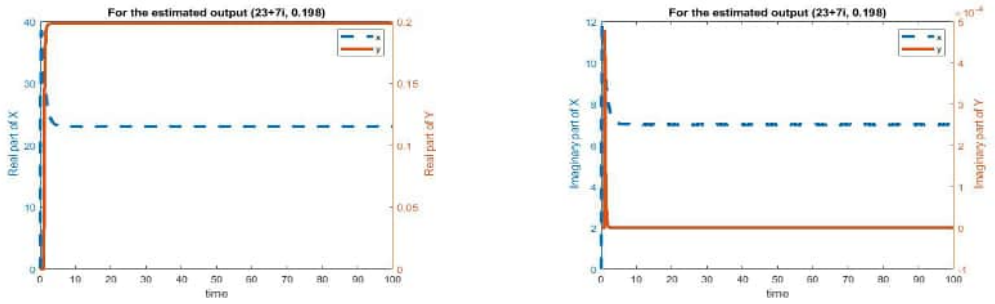

Figure 2: Input-output correlation through the system in Example 4.1.

virtue of Theorem 4.1 with $I(t)$ chosen above. The solutions approaching the a priori output (α, β) are depicted in Figures 2.

(ii) If we take $J(x) = \dfrac{x}{1+x}$, $x \neq -1$, the desired output (α, β) is restricted to the region $D = \left\{(\alpha, \beta)/9\beta - 4tanh(\beta) - \dfrac{\alpha}{1+\alpha} = 0, \right\}$. If we let $\alpha = 4 + 5i$, then we obtain $\beta = 0.178 + 0.019i$. For the input as specified above, all the other parametric conditions of Theorem 4.1 are satisfied. Hence, by Theorem 4.1, we get $(x, y) \to (\alpha, \beta) = (4 + 5i, 0.178 + 0.019i)$ as $t \to \infty$. The same is represented pictorially in Figure 3.

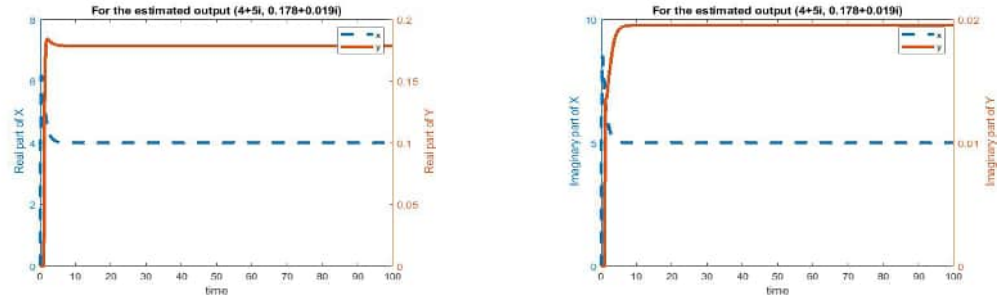

Figure 3: System eventually reaching a state desired by the client. Real and imaginary parts are shown separately.

Remark 4.2 Theorem 4.1 requires that the inputs are restricted by conditions specified by the server system as in (8) and the client should be in a position to provide them. Further, in the absence of any inputs (that is, $I(t) \equiv 0$, $J_{i_k}(x_i) \equiv 0$), it is not difficult to see [10] that $x_i \to 0$, $y_{i_k} \to 0$ as $t \to \infty$ under conditions (6), which shows that the system is going to a resting state in this case. On the other hand, when the client approaches it with suitable inputs, Theorem 4.1 establishes that the system is providing the desired solution for the client, which clearly indicates that the service provider system is client-specific only.

Remark 4.3 The very purpose of this study is to understand a real-world situation in terms of a mathematical model rather than to compare results. However, as we

have selected an existing model and modified it to suit our requirements, a question of comparison naturally arises. Mathematically, system (1) may be regarded as a general form or time delay version of (VI) from [12], which is an open problem. We notice that all the models in [12] become special cases of (1). To be specific, it may also be noted that, for $\tau_j = \delta_i = 0$, the system (4.5) from [12] is a special case of (1) for $J_{i_k}(x_i) = J_{i_k}$, system (4.7) from [12] is a special case of (1) for $I_i(t) = I_i$ and system (1) reduces to system (2.1) from [12] when $J_{i_k}(x_i) = J_{i_k}$ and $I_i(t) = I_i$ (both are mere constants). Hence, the results presented here are also applicable to systems (2.1), (4.5), and (4.7) from [12] as well. In this context, when $I(t) \equiv I$ is a fixed constant and (α, β) is an equilibrium solution of (5) satisfying $I = a\alpha - bf(\alpha) - c_1 g(\alpha, \beta)$, then it may be noticed that Theorem 4.4 from [12] becomes a special case of Theorem 4.1 here for $\delta = 0$ and for $\delta > 0$, respectively.

Since we are specifying the inputs from the client for its desired solution and making no changes in the structure of the system, the technique is not for a re-engineering of the system (e.g., [4]) but for a client-friendly system, yet rigid in its own sense. It may also be noticed that the two layers are working in coordination with each other. Thus, there is a synchronization of efforts of two layers of the network, but not a synchronization of networks (two different networks approaching a complete or almost identical state) as studied in [10].

5 Discussion

In this paper, we have considered a two-layered mathematical model to represent the dynamical interactions between the focal and non-focal parts (regarded as an outer layer and inner layer, respectively) of the server system that caters to the needs of a client system. The client system has the flexibility to vary its inputs. It is assumed that each member in the focal part is directly connected to the client system, whereas the non-focal part receives its instructions from focal members, processes them and gets back to the focal member only. They are in no way connected directly to the external client system. Basic qualitative properties of such a dynamical system, namely, the existence and uniqueness of solutions, boundedness, and the asymptotic closeness of solutions, are discussed. Since things should not get lost in carrying out such activities, the boundedness and closeness of solutions are important. Theorems 3.1, 3.2, and 3.3 take care of such situations. An expected output for the client from the focal part is defined as α, which in turn, expects a contribution of β from the non-focal part. Relations are developed, and it is established that by suitably restricting the parameters of the system, the desired solution may be attained by the focal part when the client system provides suitable inputs. This is the conclusion of Theorem 4.1. The results provided are independent of the length of time delays. Numerical examples illustrate theoretical situations. Simulations are provided to establish pictorially that the solutions of the system are reaching the desired state as envisaged by Theorem 4.1. Comparisons are made with earlier works in mathematical terms wherever possible.

Accepting a pre-specified solution from the client, working out strategies to obtain the solution, getting back to the client for suitable inputs and producing the desired solution to the client once the suitable information is received - all show that the server system is reliable. Further, the inputs need not be simple, fixed constants, but may be time-varying functions also. Only a highly proficient client can fix the inputs once for all for a possible desired solution from the service provider. Thus, our server system can

withstand variations in inputs and is flexible with the client.

References

[1] B. Dragovic, Nam Kyu Park, N. D. Zrnic and R. Mestrovic. Mathematical Models of Multi Server Queuing System for Dynamic Performance Evaluation in Port. *Mathematical Problems in Engineering* **2012** (3) (2012) 1–19.

[2] Bandana Priya, Ganesh Kumar Thakur, Sudesh Kumar Garg and M. Syed Ali. Robust Stability of Markovian Jumping Neural Networks with Time-Varying Delays. *Nonlinear Dynamics and Systems Theory* **20** (5) (2020) 535–541.

[3] Bo Xu, Ying Wang, Yu Han, Yuchang He and Ziwei Wang. Interaction patterns and coordination in two population groups: A dynamic perspective. *Chaos, Solitons and Fractals* **142** (2021) 110380.

[4] Chung-Horng Lung and Qiang Zhao. Pattern-oriented reengineering of a network system. *Journal of Systemics, Cybernetics and Informatics* **2** (4) (2004) 19–23.

[5] D. Bendel and M. Haviv. Cooperation and sharing costs in a tandem queuing network. *European Journal of Operations Research* **271** (3) (2018) 926–933.

[6] Debnath Bhattacharya, Soumita Seth and Tai-Loon Kim. Social network analysis to detect inherent communities based on constraints. *Applied Mathematics & Information sciences* **8** (1L) (2014) 385–396.

[7] Firman, Syamsuddin Toaha, Muh Nur. Asymptotic Stability of Some Class of Affine Nonlinear Control Systems through Partial Feedback Linearization. *Nonlinear Dynamics and Systems Theory* **21** (3) (2021) 238–245.

[8] Kan Li and Yin Pang. A unified community detection algorithm in complex network. *Neurocomputing* **130** (2014) 36–43.

[9] M. Y. Anshori, I. H. Santoso, T. Herlambang, M. Tafrikan, M. Adinugroho, K. Oktafianto and A. A. Firdaus. Analysis of Customer Satisfaction Survey on E-Wallets Using Simple Additive Weighting and TOPSIS. *Nonlinear Dynamics and System Theory* **24** (1) (2024) 28–40.

[10] Ruiyuan Zhu, Yingxin Guo and Fei Wang. Quasi-synchronization of heterogeneous neural networks with distributed and proportional delays via impulsive control. *Chaos, Solitons and Fractals* **141** (2020), 110322.

[11] V. B. Kolmanovskii and V. R. Nosov. *Stability of Functional Differential Equations*. Academic Press, London, 1986.

[12] V. Sree Hari Rao and P. Raja Sekhara Rao. Cooperative and Supportive Neural Network. *Physics Letters A* **371** (1) (2007) 101–110.

[13] V. Sree Hari Rao and P. Raja Sekhara Rao. Time Varying Simulations in Simple Neural Networks and Convergence to Desired Outputs. *Differential Equations and Dynamical Systems* **26** (2018) 81–104.

[14] R. Nunkoo, A. Sharma, K. K. F. So, H. Hu and A. F. Alrasheedi. Two decades of research on customer satisfaction: future research agenda and questions. *International Journal of Contemporary Hospitality Management* **37** (5) (2025) 1465–1496.

Nonlinear Dynamics and Systems Theory, **26** (1) (2026) 89–103

Analysis and Numerical Simulations of Fractional Order Model of Insect-Pest Dynamics

Y. Savadogo *, M. Barro, M. Ido and S. Traoré

Nazi Boni University, Department of Mathematics and Computer Science, LaMIA Laboratory, 01BP 1091 Bobo-Dioulasso 01, Burkina Faso

Received: January 1, 2025; Revised: February 1, 2026

Abstract: In this paper, we study a fractional-order version of the dynamics of insect-pests. We establish the existence and uniqueness of non-negative solutions and using the Laplace transform technique, we prove the boundedness of the solutions of the fractional model. Using Lyapunov's indirect method and the extension of LaSalle's invariance principle, we study the local and global stability of the equilibrium points of the fractional model. Moreover, we illustrate our theoretical results with numerical simulations of fractional model using the Adams-Bashforth-Moulton scheme.

Keywords: *Caputo fractional derivative; Riemann-Liouville fractional integral; insect-pest; numerical simulation.*

Mathematics Subject Classification (2020): 26A33, 34A08, 34A34, 37M05, 93-10.

1 Introduction

Insect-pests pose a threat worldwide, mainly in Africa, the economic and social burden of the damage caused by insect-pests such as fruit flies is increasing at both the producer and industry levels. Crop losses in these countries total billions of dollars and have a harmful impact on their economic situation and nutritional level [11]. In view of this threat, integrated pest management has been proposed to producers to combat this problem for the crops.

The massive use of pesticides as a means of controlling these insects leads to environmental pollution and economical waste. In addition, pesticides are generally harmful products and must be handled with care. Unfortunately, the precautions to be taken when handling these chemicals are unknown or ignored by producers. In this regard, the

* Corresponding author: mailto:savadogoy@outlook.fr

© 2026 InforMath Publishing Group/1562-8353 (print)/1813-7385 (online)/http://e-ndst.kiev.ua

integrated control approach against large insect invasions for the control of these fruit flies is to be favored. Thus, in order to propose an effective and inexpensive control program to reduce the proliferation of insect-pests in crops, a better knowledge of the dynamics of insect-pests is essential.

With the view of studying the impact of mating disruption control by using pheromone traps to distract males from females in order to reduce the proliferation of insect-pests, R. Anguelov *et al.* [3] introduced a generic model for insect-pests control using ordinary differential equations. In order to apply appropriate control methods against insect-pests, M. Djoukwe *et al.* [8] developed a delay model by applying strategies to control cocoa pests such as Sahlbergella singularis. In modeling, birth or growth processes are considered to be instantaneous phenomena. However, in real life, there is a time lag between the appearance of a new individual and its reproduction or activity. Therefore, to better reproduce as faithfully as possible by taking into account the total memory of past states in the dynamics of a given population, the singular or non-singular fractional differential operators are used in mathematical modeling [2,5,6]. Models based on ordinary differential equations are certainly of interest, but they do not take into account the historical life traits of pests, for example, an immature insect will go through different stages before becoming an adult capable of reproducing in turn. Fractional calculations, by allowing integrals and derivatives of integers orders as well as non-integers orders, represent a powerful tool in applied mathematics. Recently, particular attention has been focused on fractional derivatives as a tool for modeling certain real-life phenomena because of the hereditary nature and the memory effect of events. Systems described by fractional order models, using fractional differential equations based on the non-integer derivative, have attracted the interest of the scientific community. For this purpose, in [7], K. Diethelm studied the infection rate of dengue fever using a fractional model with the fractional derivative in the sense of Caputo and then compared with great success the numerical results obtained and the real data from the Cape Verde Islands.

Motivated by the applications of fractional calculus in modeling [5, 7], in this paper, we study a Caputo-type fractional model of the dynamics of insect-pests inspired by a classical model [3]. The goal of this work is to carry out the formulation and mathematical analysis of the established fractional model as well as numerical simulations to illustrate our theoretical results.

The work is organized as follows. We started by giving some useful basic notions for the analysis of fractional differential equations in the sense of Caputo in Section 2. In Section 3, we are interested in the formulation of the fractional model. Section 4 is devoted to the study of some properties of the solutions of the fractional model. In Section 5, we make numerical simulations and provide comments. We end this work by a conclusion.

2 Preliminaries on the Fractional Calculus

In this section, we recall some notions that will be used in the next sections. Let a and b be two real numbers such that $a < b$. Throughout this paper, $\mathcal{C}([a;\, b])$ denotes the space of continuous functions defined on $[a;\, b]$, $\mathcal{C}^n([a;b])$ stands for the class of all real-valued functions which are defined on $[a;\, b]$ and have continuous n-th order derivatives, and $L^1(a;b)$ is the usual Lebesgue space. Furthermore, we consider the sets $\mathbb{R}^n_+ := \{(x_1, x_2, \ldots, x_n),\, x_i \geq 0, i = 1, 2, \ldots, n\}$ and $\mathbb{R}^n_{++} := \{(x_1, x_2, \ldots, x_n),\, x_i > 0, i = 1, 2, \ldots, n\}$.

Definition 2.1 (Riemann-Liouville fractional integral [6, 10]) Let $\alpha \geq 0$, $f \in \mathcal{C}([a;b])$. The Riemann-Liouville fractional integral of order α of f is the function ${}^{RL}\mathcal{J}_a^{\alpha}[f]$ defined on $[a;b]$ by

$${}^{RL}\mathcal{J}_a^{\alpha}[f](t) := \begin{cases} \frac{1}{\Gamma(\alpha)} \int_a^t (t-\xi)^{\alpha-1} f(\xi) d\xi, & \text{if } \alpha > 0, \\ f(t), & \text{if } \alpha = 0, \end{cases}$$

where $\Gamma(\cdot)$ is Euler's Gamma function defined on $\mathbb{R}_{++}$ by

$$\Gamma(\alpha) := \int_0^{+\infty} r^{\alpha-1} e^{-r} dr.$$

Definition 2.2 (Caputo fractional derivative [6, 10]) Let $\alpha \geq 0$, $f \in \mathcal{C}^{\lceil \alpha \rceil}([a;b])$. The Caputo fractional derivative of f of order α is the function ${}^{C}\mathcal{D}_a^{\alpha}[f]$ defined on $[a;\, b]$ by

$${}^{C}\mathcal{D}_a^{\alpha}[f](t) := {}^{RL}\mathcal{J}_a^{\lceil \alpha \rceil - \alpha} \left[f^{(\lceil \alpha \rceil)} \right](t),$$

where $\lceil \cdot \rceil$ is a ceiling function defined by $\lceil \alpha \rceil := \min\{n \in \mathbb{Z} : \alpha \leq n\}$ and $f^{(\lceil \alpha \rceil)}$ denotes the $\lceil \alpha \rceil$-th derivative of f.

Let us recall the definition of the Mittag-Leffler function.

Definition 2.3 ([6]) Let $\alpha,\, \nu > 0$. Then the two-parameter Mittag-Leffler function $E_{\alpha,\nu}(\cdot)$ is defined by the series expansion

$$E_{\alpha,\,\nu}(q) = \sum_{n=0}^{\infty} \frac{q^n}{\Gamma(\nu + \alpha n)}, \quad q \in \mathbb{R}.$$

We simply denote $E_{\alpha,\,1}(\cdot)$ by $E_{\alpha}(\cdot)$.

Proposition 2.1 ([6, 10]) *Let $\alpha, \nu > 0$ and $\lambda \in \mathbb{R}$. Then*

$$\mathcal{L}\{t^{\nu-1} E_{\alpha,\nu}(\mp \lambda t^{\alpha})\}(s) = \frac{s^{\alpha-\nu}}{s^{\alpha} \pm \lambda} \quad \left(\Re(s) > 0;\, |s| > |\lambda|^{\frac{1}{\alpha}} \right), \tag{1}$$

where $\mathcal{L}\{\cdot\}$ stands for the Laplace transform and $\Re(s)$ is the real part of s.

Proposition 2.2 ([6]) *Let $\alpha,\, \nu > 0$ and $q \in \mathbb{R}$, we have*

$$E_{\alpha,\,\nu}(q) = q E_{\alpha,\,\alpha+\nu}(q) + \frac{1}{\Gamma(\nu)}.$$

In order to prove the properties of the fractional model solutions, we need the following useful lemmas.

Lemma 2.1 *Let $\alpha \in (0\,;\, 1]$, $f \in \mathcal{C}([a;b])$ and ${}^{C}\mathcal{D}_a^{\alpha}[f] \in \mathcal{C}((a;b])$. Then for all $t \in (a;b]$, there exists $\xi \in (a;\, t)$ for which*

$$f(t) = f(a) + {}^{C}\mathcal{D}_a^{\alpha}[f](\xi) \frac{(t-a)^{\alpha}}{\Gamma(\alpha+1)}.$$

Proof. Using Definition 2.1, we can write

$$^{RL}\mathcal{J}_a^{\alpha}\left[{}^{C}\mathcal{D}_a^{\alpha}\left[f\right]\right](t) = \frac{1}{\Gamma(\alpha)}\int_a^t (t-\tau)^{\alpha-1}{}^{C}\mathcal{D}_a^{\alpha}[f](\tau)d\tau.$$

By the generalized mean value theorem for integrals, there exists $\xi \in (a;\, t)$ such that

$$\begin{aligned} ^{RL}\mathcal{J}_a^{\alpha}\left[{}^{C}\mathcal{D}_a^{\alpha}\left[f\right]\right](t) &= {}^{C}\mathcal{D}_a^{\alpha}\left[f\right](\xi)\frac{1}{\Gamma(\alpha)}\int_a^t (t-\tau)^{\alpha-1}d\tau \\ &= {}^{C}\mathcal{D}_a^{\alpha}\left[f\right](\xi)\frac{(t-a)^{\alpha}}{\alpha\Gamma(\alpha)} = {}^{C}\mathcal{D}_a^{\alpha}\left[f\right](\xi)\frac{(t-a)^{\alpha}}{\Gamma(\alpha+1)}. \end{aligned} \tag{2}$$

On the other hand, it follows from the Taylor expansion for Caputo derivatives (see [6], Corollary 3.9) that for all $\alpha \in (0;1]$ and $t \in (a;\, b]$, we have

$$^{RL}\mathcal{J}_a^{\alpha}\left[{}^{C}\mathcal{D}_a^{\alpha}\left[f\right]\right](t) = f(t) - f(a). \tag{3}$$

From (2) and (3) we obtain $f(t) = f(a) + {}^{C}\mathcal{D}_a^{\alpha}\left[f\right](\xi)\frac{(t-a)^{\alpha}}{\Gamma(\alpha+1)}$. □

Remark 2.1 ([13]) Suppose that $f \in \mathcal{C}([a;b])$ and ${}^{C}\mathcal{D}_a^{\alpha}\left[f\right] \in \mathcal{C}((a;b])$, $\alpha \in (0;1]$. It follows from Lemma 2.1 that if ${}^{C}\mathcal{D}_a^{\alpha}\left[f\right](t) \geq 0$ for all $t \in (a;b)$, then f is nondecreasing on $[a;b]$ and if ${}^{C}\mathcal{D}_a^{\alpha}\left[f\right](t) \leq 0$ for all $t \in (a;b)$, then f is non-increasing on $[a;b]$.

Remark 2.2 Note that the result established in Lemma 2.1 was initially presented in the work of Z.M. Odibat *et al.* [13]. However, it contains calculation errors.

Lemma 2.2 ([6,10]) Let $\alpha > 0$ and $f \in \mathcal{C}^{\lceil\alpha\rceil}(\mathbb{R}_+)$. Moreover, suppose that $f^{(\lceil\alpha\rceil)} \in L^1(0;b)$ for any $b > 0$ is of exponential order, the Laplace transforms $\mathcal{L}\left[f\right]$ and $\mathcal{L}\left[f^{(\lceil\alpha\rceil)}\right]$ exist, and $\lim_{t\to\infty} f^{(k)}(t) = 0$ for $k = 0, 1, \ldots, \lceil\alpha\rceil - 1$. Then the Laplace transform of the fractional derivative of Caputo is

$$\mathcal{L}\left[{}^{C}\mathcal{D}_0^{\alpha}\left[f\right]\right](s) = s^{\alpha}\mathcal{L}\left[f\right](s) - \sum_{k=0}^{\lceil\alpha\rceil-1} s^{\alpha-k-1}f^{(k)}(0).$$

As a particular case, if $\alpha \in (0;\, 1]$, we have

$$\mathcal{L}\left[{}^{C}\mathcal{D}_0^{\alpha}\left[f\right]\right](s) = s^{\alpha}\mathcal{L}\left[f\right](s) - s^{\alpha-1}f(0). \tag{4}$$

Lemma 2.3 ([15]) *Let $x \in \mathcal{C}^1(\mathbb{R}_+)$ such that $x(t) > 0$ for all $t \in \mathbb{R}_+$. Then we have*

$${}^{C}\mathcal{D}_0^{\alpha}\left[x - x^* - x^*\ln\left(\frac{x}{x^*}\right)\right](t) \leq \left(1 - \frac{x^*}{x(t)}\right){}^{C}\mathcal{D}_0^{\alpha}[x](t),\ \forall\alpha \in (0;1),\ x^* \in \mathbb{R}_{++}.$$

3 Mathematical Formulation of the Model

In this section, we briefly describe the different steps in the formulation of the standard model of the dynamics of a population of insect pests such as fruit flies [3]. Thus, two main stages of development can be considered. The first stage, called the immature stage (I), which includes eggs, larvae and pupae, constitutes one class and the second stage called the adult stage is divided into three classes: the class of mating females (Y), the class of females inseminated (F) and the class of males (M). Table 1 describes the model parameters.

Parameters	**Descriptions**
b	intrinsic egg-laying rate
r	female to male ratio
K	carrying capacity
γ	females fertilized by a single male
μ_I	natural death rate of immature
μ_F	natural death rate of females
μ_M	natural death rate of males
ν_I	transfer rate from I to Y
ν_Y	transfer rate from Y to F
δ	transfer rate from F to Y

Table 1: Biological description of model parameters.

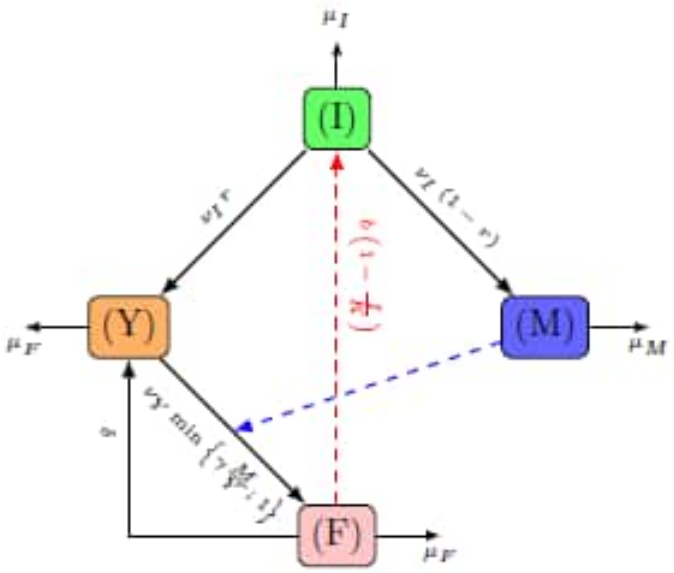

Figure 1: Compartmental representation of the different stages of insect-pest dynamics.

From Figure 1, we finally obtain the classical formulation of the model in the form of a system of the following ordinary differential equations:

$$\begin{cases} \frac{dI(t)}{dt} = b\left(1-\frac{I}{K}\right)F - (\nu_I+\mu_I)\,I, \\ \frac{dY(t)}{dt} = r\nu_I I - \nu_Y \min\{\gamma\frac{M}{Y},1\}Y + \delta F - \mu_F Y, \\ \frac{dF(t)}{dt} = \nu_Y \min\{\gamma\frac{M}{Y},1\}Y - \delta F - \mu_F F, \\ \frac{dM(t)}{dt} = (1-r)\nu_I I - \mu_M M \end{cases} \tag{5}$$

with the following initial conditions:

$$I(0) = I_0 \geq 0, \quad Y(0) = Y_0 \geq 0, \quad F(0) = F_0 \geq 0, \quad M(0) = M_0 \geq 0. \tag{6}$$

The classical model (5) above was presented and studied by R. Angelov *et al.* in [3] as part of integrated pest management (IPM) programs. It is important to note that, in the classical model (integer-order model), the state of the system does not depend on its history. However, in real life, memory plays an essential role in the dynamics of a given population. The advantage of these fractional-order models is that they allow greater degrees of freedom and incorporate the memory effect into the model. With this in mind, we propose a fractional model derived from the classical model (5).
In this paper, it is assumed that there are enough male insects to mate with all the female insects available for mating. Therefore, the transfer rate from Y to F is ν_Y^α. Using the same approach as in K. Diethelm [7], the fractional model is obtained by replacing the classical derivative in the previous system by the fractional derivative in the sense of Caputo. Then taking into account the dimensions of model parameters (5), in this context, we obtain the following fractional model:

$$\begin{cases} {}^C\mathcal{D}_0^\alpha[I](t) = b^\alpha\left(1-\frac{I}{K}\right)F - (\nu_I^\alpha+\mu_I^\alpha)\,I, \\ {}^C\mathcal{D}_0^\alpha[Y](t) = r\nu_I^\alpha I - (\nu_Y^\alpha+\mu_F^\alpha)Y + \delta^\alpha F, \\ {}^C\mathcal{D}_0^\alpha[F](t) = \nu_Y^\alpha Y - (\delta^\alpha+\mu_F^\alpha)F, \\ {}^C\mathcal{D}_0^\alpha[M](t) = (1-r)\nu_I^\alpha I - \mu_M^\alpha M, \end{cases} \tag{7}$$

where ${}^C\mathcal{D}_0^\alpha$ denotes the Caputo fractional derivative of order $\alpha \in (0;1]$, under the initial conditions (6).

4 Mathematical Analysis of the Fractional Model

4.1 Existence, uniqueness and properties of solutions

In this subsection, we study the existence and uniqueness of non-negative solution of the fractional model (7) under the initial conditions (6).
The fractional differential system (7) can be put into the following appropriate form:

$$\begin{cases} {}^C\mathcal{D}_0^\alpha\left[\Phi\right](t) = \mathcal{F}(\Phi(t)), \quad t \in \mathbb{R}_{++}, \\ \Phi(0) = \Phi_0 \geq 0 \end{cases} \tag{8}$$

with $\mathcal{F}(\cdot) := (\mathcal{F}_1(\cdot), \mathcal{F}_2(\cdot), \mathcal{F}_3(\cdot), \mathcal{F}_4(\cdot))^T$, $\Phi(t) := (I(t), Y(t), F(t), M(t))^T$ and $\Phi_0 := (I_0, Y_0, F_0, M_0)^T$, where $\mathcal{F}_1(I,Y,F,M) = b^\alpha\left(1-\frac{I}{K}\right)F - (\nu_I^\alpha+\mu_I^\alpha)\,I$, $\mathcal{F}_2(I,Y,F,M) = r\nu_I^\alpha I - (\nu_Y^\alpha+\mu_F^\alpha)Y + \delta^\alpha F$, $\mathcal{F}_3(I,Y,F,M) = \nu_Y^\alpha Y - (\delta^\alpha+\mu_F^\alpha)F$ and $\mathcal{F}_4(I,Y,F,M) = (1-r)\nu_I^\alpha I - \mu_M^\alpha M$.

Let us move on to the essential results of this paragraph.

Theorem 4.1 *The fractional system (8) admits a maximal solution.*

Proof. The function $\mathcal{F}$ is continuous. Thus, the initial value problem (8) is equivalent to the following system of nonlinear Volterra integral equations of the second kind [10]: $\Phi(t) = \Phi_0 + {}^{RL}\mathcal{J}_0^{\alpha}\left[\mathcal{F}(\Phi(\cdot))\right](t)$. Moreover, $\mathcal{F}$ is of class $\mathcal{C}^1$ since each component of $\mathcal{F}$ is of class $\mathcal{C}^1$, so it is locally Lipschitz. Then we deduce the existence and uniqueness of the maximal solution Φ of the fractional system (8) [6, 9]. □

Proposition 4.1 *The maximal solution Φ of (8) is non-negative and bounded.*

Proof. We will first show the non-negativity of the solution by proceeding to absurdity. From the uniqueness of solution, there are four possible cases.

Suppose that there exists $t_* > 0$ such that $I(t_*) = 0$, where $Y(t_*)$, $F(t_*)$, $M(t_*)$ are all non-negative and $I(t) < 0$ for all $t \in (t_*, t_1]$, where t_1 is sufficiently near t_*. Since $F(t_*) \geq 0$ and $I(t_*) = 0$, then from the second equation of the fractional system (7), we have

$$ {}^{C}\mathcal{D}_0^{\alpha}[I](t_*) = b^{\alpha}F(t_*) \geq 0.$$

Consequently, according to Lemma 2.1, we have ${}^{C}\mathcal{D}_0^{\alpha}[I](t) \geq 0$ for all $t \in [t_*, t_1]$. Therefore $I(t) \geq I(t_*)$ for all t sufficiently near t_*, which is a contradiction.
By the same way, we show that $Y(t) \geq 0$, $F(t) \geq 0$ and $M(t) \geq 0$.

We now prove the boundedness of the maximal solution.
From the first equation of (7), we get ${}^{C}\mathcal{D}_0^{\alpha}[I](t) \leq b^{\alpha}\left(1 - \frac{I(t)}{K}\right)F(t)$. So we have

$$I(t) \leq K. \tag{9}$$

From the fourth equation of the system (7) and taking into account (9), we have

$$ {}^{C}\mathcal{D}_0^{\alpha}[M](t) = (1-r)\nu_I^{\alpha}I(t) - \mu_M^{\alpha}M(t) \leq (1-r)\nu_I^{\alpha}K - \mu_M^{\alpha}M(t). \tag{10}$$

Applying the Laplace transform to the both sides of (10) and using (4), we get

$$\mathcal{L}\left[M\right](s) \leq \frac{(1-r)\nu_I^{\alpha}Ks^{-1}}{s^{\alpha} + \mu_M^{\alpha}} + \frac{s^{\alpha-1}M_0}{s^{\alpha} + \mu_M^{\alpha}}. \tag{11}$$

Now applying the inverse Laplace transform to inequality (11) and taking into account (1), we obtain

$$M(t) \leq \max\left\{\frac{(1-r)\nu_I^{\alpha}K}{\mu_M^{\alpha}};\, M_0\right\} =: K_M. \tag{12}$$

Under the assumption of male abundance in the region, i.e., $Y \leq \gamma M$, the third equation of the fractional system (7) gives

$$ {}^{C}\mathcal{D}_0^{\alpha}[F](t) \leq \nu_Y^{\alpha}\gamma M - (\delta^{\alpha} + \mu_F^{\alpha})F \leq \nu_Y^{\alpha}\gamma K_M - (\delta^{\alpha} + \mu_F^{\alpha})F. \tag{13}$$

Applying the Laplace transform to inequality (13), we get

$$\mathcal{L}\left[F\right](s) \leq \frac{\nu_Y^{\alpha}\gamma K_M s^{-1}}{s^{\alpha} + \delta^{\alpha} + \mu_F^{\alpha}} + \frac{s^{\alpha-1}F_0}{s^{\alpha} + \delta^{\alpha} + \mu_F^{\alpha}}. \tag{14}$$

Let us now apply the inverse Laplace transform to inequality (14), we have

$$F(t) \leq \max\left\{\frac{\nu_Y^{\alpha}\gamma(1-r)\nu_I^{\alpha}K}{\mu_M^{\alpha}(\delta^{\alpha} + \mu_F^{\alpha})};\, \frac{\nu_Y^{\alpha}\gamma M_0}{\delta^{\alpha} + \mu_M^{\alpha}};\, F_0\right\} =: K_F. \tag{15}$$

Similarly, from the second equation of system (7), we also have

$$Y(t) \leq \max\left\{\frac{r\nu_I^\alpha K + \delta^\alpha K_F}{\nu_Y^\alpha + \mu_F^\alpha}; Y_0\right\} =: K_Y. \tag{16}$$

□

Remark 4.1 It follows from Proposition 4.1 that the compact set Δ given by

$$\Delta := [0; K] \times [0; K_Y] \times [0; K_F] \times [0; K_M]$$

is positively invariant for the fractional system (8), where K_Y, K_F and K_M are defined by (16), (15) and (12), respectively.

Corollary 4.1 *The maximal solution Φ of (8) is a global solution.*

Proof. It follows from Proposition 4.1, that the maximal solution Φ of the fractional system (8) is bounded, then it is global [4]. □

4.2 Stability of the equilibrium points of the fractional system

In this part, we look for the equilibria of the fractional system (7) and we study their stability.

Remark 4.2 The equilibrium point without insect-pests of (7) is given by $\Phi_0^* = (0, 0, 0, 0)^T$.

Proposition 4.2 *The basic offspring number $\mathcal{N}_0$ of (7) is given as follows:*

$$\mathcal{N}_0 = \frac{b^\alpha r \nu_I^\alpha \nu_Y^\alpha}{\mu_F^\alpha(\mu_I^\alpha + \nu_I^\alpha)(\delta^\alpha + \mu_F^\alpha + \nu_Y^\alpha)}. \tag{17}$$

Proof. We will use the Van Den Driessche and Watmough method [14]. The transfer functions $\mathfrak{V}$ and $\mathfrak{F}$ are defined by

$$\mathfrak{V}(\Phi) = \begin{pmatrix} (\nu_I^\alpha + \mu_I^\alpha)\, I \\ -r\nu_I^\alpha I + (\nu_Y^\alpha + \mu_F^\alpha)Y - \delta^\alpha F \\ -\nu_Y^\alpha Y + (\delta^\alpha - \mu_F^\alpha)F \\ -(1-r)\nu_I^\alpha I + \mu_M^\alpha M \end{pmatrix} \text{ and } \mathfrak{F}(\Phi) = \begin{pmatrix} b^\alpha \left(1 - \frac{I}{K}\right) F \\ 0 \\ 0 \\ 0 \end{pmatrix}.$$

By calculating the Jacobian matrices of the functions $\mathfrak{V}$ and $\mathfrak{F}$ evaluated at the equilibrium point without insect-pests Φ_0^*, we obtain, respectively,

$$V = \begin{pmatrix} \nu_I^\alpha + \mu_I^\alpha & 0 & 0 & 0 \\ -r\nu_I^\alpha & \nu_Y^\alpha + \mu_F^\alpha & -\delta^\alpha & 0 \\ 0 & -\nu_Y^\alpha & \delta^\alpha + \mu_F^\alpha & 0 \\ -(1-r)\nu_I^\alpha & 0 & 0 & \mu_M^\alpha \end{pmatrix} \text{ and } F = \begin{pmatrix} 0 & 0 & b^\alpha & 0 \\ 0 & 0 & 0 & 0 \\ 0 & 0 & 0 & 0 \\ 0 & 0 & 0 & 0 \end{pmatrix}.$$

So, we have

$$FV^{-1} = \begin{pmatrix} \frac{b^\alpha r \nu_I^\alpha \nu_Y^\alpha}{\mu_F^\alpha(\mu_I^\alpha + \nu_I^\alpha)(\delta^\alpha + \mu_F^\alpha + \nu_Y^\alpha)} & \frac{b^\alpha \nu_Y^\alpha}{\mu_F^\alpha(\delta^\alpha + \mu_F^\alpha + \nu_Y^\alpha)} & \frac{b^\alpha(\nu_Y^\alpha + \mu_F^\alpha)}{\mu_F^\alpha(\delta^\alpha + \mu_F^\alpha + \nu_Y^\alpha)} & 0 \\ 0 & 0 & 0 & 0 \\ 0 & 0 & 0 & 0 \\ 0 & 0 & 0 & 0 \end{pmatrix}.$$

As a result, we arrive at $\mathcal{N}_0 := \rho(FV^{-1}) = \frac{b^\alpha r \nu_I^\alpha \nu_Y^\alpha}{\mu_F^\alpha(\mu_I^\alpha+\nu_I^\alpha)(\delta^\alpha+\mu_F^\alpha+\nu_Y^\alpha)}$, where $\rho(FV^{-1})$ denotes the spectral radius of the next generation matrix FV^{-1}. □

Remark 4.3 Note that $\mathcal{N}_0$ presented here in (17) stands for the average number of offspring produced by a female insect during its life provided that an abundant resource is available. In the case of fractional models, this average number is of a hereditary nature. It depends on the history of the dynamics of the insect population unlike the classical case. Note that, when taking the limit $\alpha \to 1$, the basic offspring number $\mathcal{N}_0$ associated with the fractional model (7) converges to $\mathcal{N}_0$ of the classical model [3].

The process of finding the equilibrium points of systems of fractional differential equations in Caputo's sense is analogous to classical ordinary differential equations. We can now state the following result.

Proposition 4.3 *(i) If $\mathcal{N}_0 \leq 1$, Φ_0^* is the unique equilibrium point of (7).*

(ii) If $\mathcal{N}_0 > 1$, the fractional model (7) admits a unique non-trivial equilibrium in the positive quadrant $\Phi^* = (I^*, Y^*, F^*, M^*)^T$ with $I^* = \left(1 - \frac{1}{\mathcal{N}_0}\right) K$, $Y^* = \frac{r\nu_I^\alpha(\delta^\alpha+\mu_F^\alpha)}{\mu_F^\alpha(\delta^\alpha+\mu_F^\alpha+\nu_Y^\alpha)} I^*$, $F^* = \frac{r\nu_I^\alpha\nu_Y^\alpha}{\mu_F^\alpha(\delta^\alpha+\mu_F^\alpha+\nu_Y^\alpha)} I^*$ and $M^* = \frac{(1-r)\nu_I^\alpha}{\mu_M^\alpha} I^*$, where $\mathcal{N}_0$ is given in (17).

Proof. We obtain the equilibrium points of (7) by setting its second member equal to zero. It follows that $M^* = \frac{(1-r)\nu_I^\alpha I^*}{\mu_M^\alpha}$, $Y^* = \frac{r\nu_I^\alpha(\delta^\alpha+\mu_F^\alpha)I^*}{\mu_F^\alpha(\delta^\alpha+\mu_F^\alpha+\nu_Y^\alpha)}$, $F^* = \frac{\nu_Y^\alpha r\nu_I^\alpha I^*}{\mu_F^\alpha(\delta^\alpha+\mu_F^\alpha+\nu_Y^\alpha)}$ and $I^*\left[K\left(\nu_I^\alpha\nu_Y^\alpha r b^\alpha - \mu_F^\alpha(\mu_I^\alpha+\nu_I^\alpha)(\delta^\alpha+\mu_F^\alpha+\nu_Y^\alpha)\right) - \nu_I^\alpha\nu_Y^\alpha r b^\alpha I^*\right] = 0$. Consequently, $I^* = 0$ or $I^* = \left(1 - \frac{1}{\mathcal{N}_0}\right) K$.

Thus, if $\mathcal{N}_0 \leq 1$, $I^* = \left(1 - \frac{1}{\mathcal{N}_0}\right) K \leq 0$, therefore $I^* = 0$, and in this case, Φ_0^* is the unique equilibrium point.

However, if $\mathcal{N}_0 > 1$, $I^* = \left(1 - \frac{1}{\mathcal{N}_0}\right) K > 0$, then we obtain that the non-trivial equilibrium point is Φ^*. □

Theorem 4.2 *The trivial equilibrium Φ_0^* of (7) is locally asymptotically stable if $\mathcal{N}_0 < 1$.*

Proof. The local stability of equilibria is obtained by using the Jacobian matrix $\mathbb{J}\mathcal{F}(\Phi)$ of the fractional system (7) defined as follows:

$$\mathbb{J}\mathcal{F}(\Phi) = \begin{pmatrix} -\frac{b^\alpha F}{K} - (\nu_I^\alpha + \mu_I^\alpha) & 0 & b^\alpha(1 - \frac{I}{K}) & 0 \\ r\nu_I^\alpha & -(\nu_Y^\alpha + \mu_F^\alpha) & \delta^\alpha & 0 \\ 0 & \nu_Y^\alpha & -(\delta^\alpha + \mu_F^\alpha) & 0 \\ (1-r)\nu_I^\alpha & 0 & 0 & -\mu_M^\alpha \end{pmatrix}. \tag{18}$$

By evaluating the Jacobian matrix (18) at the equilibrium point Φ_0^*, we obtain then

$$\mathbb{J}\mathcal{F}(\Phi_0^*) = \begin{pmatrix} -\epsilon_1 & 0 & b^\alpha & 0 \\ r\nu_I^\alpha & -\epsilon_2 & \delta^\alpha & 0 \\ 0 & \nu_Y^\alpha & -\epsilon_3 & 0 \\ (1-r)\nu_I^\alpha & 0 & 0 & -\mu_M^\alpha \end{pmatrix}, \tag{19}$$

where $\epsilon_1 = \nu_I^\alpha + \mu_I^\alpha$, $\epsilon_2 = \nu_Y^\alpha + \mu_F^\alpha$ and $\epsilon_3 = \delta^\alpha + \mu_F^\alpha$.
The eigenvalues of the matrix $\mathbb{J}\mathcal{F}(\Phi_0^*)$ are the roots of its characteristic polynomial

$$\mathcal{P}(\lambda) = (\lambda + \mu_M^\alpha)\left(\lambda^3 + A_1\lambda^2 + A_2\lambda + A_3\right)$$

with $A_1 = \epsilon_1 + \epsilon_2 + \epsilon_3$, $A_2 = \epsilon_1(\epsilon_2 + \epsilon_3) + \mu_F^\alpha(\epsilon_2 + \delta^\alpha)$ and $A_3 = \epsilon_1\mu_F^\alpha(\epsilon_2 + \delta^\alpha)(1 - \mathcal{N}_0)$.
It is easy to note that $\lambda_1 = -\mu_M^\alpha < 0$ is an eigenvalue of the matrix defined in (19), so it satisfies the condition $|\arg(\lambda_1)| = \pi > \frac{\alpha\pi}{2}$ for $\alpha \in (0; 1]$. The other eigenvalues are the roots of the polynomial $U(\lambda) := \lambda^3 + A_1\lambda^2 + A_2\lambda + A_3$. By applying the Routh-Hurwitz criterion on the polynomial $U(\lambda)$, we have the following sufficient conditions: $A_1 > 0$, $A_1A_2 - A_3 > 0$ and $A_3 > 0$. It is obvious that $A_1 > 0$, $A_1A_2 - A_3 > 0$ and so $\mathcal{N}_0 < 1$, $A_3 > 0$. We conclude that the other eigenvalues satisfies the condition $|\arg(\lambda)| > \frac{\alpha\pi}{2}$, when $\mathcal{N}_0 < 1$. Therefore, the trivial equilibrium point Φ_0^* of the fractional system (7) is locally asymptotically stable if $\mathcal{N}_0 < 1$. □
Note that the discriminant $\mathcal{D}(U)$ of the polynomial $U(\lambda)$ is defined (see [1]) by

$$\mathcal{D}(U) = 18A_1A_2A_3 + (A_1A_2)^2 - 4A_3A_1^3 - 4A_2^3 - 27A_3^2.$$

Using the fractional Routh-Hurwitz criterion established in [1], we deduce additional necessary and sufficient conditions for the local stability of the trivial equilibrium point.

Corollary 4.2 *The trivial equilibrium point Φ_0^* of (7) is locally asymptotically stable if and only if one of the following conditions holds:*

(i) $\mathcal{D}(U) > 0$, $A_1 > 0$, $A_3 > 0$ *and* $A_1A_2 > A_3$.

(ii) $\mathcal{D}(U) < 0$, $A_1 \geq 0$, $A_2 \geq 0$, $A_3 > 0$ *and* $\alpha < \frac{2}{3}$.

(iii) $\mathcal{D}(U) < 0$, $A_1 > 0$, $A_2 > 0$, $A_1A_2 = A_3$ *and* $\alpha \in (0, 1)$.

Remark 4.4 In the case when $\mathcal{D}(U) < 0$, $A_1 < 0$, $A_2 < 0$ and $\alpha > \frac{2}{3}$, the fractional system (7) is unstable. These instability conditions will not be treated in this model since biologically, A_1 and A_2 are always positive.

Theorem 4.3 *The trivial equilibrium point Φ_0^* of (7) is globally asymptotically stable in Δ if $\mathcal{N}_0 < 1$.*

Proof. We consider the Lyapunov candidate function $\mathcal{W}_1 : \mathbb{R}_+^4 \to \mathbb{R}$ defined by

$$\mathcal{W}_1(\Phi) = I + \frac{\nu_Y^\alpha b^\alpha}{\epsilon_2\epsilon_3 - \nu_Y^\alpha\delta^\alpha}Y + \frac{\epsilon_2 b^\alpha}{\epsilon_2\epsilon_3 - \nu_Y^\alpha\delta^\alpha}F + \frac{\epsilon_1(1 - \mathcal{N}_0)}{2(1 - r)\nu_I^\alpha}M.$$

Note that $\mathcal{W}_1(\Phi_0^*) = 0$ and $\mathcal{W}_1(\Phi) > 0$, $\forall\Phi \in \mathbb{R}_+^4 \setminus \{\Phi_0^*\}$.
By differentiating $\mathcal{W}_1$ with respect to time in the sense of Caputo and taking into account the linearity of the differential operator ${}^C\mathcal{D}_0^\alpha$, we get

$${}^C\mathcal{D}_0^\alpha[\mathcal{W}_1(\Phi)](t)|_{(7)} = -\frac{b^\alpha IF}{K} - \frac{\epsilon_1\mu_M^\alpha(1 - \mathcal{N}_0)}{2(1 - r)\nu_I^\alpha}M - \frac{\epsilon_1(1 - \mathcal{N}_0)}{2}I.$$

Consequently, as $\mathcal{N}_0 < 1$, it follows that

$${}^C\mathcal{D}_0^\alpha[\mathcal{W}_1(\Phi)](t)|_{(7)} = -\frac{b^\alpha IF}{K} - \frac{\epsilon_1\mu_M^\alpha(1 - \mathcal{N}_0)}{2(1 - r)\nu_I^\alpha}M - \frac{\epsilon_1(1 - \mathcal{N}_0)}{2}I \leq 0.$$

According to the extension of the LaSalle invariance principle [12], we conclude that the trivial equilibrium point Φ_0^* is globally asymptotically stable if $\mathcal{N}_0 < 1$. □

Theorem 4.4 *The non-trivial equilibrium Φ^* of (7) is locally asymptotically stable if $\mathcal{N}_0 > 1$.*

Proof. The local stability of the non-trivial equilibrium Φ^* is obtained by using the Jacobian matrix $\mathbb{J}\mathcal{F}(\Phi^*)$ of the fractional system (7) defined as follows:

$$\mathbb{J}\mathcal{F}(\Phi^*) = \begin{pmatrix} -\frac{b^\alpha F^*}{K} - \epsilon_1 & 0 & b^\alpha(1-\frac{I^*}{K}) & 0 \\ r\nu_I^\alpha & -\epsilon_2 & \delta^\alpha & 0 \\ 0 & \nu_Y^\alpha & -\epsilon_3 & 0 \\ (1-r)\nu_I^\alpha & 0 & 0 & -\mu_M^\alpha \end{pmatrix}. \tag{20}$$

The characteristic polynomial of $\mathbb{J}\mathcal{F}(\Phi^*)$ is

$$\mathcal{Q}(\lambda) = (\lambda + \mu_M^\alpha)\left(\lambda^3 + B_1\lambda^2 + B_2\lambda + B_3\right),$$

where $B_1 = \epsilon_1 + \epsilon_2 + \epsilon_3 + \frac{b^\alpha F^*}{K}$, $B_2 = (\epsilon_2+\epsilon_3)\left(\epsilon_1 + \frac{b^\alpha F^*}{K}\right) + \mu_F^\alpha(\epsilon_2 + \delta^\alpha)$ and $B_3 = \frac{\mu_F^\alpha b^\alpha F^*}{K}(\epsilon_2+\delta^\alpha)$. It is clear that $\lambda_1 = -\mu_M^\alpha < 0$ is an eigenvalue of the matrix defined in (20), so it satisfies the condition $|\arg(\lambda_1)| = \pi > \frac{\alpha\pi}{2}$ for $\alpha \in (0;1]$. The other eigenvalues are the roots of the polynomial $V(\lambda) := \lambda^3 + B_1\lambda^2 + B_2\lambda + B_3$. By applying the Routh-Hurwitz criterion to the polynomial $V(\lambda)$, we get the following sufficient conditions: $B_1 > 0$, $B_1B_2 - B_3 > 0$ and $B_3 > 0$. It is easy to see that $B_1 > 0$, $B_1B_2 - B_3 > 0$ and $B_3 > 0$. We conclude that the other eigenvalues satisfy the condition $|\arg(\lambda)| > \frac{\alpha\pi}{2}$ for $\alpha \in (0;1]$. Since Φ^* exists if $\mathcal{N}_0 > 1$, we deduce that the non-trivial equilibrium Φ^* of (7) is locally asymptotically stable when $\mathcal{N}_0 > 1$. □

Remark 4.5 For the non-trivial equilibrium Φ^*, we do not need additional conditions for local stability because the existence condition guarantees the local stability.

Theorem 4.5 *The non-trivial equilibrium point Φ^* of (7) is globally asymptotically stable if $\mathcal{N}_0 > 1$.*

Proof. Consider the following candidate Lyapunov function $\mathcal{W}_2 : \mathbb{R}^4_{++} \to \mathbb{R}$ given by

$$\mathcal{W}_2(\Phi) = c_1\int_{I^*}^{I}\frac{\tau - I^*}{\tau}d\tau + c_2\int_{Y^*}^{Y}\frac{\tau - Y^*}{\tau}d\tau + c_3\int_{F^*}^{F}\frac{\tau - F^*}{\tau}d\tau + c_4\int_{M^*}^{M}\frac{\tau - M^*}{\tau}d\tau,$$

where $c_1 = \frac{K}{b^\alpha}$, $c_2 = \frac{K\epsilon_1}{rb^\alpha\nu_I^\alpha}$, $c_3 = \frac{K\epsilon_1 I^*}{b^\alpha\nu_Y^\alpha Y^*} + \frac{K\epsilon_1\delta^\alpha F^*}{b^\alpha r\nu_I^\alpha\nu_Y^\alpha Y^*}$ and $c_4 = \frac{I^*}{(1-r)\nu_I^\alpha}$.
We notice that $\mathcal{W}_2(\Phi^*) = 0$ and $\mathcal{W}_2(\Phi) > 0$, $\forall\Phi \in \mathbb{R}^4_{++}\setminus\{\Phi^*\}$.
By differentiating $\mathcal{W}_2$ with respect to time in the sense of Caputo and taking into account the linearity of the fractional derivative ${}^C\mathcal{D}_0^\alpha$ and using Lemma 2.3, we have

$$\begin{aligned} {}^C\mathcal{D}_0^\alpha[\mathcal{W}_2(\Phi)](t)|_{(7)} &\leq c_1\left(1-\frac{I^*}{I(t)}\right){}^C\mathcal{D}_0^\alpha[I](t) + c_2\left(1-\frac{Y^*}{Y(t)}\right){}^C\mathcal{D}_0^\alpha[Y](t) \\ &+ c_3\left(1-\frac{F^*}{F(t)}\right){}^C\mathcal{D}_0^\alpha[F](t) + c_4\left(1-\frac{M^*}{M(t)}\right){}^C\mathcal{D}_0^\alpha[M](t). \end{aligned}$$

Using the following non-trivial equilibrium conditions: $K = \frac{K\epsilon_1 I^*}{b^\alpha F^*} + I^*$, $\delta^\alpha F^* = \epsilon_2 Y^* - r\nu_I^\alpha I^*$, $\nu_Y^\alpha Y^* = \epsilon_3 F^*$ and $\mu_M^\alpha M^* = (1-r)\nu_I^\alpha I^*$, and after some calculations, we obtain

$$\begin{aligned} {}^C\mathcal{D}_0^\alpha[\mathcal{W}_2(\Phi)](t)|_{(7)} &\leq \frac{K\epsilon_1 I^*}{b^\alpha}\left[3 - \frac{I^*F}{F^*I} - \frac{Y^*I}{I^*Y} - \frac{F^*Y}{Y^*F}\right] - IF\left(1-\frac{I^*}{I}\right)^2 \\ &+ \frac{K\epsilon_1\delta^\alpha F^*}{b^\alpha r\nu_I^\alpha}\left[2 - \frac{Y^*F}{F^*Y} - \frac{F^*Y}{Y^*F}\right] + I^*\left[1 - \frac{M}{M^*} - \frac{M^*I}{I^*M} + \frac{I}{I^*}\right]. \end{aligned}$$

By subtracting then adding $\frac{I^*}{I}+2$ to the expression $1-\frac{M}{M^*}-\frac{M^*I}{I^*M}+\frac{I}{I^*}$, we obtain

$$\begin{aligned} {}^C\mathcal{D}_0^\alpha[\mathcal{W}_2(\Phi)](t)|_{(7)} &\leq \frac{K\epsilon_1 I^*}{b^\alpha}\left[3-\frac{I^*F}{F^*I}-\frac{Y^*I}{I^*Y}-\frac{F^*Y}{Y^*F}\right]+I\left(1-F\right)\left(1-\frac{I^*}{I}\right)^2 \\ &+ \frac{K\epsilon_1\delta^\alpha F^*}{b^\alpha r\nu_I^\alpha}\left[2-\frac{Y^*F}{F^*Y}-\frac{F^*Y}{Y^*F}\right]+I^*\left[3-\frac{M}{M^*}-\frac{M^*I}{I^*M}-\frac{I^*}{I}\right]. \end{aligned}$$

By rewriting the above expression with the Volterra type function, it turns out that

$$\begin{aligned} {}^C\mathcal{D}_0^\alpha[\mathcal{W}_2(\Phi)](t)|_{(7)} &\leq -\frac{K\epsilon_1 I^*}{b^\alpha}\left\{\psi\left(\frac{I^*F}{F^*I}\right)+\psi\left(\frac{Y^*I}{I^*Y}\right)\right\}-I\left(F-1\right)\left(1-\frac{I^*}{I}\right)^2 \\ &- \frac{K\epsilon_1 I^*}{b^\alpha}\psi\left(\frac{F^*Y}{Y^*F}\right)-\frac{K\epsilon_1\delta^\alpha F^*}{b^\alpha r\nu_I^\alpha}\left\{\psi\left(\frac{Y^*F}{F^*Y}\right)+\psi\left(\frac{F^*Y}{Y^*F}\right)\right\} \\ &- I^*\left\{\psi\left(\frac{M}{M^*}\right)+\psi\left(\frac{M^*I}{I^*M}\right)\right\}-I^*\psi\left(\frac{I^*}{I}\right), \end{aligned}$$

where $\psi(x)=x-1-\ln(x)$ for all $x\in\mathbb{R}_{++}$. Therefore, we have ${}^C\mathcal{D}_0^\alpha[\mathcal{W}_2(\Phi)](t)|_{(7)}\leq 0$. Then we can apply LaSalle's fractional invariance principle [12] to the limit set, where each solution is contained in the largest invariant set $\mathcal{E}$ defined by $\mathcal{E}=\left\{(I,Y,F,M)\in\Delta:{}^C\mathcal{D}_0^\alpha\mathcal{W}_2(\Phi)|_{(7)}=0\right\}$. It is easy to see that the largest invariant set in $\mathcal{E}$ is just the singleton $\{\Phi^*\}$. It is concluded that the non-trivial equilibrium point Φ^* is globally asymptotically stable in the interior of Δ when $\mathcal{N}_0>1$. □

5 Numerical Simulations and Interpretations

In this section, we perform some numerical simulations to illustrate the theoretical results obtained in the previous sections. For this, we use the Python software and the Adams-Bashforth-Moulton numerical scheme (see [6]). The graphs resulting from the numerical simulation give the dynamics of the different compartments of the fractional model with different values of fractional derivation order $\alpha\in(0;1]$ and the basic offspring number $\mathcal{N}_0$. Furthermore, the numerical values used are summarized in Table 2.

	Values		**References**		
Parameters	$\mathcal{N}_0<1$	$\mathcal{N}_0>1$	$\mathcal{N}_0<1$	$\mathcal{N}_0>1$	**Dimensions**
b	1	3.28	estimated	estimated	day^{-1}
r	0.57	0.57	[3]	[3]	–
K	1000	1000	[3]	[3]	–
γ	1	4	estimated	[3]	–
μ_I	0.01	0.01	estimated	estimated	day^{-1}
μ_F	0.08	0.08	estimated	estimated	day^{-1}
μ_M	0.001	0.001	estimated	estimated	day^{-1}
ν_I	1/250	1/25	estimated	[3]	day^{-1}
ν_Y	1/100	0.5	estimated	[3]	day^{-1}
δ	0.1	0.1	[3]	[3]	day^{-1}

Table 2: The numerical values of the model parameters.

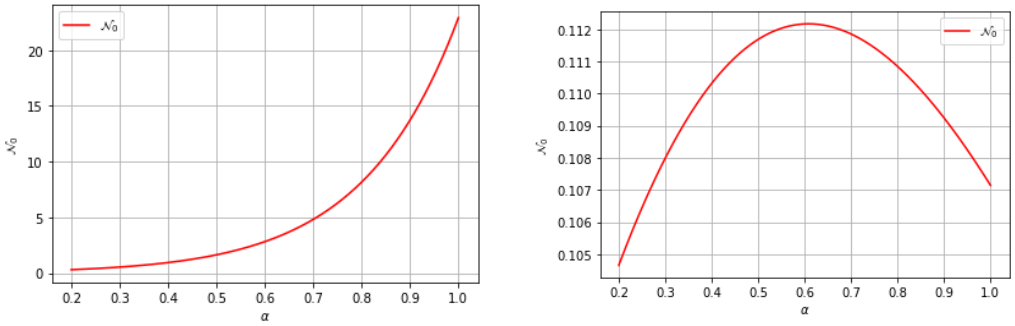

(a) (b)

Figure 2: Graph of offspring number $\mathcal{N}_0$ of the fractional model (7).

Figure 2 shows the influence of the derivation order on the offspring number with the data in Table 2, when $\mathcal{N}_0 > 1$ (Figure 2 (a)) and $\mathcal{N}_0 < 1$ (Figure 2 (b)).

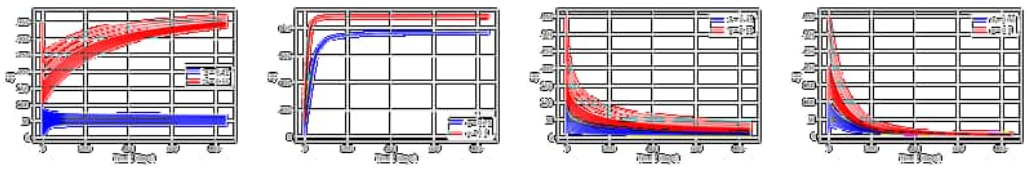

(a) (b) (c) (d)

Figure 3: Simulation of the global asymptomatic behavior of the class of immature insects of the fractional model (7).

We observe that if $\mathcal{N}_0 > 1$ (Figure 3 (a) and (b)), we have a persistence of the population of immature insects. And if $\mathcal{N}_0 < 1$ (Figure 3 (c) and (d)), we see an extinction of the population of immature insects.

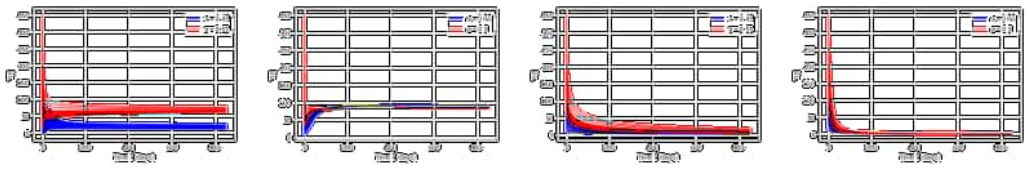

(a) (b) (c) (d)

Figure 4: Simulation of the global asymptomatic behavior of the class of female insects ready for mating of the fractional model (7).

We notice that if $\mathcal{N}_0 > 1$ (Figure 4 (a) and (b)), we have a persistence of the population of female insects ready for mating. And if $\mathcal{N}_0 < 1$ (Figure 4 (c) and (d)), we see an extinction of the population of female insects ready for mating of the fractional model (7).

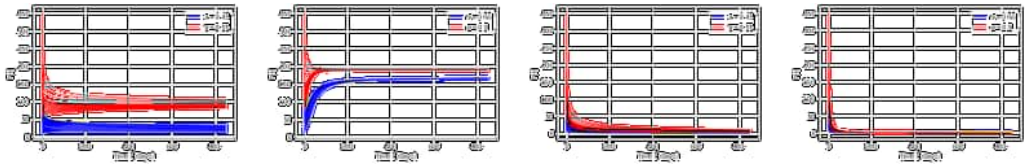

(a) (b) (c) (d)

Figure 5: Simulation of the global asymptomatic behavior of the class of females insects inseminated of the fractional model (7).

We observe that if $\mathcal{N}_0 > 1$ (Figure 5 (a) and (b)), we have a persistence of the population of females insects inseminated and if $\mathcal{N}_0 < 1$, (Figure 5 (c) and (d)), we see an extinction of the population of females insects inseminated.

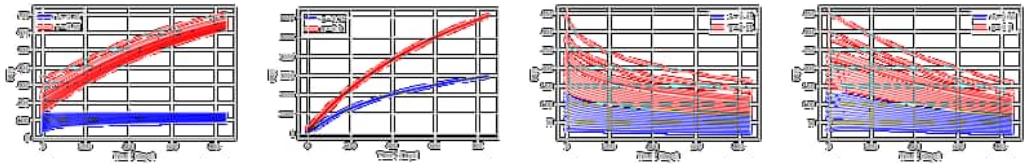

(a) (b) (c) (d)

Figure 6: Simulation of the global asymptomatic behavior of the class of male insects of (7).

We notice that if $\mathcal{N}_0 > 1$ (Figure 6 (a) and (b)), we observe a persistence of the population of male insects and $\mathcal{N}_0 < 1$ (Figure 6 (c) and (d)), we see an extinction of the population of male insects of the fractional order model (7).

6 Conclusion

In this paper, we have proposed and studied an extension of a model of the nonlinear dynamics of insect pests which is governed by Caputo-type fractional order differential equations. We have proved the existence and uniqueness of non-negative solutions of the fractional model. Then, using the Laplace transform technique, we have also shown the boundedness of the solutions. On one hand, by applying the classical Routh-Hurwitz criterion, we have established that the trivial and non-trivial equilibrium points are locally asymptotically stable, when $\mathcal{N}_0 < 1$ and $\mathcal{N}_0 > 1$, respectively. On the other hand, the use of fractional Routh-Hurwitz criteria has allowed us to determine additional conditions ensuring the asymptotic stability of the trivial equilibrium point of the fractional-order model. Using LaSalle's fractional invariance principle, we have shown that the trivial and non-trivial equilibrium points are globally asymptotically stable respectively, when $\mathcal{N}_0 < 1$ and $\mathcal{N}_0 > 1$. We have performed numerical simulations to illustrate our theoretical results. These numerical results are obtained with the values of the fractional order of derivative $\alpha \in \{0.9, 0.75, 0.55, 0.45\}$. The fractional model can capture richer and more realistic dynamics, thus improving predictions and the management of infestations.

Acknowledgment

The authors would like to express their sincere gratitude to the anonymous reviewers, whose valuable comments have greatly contributed to improving the quality of this work.

References

[1] E. Ahmed, A. M. A. El-Sayed and H. A. A. El-Saka. On some Routh-Hurwitz conditions for fractional order differential equations and their applications in Lorenz, Rössler, Chua and Chen Systems. *Physics Letters A* **358** (1) (2006) 1–4.

[2] R. Amira and F. Hannachi. A novel fractional-order chaotic system and its synchronization via adaptive control method. *Nonlinear Dynamics and Systems Theory* **23** (4) (2023) 359–366.

[3] R. Anguelov, C. Dufourd and Y. Dumont. Mathematical model for pest-insect control using mating disruption and trapping. *Applied Mathematical Modelling* **52** (2017) 437–457.

[4] L. Bourdin. Cauchy-Lipschitz theory for fractional multi-order dynamics : state-transition matrices, Duhamel formulas and duality theorems. *Differential Integral Equations* **31** (7-8) (2018) 559–594.

[5] S. Daudi, L. Luboodi, M. Kgosimore, D. Kuznetsov and S. Mushayabasa. A mathematical model for fall armyorm management on maize biomass. *Advances in Difference Equations* **2021** (99) (2021) 1–27.

[6] K. Diethelm. *The Analysis of Fractional Differential Equations, An Application-Oriented Exposition Using Differential Operators of Caputo Type*. Springer: Berlin, Germany, 2004, 2010.

[7] K. Diethelm. A fractional calculus based model for the simulation of an outbreak of dengue Fever. *Nonlinear Dynamics* **71** (4) (2013) 613–619.

[8] M. Djoukwe Tapi, L. Bagny-Beilhe and Y. Dumont. Miridae control using sex-pheromone traps. Modeling, analysis and simulations. *Nonlinear Analysis: Real World Applications* **54** (2020), 103082.

[9] V. D. Gejji and A. Babakhani. Analysis of a system of a fractional differential equations. *Journal of Mathematical Analysis and Applications* **293** (2) (2004) 511–522.

[10] A. A. Kilbas, H. M. Srivastava and J. J. Trujillo. *Theory and Applications of Fractional Differential Equations*. North-Holland Mathematics Studies, **204**, Amsterdam, Elsevier, (2006).

[11] R. Kumar. *Insect Pest Control: With Special Reference to African Agriculture*. Edward Arnold, ISBN 9780713184532, 1984.

[12] P. A. Naik. Global dynamics of a fractional-order SIR epidemic model with memory. *International Journal of Biomathematics* **13** (8) (2020), 2050071.

[13] Z. M. Odibat and N. T. Shawagfeh. Generalized Taylor's formula. *Applied Mathematics and Computation* **186** (1) (2007) 286–293.

[14] P. Van Den Driesche and J. Watmough. Reproduction numbers and subthreshold endemic equilibria for the compartmental models of disease transmission. *Mathematical Biosciences* **180** (2) (2002) 29–48.

[15] C. Vargas-De-León. Volterra-type Lyapunov functions for fractional-order epidemic systems. *Commun Nonlinear Sci. Numer. Simul.* **24** (3) (2015) 75–85.

Nonlinear Dynamics and Systems Theory, **26** (1) (2026) 104–114

An Analytical Study of Areas with Intellectual Disability in East Java and Their Prediction Using Ensemble Filtering

R. B. Utami [1,4*], M. Fannani [2], S. Sumardiyono [2] and T. Herlambang [3]

[1] *Doctoral Program on Public Health, Universitas Sebelas Maret, Surakarta, Indonesia.*
[2] *Department of Occupational Health and Safety, Vocational School, Universitas Sebelas Maret, Surakarta 57126, Indonesia.*
[3] *Department of Information System, Faculty of Economic Business and Digital Technology, Universitas Nahdlatul Ulama, Surabaya, Indonesia.*
[4] *Satria Bhakti College of Health Sciences, Nganjuk, Indonesia.*

Received: March 30, 2025; Revised: February 2, 2026

Abstract: According to the WHO, intellectual disability refers to individuals with limited intellectual abilities, who face difficulties in meeting basic needs. This condition affects both children and adults, with children requiring full support from parents and their environment, as they are prone to discrimination. It is common in several Indonesian provinces, notably West Java, Central Java, and East Java, particularly in rural or remote areas where access to health facilities and knowledge is limited. In this study, the prevalence of intellectual disability in East Java is analyzed and predicted using machine learning methods based on the number of affected regions per district/city. The methods applied are the Ensemble Kalman Filter (EnKF) and Ensemble Kalman Filter Square Root (EnKF-SR), both of which are developments of the Kalman Filter. The EnKF method achieved the best RMSE of 50.68 with 600 ensembles and R = 0.01, while the EnKF-SR achieved the best RMSE of 69.16 with 800 ensembles and R values of 0.01 and 0.03.

Keywords: *intellectual disability; East Java; prediction; machine learning; ensemble filtering.*

Mathematics Subject Classification (2020): 62M20, 68T07, 92C50.

* Corresponding author: mailto:budiutami2201@gmail.com

© 2026 InforMath Publishing Group/1562-8353 (print)/1813-7385 (online)/http://e-ndst.kiev.ua

1 Introduction

The World Health Organization's International Classification of Disease (ICD-10) defines intellectual disability as a mental disorder that simultaneously refers to the people of below average intellectual capability marked by the limitation of two or more skills, namely communication, self-care, social skills, safety, and personal health. In Indonesia, intellectual disability is experienced not only by adults, but also by children. According to Pendataan Program Perlindungan Sosial (PPLS) in 2011, the number of children with intellectual disability was 30,460 children out of a total of 13,572. This data is spread throughout Indonesia, with the most provinces in Central Java, East Java, and West Java [1].

According to the Basic Health Research Indonesia, 2013 (Riset Kesehatan Dasar known as Riskesdas), 14.3% of Indonesian household have a patient with a mental disorder and a majority are in rural area [2]. Knowledge, economic, and information factors and access to health facilities in rural areas are also limited. This lack of knowledge, for example, can be evidenced by the many cases of shackling that occur. Until now, most cases of shackling are in rural areas with the main factors being low economic problems and the inability to go to a mental hospital [3].

Almost all of Indonesia is familiar with the term "Pasung". Pasung is a long-standing custom in West Java and beyond. Pasung has traditionally involved a person who is agitated or considered at high risk of doing harm, either to themselves or others, being shackled using a wooden log [4]. Although it sounds less humane, it is still widely found in rural areas in Indonesia.

Especially for people with intellectual disability who are still children, this requires special attention and treatment. One of the most significant factors that can help improve quality of life for children with developmental disabilities is parental resilience [5]. On a broader scale, the role of the local government is needed as a health facilitator so that all people with intellectual disability have the same rights and access to health services in terms of legal guarantees in the form of Regional Regulations (Perda) [6].

In this research, the authors try to analyze and predict the number of regions in East Java province with intellectual disability survivors. Predictions are performed using Machine Learning (ML). ML is a subset of Artificial Intelligence [7]. Machine Learning (ML) has potential to enable a machine to learn from experience and apply this learning in future uncertainties [8]. ML methods can be divided into supervised learning, unsupervised learning, and reinforce learning [9].

The prediction methods used in this research are Ensemble Kalman Filter (EnKF) and Ensemble Kalman Filter-Square Root (EnKF-SR). The Ensemble Kalman Filter (EnKF) is an algorithm which is widely employed in the engineering community for the estimation of the state of partially-observed dynamical systems whose dynamics are governed by a nonlinear agent [10]. In the EnKF, the system's mean and covariance are approximated by an ensemble of states randomly sampled from the probability distribution. In the forecast, each state is advanced by the dynamical model; in the analysis step, each ensemble member is updated with the new observation to minimize the posterior covariance [11]. Meanwhile, EnKF-SR is a development of EnKF.

Previously, in 2023, S. Yoo et al. [12] conducted research about predicting wildfire spread using Ensemble Kalman Filter and polyline simplification. The result is algorithm successfully reduced computational time required for data assimilation [12]. In 2022, M. Y. Anshori et al. [13] conducted research about estimation XYZ company profitability

using H-Infinity and Ensemble Kalman Filter (EnKF). The result is that the performance of EnKF is more promising than H-Infinity with error percentage around 5-8% [13]. Still in 2022, A. Muhith et al. [14] conducted research about the stock of TC blood in PMI Gresik. The result is that EnKF-SR is better than UKF with an error less than 3% [14].

R. Ghostine et al. [15] in 2021, employed EnKF to predict COVID-19 pandemic evolution in Saudi Arabia complementing SEIR with vaccination and achieved promising short-term predictions with a relatively small ensemble size [15]. In 2021, H. Cevallos et al. [16] conducted research about electrical estimation using EnKF and Particle Filter. The result is that the Particle Filter achieves greater stability, higher estimation accuracy, and better performance [16]. In 2020, E. K. Korir et al. [17] conducted research on forecasting electricity prices using EnKF. The result is that EnKF gives better prediction with an RMSE value of 0.0089 [17].

2 Research Method

In this research, the data source refers to the official website of BPS Jatim (`www.jatim.bps.go.id`). The data contains 3 columns and 30 rows which represent the results recorded in 2014 and 2018. After that, the data is processed statistically to find insights and identify patterns. Table 1 shows the dataset used in this research, while Figure 1 illustrates the research methodology.

City/Regency	Number of Villages with Intellectual Disability in 2014	Number of Villages with Intellectual Disability in 2018
Pacitan	150	142
Ponorogo	236	238
Trenggalek	137	139
Tulungagung	239	243
Blitar	227	226
Kediri	277	298
Malang	338	303
Lumajang	147	140
Jember	192	169
Banyuwangi	166	172
Bondowoso	169	151
Situbondo	99	86
Probolinggo	254	209
Pasuruan	274	248
Sidoarjo	273	265
Mojokerto	234	229
Jombang	266	279
Nganjuk	231	214
Madiun	182	159
Magetan	202	199
Ngawi	175	159
Bojonegoro	345	327
Tuban	235	247
Lamongan	360	325
Gresik	276	235
Bangkalan	173	150
Sampang	145	148
Pamekasan	136	122
Sumenep	231	209
Kota Kediri	35	37
Kota Blitar	18	18
Kota Malang	24	38
Kota Probolinggo	27	26
Kota Pasuruan	27	26
Kota Mojokerto	28	28
Kota Madiun	9	17
Kota Surabaya	21	20
Kota Batu	22	20

Table 1: Dataset.

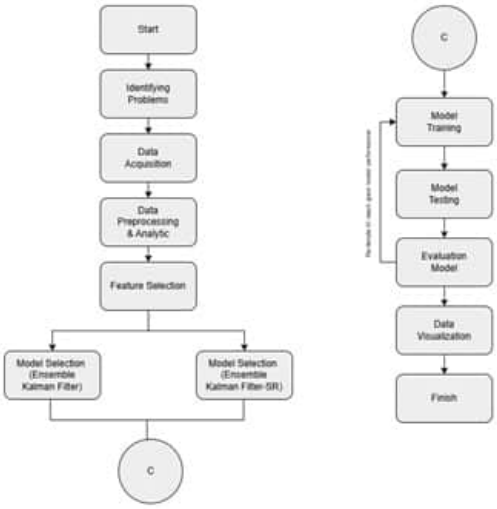

Figure 1: Research Methodology.

2.1 Exploratory Data Analysis (EDA)

Exploratory Data Analysis (EDA) is a statistical approach that examines the presence of multiple hidden features and patterns in a dataset [18]. In other words, Exploratory Data Analysis (EDA) is a way to explore the data with the aim of extracting useful and actionable information from it [19]. The data was collected in 2014 and 2018 and covers the entire province of East Java. Table 2 presents a summary of the central tendency of the data and Figure 2 plots the number of villages with intellectual disability in East Java.

Statistic	Number of Villages with Intellectual Disability in 2014	Number of Villages with Intellectual Disability in 2018
mean	174.97	38.0
min	9.0	17.0
max	360.0	327.0
std	100.24	93.73

Table 2: Measurement of the central tendency of villages with intellectual disability in East Java.

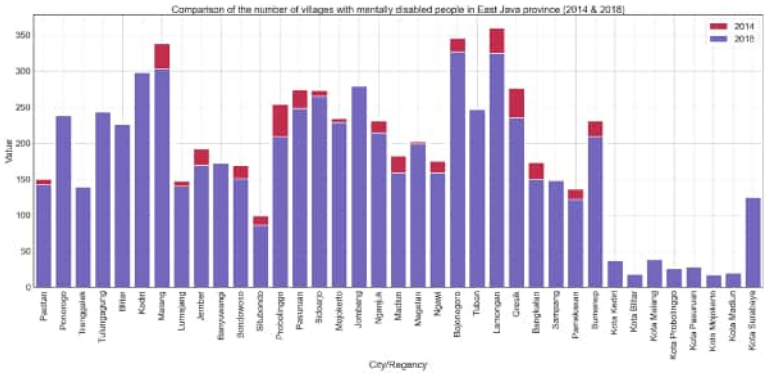

Figure 2: Plot comparison of the number of areas with people with intellectual disability in East Java.

From Figure 2, it can be seen that in some areas of East Java province, there has been an increase in areas with people with intellectual disability. Lamongan district has the highest level of mentally retarded people in East Java province and Blitar City along with Mojokerto City became the regions with the lowest levels. Then, the previous dataset can be tested using the Wilcoxon test to determine the relationship between condition variables in 2014 and 2018. Below, Figures 3 and 4 plot the distribution of data and Table 3 presents the result of the Wilcoxon test.

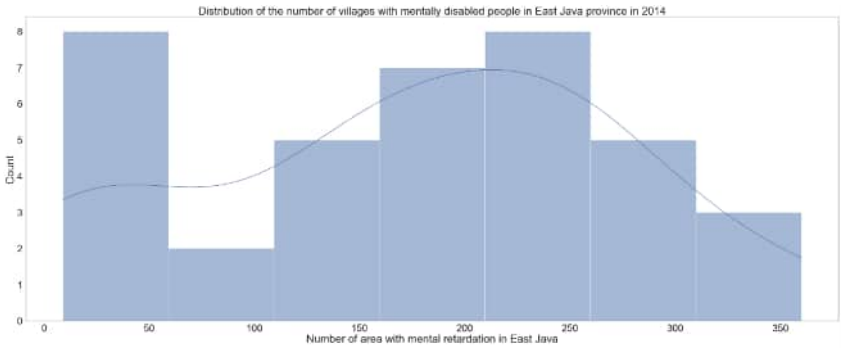

Figure 3: Histogram of distribution of data in 2014.

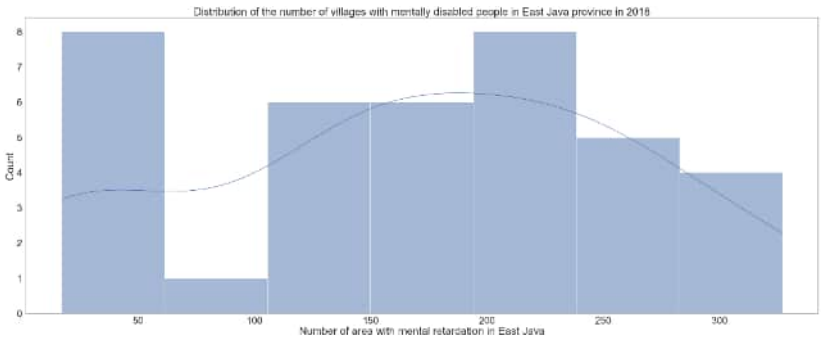

Figure 4: Histogram of distribution of data in 2018.

Wilcoxon statistic	176.0
P-Value	0.013

Table 3: Result of the Wilcoxon test.

From Figures 3 and 4 and also Table 3 above, it can already be determined which distribution of data is not normal and based on the Wilcoxon test, it is clear that there is a relationship between the values in the columns in 2014 and 2018. Indeed, many papers apply non-parametric tests such as the Mann-Whitney test or the Wilcoxon test to compare groups when the data do not seem completely normally distributed [20].

2.2 Preprocessing

After that, the next step is normalization. It refers to scaling the dataset so that the data values lie between 0 and 1 [21]. One advantage of MinMax Scaler is that it allows mapping features with very different ranges into the same interval while keeping all information since distance ratios are preserved [22]. Below in Equation (1) is the MinMax Scaler function

$$x^1 = \frac{x_i - \min(x)}{\max(x) - \min(x)}. \tag{1}$$

2.3 Feature selection

Next, the process moves on to feature selection. Based on the case study and dataset variables, the variable *Number of Villages with Impaired Patients in 2018* is selected as the dependent/target variable.

2.4 Ensemble Kalman Filter (EnKF) prediction model

The EnKF was developed as a version of the Kalman Filter for large-scale problems. It is a Monte Carlo based implementation of the Kalman Filter for non-linear state estimation problems [23]. Similar to the KF, the EnKF consists of recursive application of a forecast step and an analysis step [24]. Below in Figure 5, the EnKF algorithms are presented.

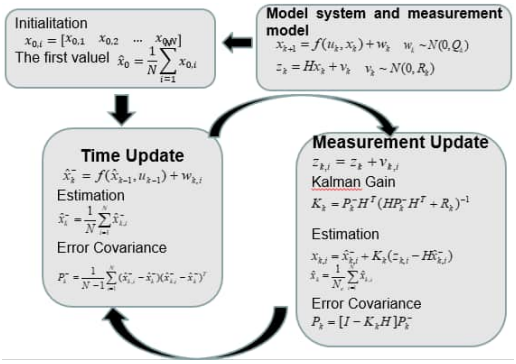

Figure 5: Ensemble Kalman Filter (EnKF) algorithm.

2.5 Ensemble Kalman Filter Square Root (EnKF-SR) prediction model

Below Figure 6 present the function of Ensemble Kalman Filter Square Root.

2.6 Model evaluation

At the evaluation stage, the model trained and tested is calculated for accuracy based on the resulting error value. The root mean squared error (RMSE) and the mean absolute error (MAE) are two standard metrics used in model evaluation. This study uses the Root Mean Square Error (RMSE) method to calculate the error value generated by the

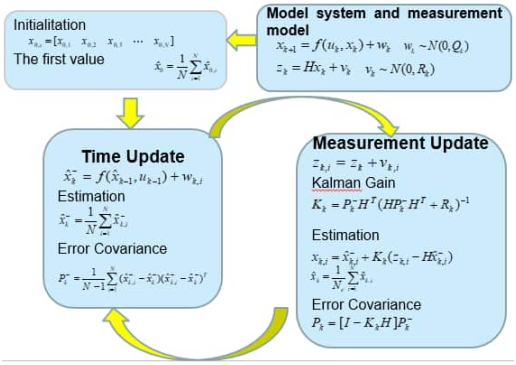

Figure 6: Ensemble Kalman Filter Square Root (EnKF-SR) algorithm.

model. The function of the Root Mean Square Error (RMSE) is presented in Equation (2) as follows:

$$\text{RMSE} = \sqrt{\frac{1}{n}\sum_{i=1}^{n}(y_i - \hat{y}_i)^2}. \tag{2}$$

3 Results and Discussion

In this research, the authors tried to implement Ensemble Kalman Filter (EnKF) and Ensemble Kalman Filter Square Root (EnKF-SR) to predict the number of areas in East Java with people with intellectual disability. The ensemble numbers used are 600 and 800. The overall simulation results are shown in Figures 7 to 10.

3.1 Simulation result of EnKF and EnKF-SR with 600 ensembles

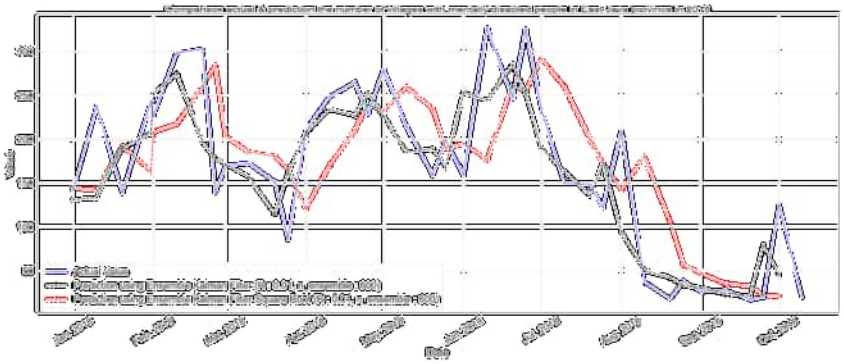

Figure 7: 1st Simulation Plot with EnKF and EnKF-SR with 600 ensembles and R value 0,01.

The first simulation can be seen in Figure 7, it shows the result of comparison between Ensemble Kalman Filter (EnKF) and Ensemble Kalman Filter Square Root (EnKF-SR). EnKF prediction results are shown by the black line, while those of EnKF-SR are shown

by the red line. All methods use 600 ensembles and R value is 0,01. The result of EnKF with 600 ensembles and R value of 0,01 has a better accuracy value with an RMSE value of 50,68. Meanwhile, EnKF-SR gives an RMSE value of 69.19.

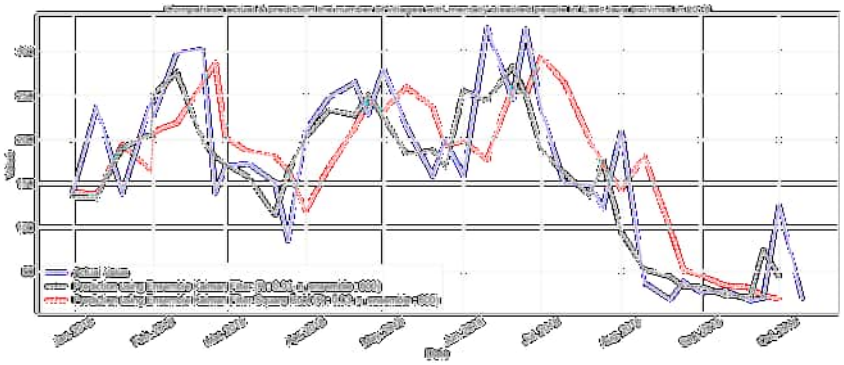

Figure 8: 2nd Simulation Plot with EnKF and EnKF-SR with 600 ensembles and R value 0,03.

The second simulation can be seen in Figure 8, it shows the result of comparison between Ensemble Kalman Filter (EnKF) and Ensemble Kalman Filter Square Root (EnKF-SR). EnKF prediction results are shown by the black line, while those of EnKF-SR are shown by the red line. All methods use 600 ensembles and R value is 0,03. The result of EnKF with 600 ensembles and R value of 0,03 has a better accuracy value with an RMSE value of 50,80. Meanwhile, EnKF-SR gives an RMSE value of 69.64.

3.2 Simulation result of EnKF and EnKF-SR with 800 ensembles

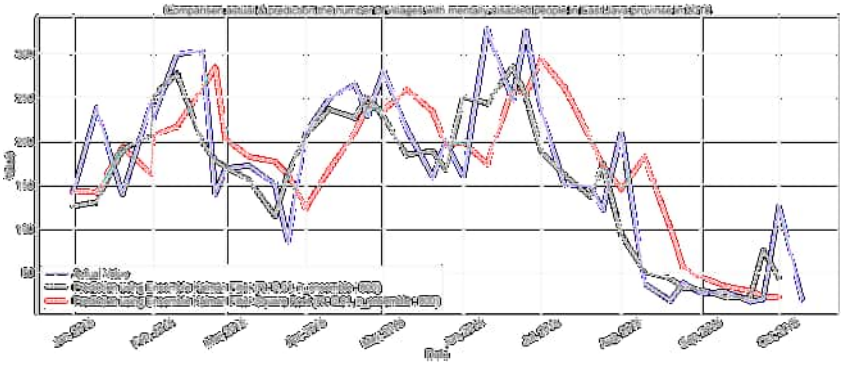

Figure 9: 3rd Simulation Plot with EnKF and EnKF-SR with 800 ensembles and R value 0,01.

The third simulation can be seen in Figure 9, it shows the result of comparison between Ensemble Kalman Filter (EnKF) and Ensemble Kalman Filter Square Root (EnKF-SR). EnKF prediction results are shown by the black line, while those of EnKF-SR are shown by the red line. All methods use 800 ensembles and R value is 0,01. The result of EnKF with 800 ensembles and R value of 0,01 has a better accuracy value with an RMSE value of 50,89. Meanwhile, EnKF-SR gives an RMSE value of 69.16.

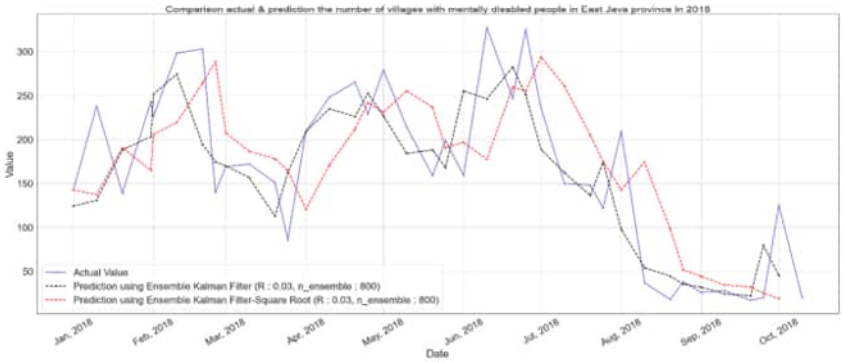

Figure 10: 4th Simulation Plot with EnKF and EnKF-SR with 800 ensembles and R value 0,03.

The fourth simulation can be seen in Figure 10, it shows the result of comparison between Ensemble Kalman Filter (EnKF) and Ensemble Kalman Filter Square Root (EnKF-SR). EnKF prediction results are shown by the black line, while those of EnKF-SR are shown by the red line. All methods use 800 ensembles and R value is 0,03. The result of EnKF with 800 ensembles and R value of 0,03 has a better accuracy value with an RMSE value of 50,99. Meanwhile, EnKF-SR gives an RMSE value of 69.16. For a clearer interpretation, below is a recapitulation table of all simulations shown in Tables 4 and 5

3.3 Comparison of RMSE Values

Method	Number of Ensembles	R Value	RMSE Value
EnKF	600	0.01	50.68
		0.03	50.80
EnKF-SR	600	0.01	69.19
		0.03	69.64

Table 4: Comparison of RMSE values of EnKF and EnKF-SR using 600 ensembles.

Method	Number of Ensembles	R Value	RMSE Value
EnKF	800	0.01	50.89
		0.03	50.99
EnKF-SR	800	0.01	69.16
		0.03	69.16

Table 5: Comparison of RMSE values of EnKF and EnKF-SR using 800 ensembles.

From Tables 4 and 5, it can be seen that both methods perform well. The EnKF method achieves the best RMSE value when the number of ensembles is 600 with an R value of 0.01. Meanwhile, the EnKF-SR method achieved the best RMSE value when the number of ensembles was 800 with R values of 0.01 and 0.03. Overall, the accuracy

rate produced by the EnKF method is about 80 percent. Meanwhile, the accuracy rate produced by the EnKF-SR method is around 77 percent.

4 Conclusion

From the overall simulation results that have been obtained using the EnKF and EnKF-SR methods, the prediction performance is quite good. Both methods maximize the accuracy value based on the number of ensembles and the R value. The EnKF method achieves the best RMSE value of 50,68 when the number of ensembles is 600 with an R value of 0.01. Meanwhile, the EnKF-SR method achieved the best RMSE value of 69,16 when the number of ensembles was 800 with R values of 0.01 and 0.03. Both methods can be used and optimized with other variations.

References

[1] M. H. Imaduddin, N. Febriyana, Y. Setiawati and I. Irwanto. Risk Factor Mild Mental Retardation in Extraordinary School at Surabaya. *Surabaya Journal of Psychiatry* **9** (2) (2020) 34—45.

[2] M. A. Wahyu and T. M. A. Elven. Protecting the Rights of Mental Health Patients: Comparative Study between Indonesia and Taiwan. *Indonesian Comparative Law Review* **2** (2) (2020) 110—125.

[3] N. V. E. S. Hidayanti, G. Alfianto, N. M. A. Kurniyanti and N. Soebagijono. Case Study: People with Severe Mental Disorders with Physical Mobility Barriers After in Pasung. *Journal of Health Research and Technology* **1** (1) (2023) 36—46.

[4] M. T. Hidayat, C. Oster, E. Muir-Cochrane and S. Lawn. Indonesia Free from Pasung: A Policy Analysis. *International Journal of Mental Health Systems* **17** (1) (2023) 1—22.

[5] Y. Widyawati, R. H. J. Scholte, T. Kleemans and R. Otten. Positive parenting and its mediating role in the relationship between parental resilience and quality of life in children with developmental disabilities in Java Island, Indonesia. *Research in Developmental Disabilities*. **112** (2021) 103911.

[6] T. I. Pramesti and S. Wibawani. Implementation of the Protection Policy for Children with Disabilities in the Rumah Anak Prestasi Surabaya City. *Journal La Sociale* **5** (4) (2024) 1139—1151.

[7] A. Sircar, K. Yadav, K. Rayavarapu, N. Bist and H. Oza. Application of machine learning and artificial intelligence in oil and gas industry. *Petroleum Research* **6** (4) (2021) 379—391.

[8] P. Kumar and M. Sharma. Data, Machine Learning, and Human Domain Experts: None Is Better than Their Collaboration. *International Journal of Human-Computer Interaction* **38** (14) (2021) 1307—1320.

[9] N. Peiffer-Smadja et al. Machine learning for clinical decision support in infectious diseases: a narrative review of current applications. *Clinical Microbiology and Infection* **26** (5) (2019) 584—595.

[10] A. Abdulle, G. Garegnani and A. Zanoni. Ensemble Kalman filter for multiscale inverse problems. *Multiscale Modeling and Simulation* **18** (4) (2020) 1565—1594.

[11] M. L. Provost and J. D. Eldredge. Ensemble Kalman filter for vortex models of disturbed aerodynamic flows. *Physical Review Fluids* **6** (5) (2021).

[12] S. Yoo and J. Song. Rapid prediction of wildfire spread using ensemble Kalman filter and polyline simplification. *Environmental Modelling & Software* **160** (2022) 105610.

[13] M. Y. Anshori, T. Herlambang, P. Katias, F. A. Susanto and R. R. Rasyid. Profitability estimation of XYZ company using H-infinity and Ensemble Kalman Filter. *Journal of Physics Conference Series* **2157** (2022) 012027.

[14] A. Muhith, T. Herlambang, D. Rahmalia, N. Irhamah and D. F. Karya. Estimation of Thrombocyte Concentrate (TC) in PMI Gresik using unscented and square root Ensemble Kalman Filter. *Journal of Physics Conference Series* **2157** (1) (2022) 012029.

[15] R. Ghostine, M. Gharamti, S. Hassrouny and I. Hoteit. An Extended SEIR Model with Vaccination for Forecasting the COVID-19 Pandemic in Saudi Arabia Using an Ensemble Kalman Filter. *Mathematics* **9** (6) (2021) 636.

[16] H. Cevallos, G. Intriago, and D. Plaza. Ensemble kalman filter and particle filter-based state estimation on electrical power systems. *Mathematics* **2090** (1) (2021) 012016.

[17] E. K. Korir, J. Aduda and T. Mageto. Forecasting Electricity Prices Using Ensemble Kalman Filter Forecasting Using Ensemble kalman Filter. *Journal of Statistical and Econometric Methods* **9** (1) (2020) 27–45.

[18] U. Javed et al. Exploratory Data Analysis Based Short-Term Electrical Load Forecasting: A Comprehensive analysis. *Energies* **14** (17) (2021) 1-22.

[19] N. S. Mittal et al. An exploratory data analysis of COVID-19 in India. *International Journal of Engineering Research* **9** (4) (2020) 580.

[20] S. L. Cessie, J. J. Goeman and O. M. Dekkers. Who is afraid of non-normal data? Choosing between parametric and non-parametric tests. *European Journal of Endocrinology* **182** (2) (2020) E1—E3.

[21] W. M. Ridwan et al. Rainfall forecasting model using machine learning methods: Case study Terengganu, Malaysia. *Ain Shams Engineering Journal* **12** (2) (2021) 1651—1663.

[22] D. Chanal, N. Y. Steiner, D. Chamagne and M. -C. Pera. Impact of standardization applied to the diagnosis of LT-PEMFC by Fuzzy C-Means clustering. *2021 IEEE Vehicle Power and Propulsion Conference (VPPC)* (2021).

[23] B. Nilam and S. T. Ram. Forecasting Geomagnetic activity (Dst Index) using the ensemble kalman filter. *Monthly Notices of the Royal Astronomical Society* **511** (1) (2022) 723—731.

[24] M. Fan, Y. Bai, L. Wang and L. Ding. Combining a fully connected neural network with an ensemble Kalman filter to emulate a dynamic model in data assimilation. *IEEE Access* **9** (2021) 144952–144964.